DETERMINATION OF IN-SITU STRESSES AROUND UNDERGROUND EXCAVATIONS BY MEANS OF HYDRAULIC FRACTURING

Bezalel C. Haimson

Wisconsin University

Prepared for:

Advanced Research Projects Agency
Bureau of Mines

1 April 1974

UNCLASSIFIED

SECURITY CLASSIFICATION OF THIS PAGE (When Data Entered)

REPORT DOCUMENTATION PAGE		READ INSTRUCTIONS BEFORE COMPLETING FORM
1. REPORT NUMBER	2. GOVT ACCESSION NO.	3. RECIPIENT'S CATALOG NUMBER AD-780 220
4. TITLE (and Subtitle) Determination of In-Situ Stresses Around Underground Excavations by Means of Hydraulic Fracturing		5. TYPE OF REPORT & PERIOD COVERED Final 7/1/72 - 3/31/74 6. PERFORMING ORG. REPORT NUMBER
7. AUTHOR(s) Bezalel C. Haimson		8. CONTRACT OR GRANT NUMBER(s) H0220080
9. PERFORMING ORGANIZATION NAME AND ADDRESS University of Wisconsin Madison, Wisconsin 53706		10. PROGRAM ELEMENT, PROJECT, TASK AREA & WORK UNIT NUMBERS 62701D/1579/F53408
11. CONTROLLING OFFICE NAME AND ADDRESS Advanced Research Projects Agency 1400 Wilson Blvd. Arlington, Virginia 22209		12. REPORT DATE April 1, 1974 13. NUMBER OF PAGES 113
14. MONITORING AGENCY NAME & ADDRESS(if different from Controlling Office) U.S. Bureau of Mines Spokane Mining Research Center 1430 N. Washington Street Spokane, Washington 99201		15. SECURITY CLASS. (of this report) Unclassified 15a. DECLASSIFICATION/DOWNGRADING SCHEDULE

16. DISTRIBUTION STATEMENT (of this Report)

Distribution of this document is unlimited.

17. DISTRIBUTION STATEMENT (of the abstract entered in Block 20, if different from Report)

18. SUPPLEMENTARY NOTES

19. KEY WORDS (Continue on reverse side if necessary and identify by block number)

Rock Mechanics
Hydraulic Fracturing
Mechanical Properties of Rock
Stress Determination

20. ABSTRACT (Continue on reverse side if necessary and identify by block number)

Laboratory tests have been conducted to determine the mechanical properties of Coeur d'Alene quartzite and to establish whether this highly inhomogeneous, precracked variable rock is suitable for hydraulic fracturing as a method of in-situ stress measurement. It was found that basically the Coeur d'Alene quartzite is amenable to hydraulic fracturing testing. The rock has no consistent anisotropy, but is inhomogeneous with physical

DD FORM 1 JAN 73 1473 EDITION OF 1 NOV 65 IS OBSOLETE

UNCLASSIFIED

SECURITY CLASSIFICATION OF THIS PAGE (When Data Entered)

20. ABSTRACT (Continued)

property variations depending on fabric changes and existence of fractures and mica inclusions. Bedding inclination does not affect hydraulic fracturing results. Neither do existing cracks not crossing the pressurized borehole. Plaster lining of the hole remedies those situations where open cracks traverse the fracturing zone. Theoretical stress-hydrofracturing pressure relationships for permeable and impermeable rock provide the range within which the experimental results fall. Hydrofracture direction is always perpendicular to the smallest horizontal stress notwithstanding rock condition. Field stress measurements in the Coeur d'Alene mines using the hydraulic fracturing technique are recommended.

DETERMINATION OF IN-SITU STRESSES AROUND UNDERGROUND EXCAVATIONS BY MEANS OF HYDRAULIC FRACTURING

Final Technical Report

July 1972 - March 1974

B.C. Haimson
Principal Investigator
(608) 262-2563

Department of Metallurgical & Mineral Engineering
and the
Engineering Experiment Station
College of Engineering
The University of Wisconsin-Madison
Madison, Wisconsin 53706

Sponsored by Advanced Research Projects Agency,
ARPA Order No. 1579, Amendment 3
Program Code No. 2F10
Contract No. H0220080

Contract Period: July 1, 1972 - March 31, 1974
Amount of Contract: $46,410

ACKNOWLEDGEMENTS

This research was supported by the Advanced Research Projects Agency of the Department of Defense and was monitored by the Bureau of Mines under Contract No. H0220080.

Most of the experimental work was carried out by Mr. J.M. Avasthi, graduate research assistant. Considerable assistance in rock preparation and mechanical property testing was given by Messrs. C.M. Kim, J. Edl, K. Kim and V. Rajaram.

Star mine generously supplied rock blocks for laboratory testing.

Mr. T.O. Meyer, contract technical officer, provided substantial support with logistic and technical details.

TABLE OF CONTENTS

ACKNOWLEDGEMENTS	ii
SUMMARY	iv
LIST OF FIGURES	vii
LIST OF TABLES	xi
INTRODUCTION	1
PREVIOUS STUDIES	2
THEORY	7
RESEARCH PROGRAM	15
ROCK, LABORATORY EQUIPMENT, AND EXPERIMENTAL PROCEDURES	16
Coeur d'Alene Mining District	16
The Star Mine	17
Rock Type	17
Specimen Repraration	17
Apparatus	20
MECHANICAL PROPERTIES OF REVETT QUARTZITE	34
Dynamic Properties	35
Uniaxial Compression	37
Uniaxial Tension	52
Triaxial Compression	60
Jacketed and Unjacketed Compressibilities	60
HYDRAULIC FRACTURING	64
Equal Horizontal Stresses	64
Unequal Horizontal Stresses	80
CONCLUSIONS	96
REFERENCES	99

SUMMARY

An extensive laboratory investigation has been undertaken to establish the applicability of hydraulic fracturing as a method of in-situ stress measurement around underground excavations in inhomogeneous, anisotropic, prefractured rock subjected to high compressive stresses. In particular, the applicability of the method to the Coeur d'Alene Revett quartzite has been studied. The laboratory study consisted of hydraulic fracturing tests under simulated field conditions in rock from selected sites in the Star mine where conditions such as discing could be expected to preclude stress measurement by overcoring methods. The specific objectives of the study were to determine the validity of current hydraulic fracturing theory with respect to the tested rock and to make recommendations regarding continuation of the study in-situ.

Hydraulic fracturing (hydrofracturing) is a relatively simple method of estimating in-situ stresses, which makes use of instruments and parts that are commercially readily available for rent or purchase. It consists of sealing-off a section of a borehole at the location of interest by means of two rubber packers, and pressurizing the packed-off segment by pumping in a fluid. At a certain critical pressure (called "breakdown pressure") a fracture occurs, which can be extended indefinitely by continuous pumping. Where pumping is stopped the 'shut-in' pressure necessary to keep the fracture open is recorded. The breakdown and the shut-in pressure can be related to the acting in-situ stresses. An impression packer is used after the pressurizing test to determine the exact direction and inclination of the hydraulic fracture, which in turn yields the direction of the smallest principal stress. In this manner the complete state of stress can often be evaluated. Most of the theoretical, laboratory and field work experience, however, had been with isotropic intact rock, and the reaction of a material

like the Coeur d'Alene quartzite was unknown and unpredictable.

The reported experimental program was a three prong effort. The basic mechanical properties of Revett quartzite from three different levels in the Star mine, Idaho (6100 ft, 7500 ft and 7700 ft levels) were determined, the response of same rock to hydraulic fracturing pressures under equal horizontal stresses was studied, and the effect of the most general state of stress on fracture initiation and direction was established.

The mechanical property testing has shown that the rock is inhomogeneous and possibly anisotropic with physical property variations depending on fabric changes and existence and extent of fractures. This implies that the characteristics of the rock at each stress measuring site will have to be determined separately for maximum accuracy. However, this is not strictly necessary since average variations are not exceedingly high.

The hydrofracturing testing has shown that the frequently visible bedding planes have no effect on the breakdown pressures. Existing cracks that do not cross the borehole do not appear to effect hydrofracturing results. In those cases where existing cracks do cross the pressurized borehole a lining of plaster of paris provides a good seal for the fracturing fluid and resulting hydrofracturing pressures are unaffected by rock condition. In all tested specimens the relationship between the breakdown pressure and the tangential stress at the borehole could be approximated by a straight line. This line, as well as the great majority of the experimental points, were bounded above by the expected pressure-stress relationship as predicted by theory for a perfectly impermeable rock, and by the similar expected relationship for permeable rock below. The scatter of fracturing pressure results, although not insignificant, was seldom in excess of $\pm$ 15% from the linear approximation in the range of horizontal stresses anticipated in the deep levels of the Coeur d'Alene mines.

All the hydraulic fractures initiated and extended vertically in a direction perpendicular to the minimum horizontal in-situ stress. Only when the difference between the two horizontal principal stresses was 100 psi or less was the vertical hydrofracture direction at random. Existing cracks, joints, partings, bedding planes did not affect fracture initiation direction which remained completely controlled by the horizontal principal stresses even under most severe conditions. Away from the hole hydrofractures would either cross existing discontinuities or join them, depending on local conditions.

The major conclusion of the investigation is that the Revett quartzite, in spite of some unusual mechanical behavior and excessive inhomogeneity, is basically amenable to hydraulic fracturing stress measurements without modifying the present theory. The quartzite reaction to hydraulic fracturing is sufficiently consistent to warrant field testing notwithstanding the rock inherent imperfections and discontinuities. Hydraulic fracturing could become the only reliable stress measuring method in the Coeur d'Alene mines because of its simplicity and relative insensitivity to deviations from idealized rock conditions.

LIST OF FIGURES

Fig. 1 (a) Vertical cross-section of a hydrofracturing specimen.

(b) Vertical cross-section of a prefractured hydrofracturing specimen treated with plaster of paris.

Fig. 2 Vertical cross-section of a hydrofracturing specimen with inclined hole.

Fig. 3 Vertical cross-section of the triaxial cell.

Fig. 4 Hydraulic circuit for hydrofracturing testing in the triaxial cell.

Fig. 5 General view of the hydrofracturing testing system using the triaxial cell.

Fig. 6 Triaxial cell, top nut and specimen attached to top and bottom platens.

Fig. 7 Horizontal and vertical cross-section (without pistons) of the polyaxial cell.

Fig. 8 Hydraulic circuit for hydrofracturing testing in the polyaxial cell.

Fig. 9 Block diagram of loading systems and recordings in polyaxial cell testing.

Fig. 10 General view of the hydrofracturing testing system using the polyaxial cell.

Fig. 11 Polyaxial cell with specimen in place

Fig. 12 Typical pressure-time plot during a hydrofracturing test in the polyaxial cell.

Fig. 13 Acoustic bench used for the determination of dynamic properties.

Fig. 14 Loading machine used for the determination of static properties.

Fig. 15 Typical recording of linear stress-axial strain curve and the corresponding stress-lateral strain.

Fig. 16 Typical recording of nonlinear stress-axial strain curve. Such curves can often be approximated by two straight lines (bilinear).

Fig. 17 Recorded stress-lateral strain curve corresponding to the plot in Fig. 16. Note the positive strain (contraction) in the first 12, 000 psi of loading.

Fig. 18 Typical stress-strain curves representing groups I and II.

Fig. 19 Calculated stress-volumetric strain curves corresponding to plots in Fig. 18.

Fig. 20 Variation of Poisson's Ratio with stress in selected typical specimens of groups I and II.

Fig. 21 Typical recording of stress-axial strain curve in uniaxial tension.

Fig. 22 Typical recording of stress-lateral strain curve in uniaxial tension (corresponding to Fig. 21).

Fig. 23 Variation of Biot coefficient with pressure in Revett quartzite.

Fig. 24 Breakdown pressure results as a function of tangential stress (cylindrical specimens, first shipment).

Fig. 25 Breakdown pressure results as a function of tangential stress (cylindrical specimens, second shipment).

Fig. 26 Vertical hydrofracture crossed preexisting inclined crack.

Fig. 27 Vertical hydrofracture (H_f) was unaffected by preexisting vertical crack, but was stopped from extending downward by horizontal crack.

Fig. 28 Breakdown pressure results as a function of tangential stress (cylindrical specimens, third shipment).

Fig. 29 Plaster of paris lining resulted in a vertical hydrofracture (H_f) unaffected by preexisting inclined crack running through the borehole.

Fig. 30 Typical vertical hydrofracture in an inclined borehole.

Fig. 31 Breakdown pressure as a function of tangential stress (all cylindrical specimens combined).

Fig. 32 Breakdown pressures as a function of tangential stress (cylindrical specimens with inclined holes, second and third shipments).

Fig. 33 Breakdown pressure as a function of tangential stress (prismatic specimens, third shipment).

Fig. 34 Breakdown pressure as a function of tangential stress (prismatic specimens, fourth shipment, block 12).

Fig. 35 Breakdown pressure as a function of tangential stress (prismatic specimens, fourth shipment, block 14).

Fig. 36 Vertical hydrofracture at random direction, as expected when $\sigma_x \cong \sigma_y$.

Fig. 37 Typical vertical hydrofracture perpendicular to the smallest horizontal stress (intact specimen with $\sigma_x \neq \sigma_y$).

Fig. 38 Vertical hydrofracture (H_f) crossed preexisting inclined discontinuity and maintained its expected direction.

Fig. 39 Vertical hydrofracture (H_f) crossed preexisting inclined fracture and maintained its expected direction.

Fig. 40 Vertical hydrofracture (H_f) developed in its expected direction joined preexisting fracture. Fracturing hole lined with plaster of paris.

Fig. 41 The presence of a preexisting crack at the hole did not affect the initiation and direction of the hydrofracture, probably because of the plaster of paris lining. Away from the hole the hydrofracture joined the inclined crack.

Fig. 42 Vertical hydrofracture in the expected direction, unaffected by preexisting inclined fracture.

Fig. 43 Horizontal section of the specimen shown in Fig. 42.

Fig. 44 Vertical section of a specimen traversed by preexisting fractures including two horizontal cracks cutting through the hole. With the help of plaster lining the hydrofracture obtained was unaffected by discontinuities.

Fig. 45 Vertically sectioned specimen showing preexisting cracks and bands cutting into the hole. The hydrofracture, initiated through a plaster lining, was controlled only by the principal stress directions.

Fig. 46 A pennsylvanian slate specimen with thin beds dipping at 30° yielded a hydrofracture controlled only by the direction of the smallest horizontal stress. Hole was lined with plaster of paris.

Fig. 47 A pennsylvanian slate specimen with t in beds dipping at 60° yielded a hydrofracture controlled only by the direction of the smallest horizontal stress. Hole was lined with plaster of paris.

LIST OF TABLES

Table 1. Longitudinal velocity results

Table 2. Uniaxial compression results
First shipment - x, y, z directions

Table 3. Uniaxial compression results
First shipment - different bedding inclinations

Table 4. Uniaxial compression results
Second shipment

Table 5. Uniaxial compression results
Third shipment

Table 6. Uniaxial compression results
Fourth shipment

Table 7. Uniaxial compression results
Comparison

Table 8. Uniaxial tension results
First shipment

Table 9. Uniaxial tension results
Second shipment

Table 10. Uniaxial tension results
Third shipment

Table 11. Uniaxial tension results
Fourth shipment

Table 12. Uniaxial tension results
Comparison

Table 13. Hydraulic fracturing results
First shipment

Table 14. Hydraulic fracturing results
Second shipment

Table 15. Hydraulic fracturing results
Third shipment

Table 16. Hydraulic fracturing results
Inclined holes-second and third shipments

LIST OF TABLES (Continued)

Table 17. Hydraulic fracturing results
Third shipment - prismatic specimens

Table 18. Hydraulic fracturing results
Fourth shipment - prismatic specimens (block 12)

Table 19. Hydraulic fracturing results
Fourth shipment - prismatic specimens (block 14)

INTRODUCTION

This report summarizes the work performed under Contract H0220080. The main objective of the program has been to investigate the applicability of hydrofracturing as a technique for measuring underground in-situ stresses in the Coeur d'Alene mines.

The major characteristic of the tested Coeur d'Alene Revett quartzite is that it is highly fractured, inhomogeneous, possibly anisotropic, and subjected to very high in-situ stresses. As a result, extreme difficulties have been encountered in using overcoring stress measuring techniques due to drilling problems, discing and erratic readings.

The research program as originally conceived was divided into two stages: a comprehensive laboratory investigation, followed by a field study in which the laboratory recommendation would be used to determine the in-situ stresses. Due to budget restrictions the field testing could not be undertaken in the first year of the contract. The second year of the contract did not materialize because of the discontinuation of the ARPA-USBM program. This report, therefore, presents the results of a laboratory study of simulated hydrofracturing in Revett quartzite and makes recommendations regarding the feasibility of successful use of the method in the Coeur d'Alene mines.

PREVIOUS STUDIES

The state of stress in underground formations has always been a subject of much interest to earth scientists. The problem of directly and indirectly measuring stress in the earth's crust has received considerable attention from rock mechanics researchers in recent years. Most of the techniques suggested for this purpose require delicate instrumentation to be installed in boreholes, with electrical connections to the point of access (surface or underground opening). The measurement is conducted by determining the state of deformation in the borehole before and after overcoring. The instrumentation as well as the method limit such techniques as "borehole deformation" or "door-stopper" to within a few tens of feet from the access point. At such distances the measurements, if conducted underground, could be affected by the vicinity of the mine openings and yield erroneous results. In addition, the calculation of the stresses requires knowledge of rock moduli, which are seldom easy to determine. In high-stress regions, discing occurs when overcoring the instrumented hole and measurements become extremely difficult.

Indeed, the history of stress measurements in the Coeur d'Alene mining district has not been too successful due to problems such as those indicated above. The local quartzite is highly variable, prefractured, and subjected to relatively high in-situ stresses. Chan (1972) reports that out of 42 overcoring runs he conducted in the Silver Summit mine using the Bureau of Mines borehole deformation gage only three were successfully carried out. Blake (1970) reports on previous measurements in the Galena mine where out of three overcoring holes at 4300 level only one reliable measurement was obtained. Ageton (1967) determined the vertical stress at the 6100 level of the Star mine using both the flatjack and the borehole deformation methods, but the tests were run at only two feet into the rib along a haulage drift,

much too close to be unaffected by the mine opening.

To overcome the apparent impracticality of overcoring techniques, the present research project is proposing to use the hydraulic fracturing (hydrofracturing) method of stress determination. This method has the advantage of not being limited by any particular distance between the operator and the measured spot, and does not require knowledge of rock moduli, nor does it necessitate overcoring. The hydrofracturing technique was designed by Clark (1948) for the purpose of oil well production stimulation. It consisted of sealing off a section of the well with rubber packers, pressurizing it hydraulically until rock fractures, and extending the artificial fracture by continuous fluid injection. The newly created parting, propped with sand or glass beads, provided a generous increase in the overall permeability of the oil bearing formation,almost invariably resulting in a production increase. During the 1950's, several attempts were made to correlate hydrofracturing results to in-situ or regional stresses. The most significant results were reported by Hubbert and Willis (1957), who assumed that the underground condition is one of unequal principal stresses and proceeded to develop the relationship between them and the hydrofracturing pressures and directions. They suggested that under the condition that one of the principal stresses is vertical and parallel to the wellbore axis, all hydrofractures are either vertical or horizontal tensile ruptures depending on the pressure required to extend the fracture (P_f). Their theory, based on linear elasticity, is still widely accepted today. However, a number of modifications have since been added.

Scheidegger (1962) introduced the rock tensile strength value in the pressure-stress relationships developed by Hubbert and Willis. He was probably the first to suggest that tectonic stresses could be estimated from results of hydraulic fracturing jobs.

Kehle (1964) made an analytical study of an open hole well model under hydrofracturing and determined the stress distribution at the wellbore walls in a finite packed-off region. Based upon his study, he determined different possible fracturing situations. He also concluded that rather than the fracture extension pressure (P_f), the instantaneous shut-in pressure (P_s) determines the magnitude of the minimum principal compressive stress.

Fairhurst (1964) should be credited with the idea of employing hydrofracturing as a stress measuring technique. He was the first to point out the advantages of the method over the instrumental ones and suggested using it in underground excavations by fracturing holes drilled from tunnels into the undisturbed zones of the formation. He also pointed out the theoretical difficulties of estimating stresses in anisotropic rock.

Haimson (1968) and Haimson and Fairhurst (1967, 1970) modified the theoretical pressure-stress relationships by incorporating the effect of fracturing fluid penetration into the rock during the pressurization of the hole. Such effect was shown to be significant and extensive laboratory tests under simulated conditions of three unequal principal stresses yielded results that confirmed the theoretical expectation. Results (Haimson and Stahl, 1969, Haimson, 1974) from three hydrofracturing jobs in different oil fields clearly indicated the close relationship between recorded pressures and fracture directions and the regional stresses.

von Schonfeldt (1970) tested the method in a quarry and a few underground sites and obtained a number of significant results. He reported that an increase in the magnitude of measured stresses was recorded as the face of an opening was approached from inside the rock. This observation is quite in agreement with the predicted state of stress around openings. Another convincing feature which he observed during his field study was the occurrence of horizontal fractures in horizontal holes drilled in areas of high lateral stresses, further evidence that hydraulic fractures extend in a direction perpendicular to the least compressive stress. Based upon these

observations and field experiment results, he found the method suitable for the determination of in-situ stress fields provided the rupture strength of the rock is known. Dahl and Parsons (1971) used hydrofracturing successfully in a coal mine in West Virginia. Haimson (1973) conducted the deepest stress measurement ever undertaken from the surface. The stresses were required in connection with a field experiment undertaken by the U.S. Geological Survey at Rangely, Colorado to determine the pore pressure effect on triggering of earthquakes (Raleigh et al, 1972). Knowledge of the local stress configuration was needed to confirm the type and direction of movement along an existing fault, establish the critical pore pressure necessary to induce slip along the fault, and provide a basis for critical pore pressure estimates in future research of earthquake control. The hydrofracturing test was conducted in a newly drilled oil well at 6,300 ft. below surface. The in-situ stresses as determined by the method were in accord with the expected condition for the type and the slip direction of the fault. The calculated critical pore pressure was within 10% of the actual pressure as monitored during the period of earthquake activity. Roegiers and Fairhurst (1973) have recently recommended that the impression and the fracturing packers be interconnected and lowered together into the hole, thus eliminating extra "trips" and bringing down the costs. They tested their idea in a quarry in Texas and determined the stresses at about 1,000 ft. below surface.

The success of hydrofracturing field measurements encouraged different groups and agencies to use the method for stress determination and other purposes. The Los Alamos Scientific Laboratory has been testing hydrofracturing primarily for dry-rock geothermal energy extraction but also for stress determination (Smith, 1973); the U.S. Geological Survey has been measuring the stresses in northwestern Colorado (Bredehoeft, 1973); Sandia Corporation is preparing to use the method for coal gasification (Sandia Laboratories, 1973), Defense Nuclear Agency has recently determined successfully the stresses near tunnel U12n, Nevada Test Site (Haimson et al, 1974).

The research on the applicability of hydraulic fracturing to measuring in-situ stresses is far from complete. Currently, at the University of Wisconsin, there are three major hydrofracturing research studies underway:

1) The effect of very high stresses and high temperatures on hydrofracturing results.
2) The effect of anisotropy due to weak bedding plane inclination on hydrofracturing results.
3) The effect of inhomogeneity and preexisting cracks on hydrofracturing results.

The latter study is part of the program communicated in this report.

THEORY

The theory of hydraulic fracturing that has withstood the scrutiny of laboratory and field testing is that applied to a brittle, isotropic, linearly elastic rock. It is well known that no rock possesses any of these ideal characteristics but in the whole it has become apparent that in average rock types these assumptions do not usually lead to erroneous results in hydraulic fracturing.

When employing the hydraulic fracturing method from the surface of the earth, vertical holes (either oil or water wells or specially drilled boreholes) are used whose axis is considered parallel to one of the principal stresses. In underground tests, boreholes could be drilled in all directions. It is extremely beneficial, however, if the directions chosen are those approximately parallel to one of the principal stresses. The sequence recommended for underground hydrofracturing is detailed later in this chapter. The theory developed here is based on the assumption that one of the tectonic principal stresses (S_{33}) acts in the borehole axial direction. The other two (S_{11}, S_{22}) are in a plane normal to the borehole.

When a borehole is introduced, the tectonic stresses redistribute themselves around the cylindrical cavity according to Kirsch's solution (Timoshenko and Goodier, 1951). With the pressurization of the borehole at the required distance, two additional stress fields arise. One is due to the pressure P_w at the borehole wall which can be viewed as an internal pressure acting on a hollow infinitely thick cylinder. The other stress field is introduced if the fracturing fluid used to pressurize the borehole actually penetrates the formation and flows through its pores. Its stress distribution can be determined by using Nowacki's (1962) solution to thermal inclusions in hollow infinite cylinders and utilizing the analogy between thermoelasticity and porous elasticity (Biot, 1956).

The complete stress distribution around the borehole is obtained by superposing the three stress fields mentioned above. At the borehole wall and away from the ends of the pressurized interval, the superposed principal stresses are (compression is taken as positive)

$$S_{rr} = +P_w$$

$$S_{\theta\theta} = S_{11} + S_{22} - 2(S_{11} - S_{22}) \cos 2\theta - P_w + \alpha \frac{1-2\nu}{1-\nu} (P_w - P_o)$$

$$S_{zz} = S_{33} - 2\nu (S_{11} - S_{22}) \cos 2\theta + \alpha \frac{1-2\nu}{1-\nu} (P_w - P_o) \qquad (1)$$

where

S_{rr}, $S_{\theta\theta}$, S_{zz} are the radial, tangential and axial stresses, respectively.

P_o is the initial pore fluid pressure in the formation.

θ is the angle measured counterclockwise from the radius in the direction of S_{11}.

ν is Poisson's ratio of the rock.

α is the porous-elastic parameter of the rock as defined by Biot and Willis (1957). It's value is given by $\alpha = 1 - \frac{C_r}{C_b}$ and can be found in the laboratory. (C_r = material matrix compressibility, C_b = material bulk compressibility.)

Terzaghi (1943) and Hubbert & Rubey (1959) have found that failure of porous permeable rock is directly related to the distribution of "effective stresses" (σ_{ij}), where $\sigma_{ij} = \begin{matrix} S_{ij} - P \text{ for } i = j \\ S_{ij} \quad \text{for } i \neq j \end{matrix}$ (P is the pore fluid pressure). At the borehole wall, the pore pressure in permeable rock is P_w, while at a great distance from the borehole the pore pressure remains P_o. Hence, in terms of effective stresses, equation (1) becomes:

$$\sigma_{rr} + P_w = + P_w$$

$$\sigma_{\theta\theta} + P_w = \sigma_{11} + \sigma_{22} + 2P_o - 2(\sigma_{11} - \sigma_{22}) \cos 2\theta - P_w + \alpha \frac{1 - 2\nu}{1 - \nu}(P_w - P_o)$$

$$\sigma_{zz} + P_w = \sigma_{33} + P_o - 2\nu(\sigma_{11} - \sigma_{22}) \cos 2\theta + \alpha \frac{1 - 2\nu}{1 - \nu} (P_w - P_o) \qquad (2)$$

As P_w is gradually increased, both the tangential and the axial effective stresses at the borehole can eventually become tensile.

Axial Fractures

The points around the hole where the tangential effective stress is minimum are at $\theta = 0, \pi$ (assuming $S_{22} < S_{11}$). There, $\sigma_{\theta\theta}$ is given by:

$$\sigma_{\theta\theta} = 3\sigma_{22} - \sigma_{11} - (2 - \alpha \frac{1 - 2\nu}{1 - \nu})(P_w - P_o) \qquad (3)$$

An axial tensile fracture at $\theta = 0, \pi$ will occur when P_w reaches such a critical value (P_c^p) that the effective tangential stress (Eq. 3) becomes equal or larger than the hydrofrac tensile strength of the rock in the normal plane (T):

$$P_c^p - P_o = \frac{T + 3\sigma_{22} - \sigma_{11}}{2 - \alpha \frac{1 - 2\nu}{1 - \nu}} \qquad (4)$$

where P_c^p is the breakdown (critical) pressure in permeable rock. As $0 \leq \alpha \leq 1$ and $0 \leq \nu \leq 0.5$ for rock, it follows that:

$$1 \leq 2 - \alpha \frac{1 - 2\nu}{1 - \nu} \leq 2 \qquad (5)$$

If the rock parameters (T, ν, α) are known, Eq. (4) gives a direct relationship between the normal effective principal stresses and the recorded breakdown pressure. If it is assumed that $\sigma_{11} \cong \sigma_{22} (= \sigma_H)$:

$$P_c^p - P_o = \frac{T + 2\sigma_H}{2 - \alpha \frac{1 - 2\nu}{1 - \nu}} \qquad (6)$$

where the only unknown is σ_H, the hydrostatic normal effective stress.

In rock that is impermeable to the fracturing fluid, the pore pressure is P_o everywhere, and Eqs. (4) and (6) become (Haimson, 1968):

$$P_c^i - P_o = T + 3\sigma_{22} - \sigma_{11} \tag{7a}$$

$$P_c^i - P_o = T + 2\sigma_H \tag{7b}$$

where P_c^i is the breakdown (critical) pressure in the impermeable case. Equations (7) are identical to the axial fracturing criteria suggested by Scheidegger (1967).

Knowledge of only one rock parameter is required in this case. T should be measured in the laboratory on identical rock under conditions of simulated hydraulic fracturing in impervious formations. From Eqs. (7), T is then equal to P_c^i if $\sigma_{11} = \sigma_{22} = P_o = 0$. T can also be determined in the field.

Normal Fractures

From Eqs. (2), a criterion for normal fracturing away from the ends of the hole can also be established (6):

$$P_c^p - P_o = \frac{T^a + \sigma_{33}}{1 - \alpha \dfrac{1 - 2\nu}{1 - \nu}} \tag{8}$$

where T^a is the hydrofrac tensile strength of the rock in the axial direction. If the rock is impermeable to the fracturing fluid, P_o is the pore pressure everywhere and P_w does not influence the value of σ_{zz}; hence, no normal fracture initiation is possible in this case. However, normal fractures could be started if the borehole wall were precracked or prenotched.

Comparing Eqs. (6) and (8), it is apparent that a normal fracture in porous rock would be initiated if the average normal tectonic effective stress (σ_H) were much larger than σ_{33}. This is seldom the case in most formations.

Kehle (1964) has investigated the conditions of normal fracture initiation near the ends of the pressurized hole. His model included a finite pressurized interval between two solid packers which, under the pressure P_w, transmitted a shear load to the borehole wall. By incorporating in Kehle's solution an approximation of the stresses due to injected fluid flow into the formations, the criterion for normal fracturing near one of the hole ends becomes (Haimson, 1968):

$$P_c^p - P_o \simeq \frac{T^a + \sigma_{33}}{1.94 - \alpha\frac{1 - 2\nu}{1 - \nu}} \tag{9}$$

In the impermeable case, Eq. (9) reduces to Kehle's (1964) criterion:

$$P_c^i - P_o = \frac{T^a + \sigma_{33}}{0.94} \tag{10}$$

In all the above fracturing criteria, the breakdown (critical) pressure in the permeable case (P_c^p) is always lower than P_c^i for otherwise identical formations and tectonic conditions.

It should be noted that Kehle's model has some grave limitations. It assumes that a packer is a rigid cylinder in full contact with the borehole wall, which, in response to an axial load at one end, applies a shear stress to the rock. In many field applications, however, rubber packers are used. Rubber is a "liquid-solid" elastomer which under the axial load mentioned would probably apply a similar radial load to the rock. This would have a negative effect on the stress concentration in the vertical direction, and chances of horizontal fracturing would thus be minimized. Experimental results have verified this hypothesis (Haimson, 1968).

Fracture Extension

Once the fracture is initiated, additional pumping of fracturing fluid (at bottom-hole injection pressure P_f) will extend the rupture along the path of least resistance, i.e., perpendicular to the direction of the smallest compressive stress. When pumping is stopped with the borehole still sealed, the bottom-hole pressure will be indicative of the pressure in the fracture for no friction losses will exist. This "instantaneous shut-in pressure" (P_s) is equal to or slightly larger than the compressive stress that is perpendicular to the fracture plane. If P_s were smaller than the compressive

stress, the fracture would have stayed closed; if P_s were much larger than the compressive stress, the fracture would extend an additional amount until a balance was reached. In general, then:

$$P_f \geq P_s \geq S_{22} \qquad \text{(axial fractures)} \qquad (11a)$$

$$P_f \geq P_s \geq S_{33} \qquad \text{(normal fractures)} \qquad (11b)$$

A number of attempts have been made to establish accurate relationships between P_s or P_f and S_{22} or S_{33} in both porous and nonporous rocks (Haimson, 1968). All these relationships require knowledge of fracture dimensions which are not measurable as yet. When approximate values are used for width and length of the fracture, P_s is ordinarily within 200 psi larger than the smallest compressive stress. Since the determination of in-situ stresses at great depth is not expected to be extremely accurate, it can be approximated that P_s is roughly equal to the smallest compressive stress. If the value of P_s is not available, P_f can be used as a rougher estimate.

In summary, the magnitudes of P_o, P_c, P_f, P_s, which are recorded during a hydraulic fracturing test, provide the basic values from which tectonic stresses can be estimated. One remaining problem is the detection of fracture initiation and direction. At the borehole wall, techniques like the borehole televiewer or the oriented impression packer can accurately deter. ne fracture type and azimuth. But no method is yet available that can follow fracture orientation or direction away from the hole.

Stress Determination

When a formation is hydraulically fractured, a number of possibilities exist:

(a) The fracture is axial. In this case, Eqs. (11a) and (4) or (7a) can be used to uniquely determine S_{11} and S_{22}. The directions of

S_{11} and S_{22} can be found from oriented packer impressions. If the hole is vertical, S_{33} is generally accepted to be equal to the weight of the overlying rock (usually taken at 1 psi/ft of depth). If the underground conditions permit, an additional test in a horizontal hole drilled in the direction of S_{11} should yield the magnitude of S_{33} and confirm that of S_{22}.

(b) The fracture is normal. In this case only S_{33} can be determined, but it is also noted that S_{33} is then the smallest compressive stress. If the hole is vertical then S_{11} and S_{22} are in the horizontal plane. Three additional hydrofracturing in horizontal holes drilled at 45° or 60° from each other could then yield the magnitudes and directions of S_{11} and S_{22}.

This possibility is considered remote, because the experimental evidence shows that with rubber packers normal fractures in intact rock are almost never obtained. Possibility (c) appears more applicable to the case when S_{33} is the minimum principal stress.

(c) The fracture initiates axially but extends normally. This type of fracture can exist when the borehole wall is smooth and not precracked, and the packers used are such that no vertical stress concentration is allowed at the hole ends. Equation (6) or (7b) then provides an estimate of the normal principal in-situ stresses, and Eq. (11b) gives the value of S_{33} which is also the smallest compressive in-situ stress. Oriented packer impressions will determine the directions of S_{11} and S_{22}.

If the hole is vertical, only one additional test is required in a horizontal hole in the direction of S_{11} to uniquely yield all the principal stresses and their direction.

In conclusion, from a theoretical standpoint the determination of stresses underground by means of hydrofracturing should be started by testing a vertical hole. Depending on the results obtained, none, one or three

additional horizontal holes may be required to complete the test.

The purpose of the experimental program described in the following chapters was to verify the extent to which the theoretical analysis as described above can be applied to the Coeur d'Alene quartzite.

RESEARCH PROGRAM

The reported research program was an investigation of the applicability of hydraulic fracturing as a method of in-situ stress measurement in underground mines, with particular reference to rocks that may be anisotropic, nonhomogeneous, prefractured, and under high compressive stresses. These types of rocks are often encountered in the Coeur d'Alene mines. The major effort was a laboratory study of hydraulic fracturing under simulated field stress conditions comparable to those encountered in the deep mines of the area.

The program plan was divided into three phases. In Phase I, rock specimens were obtained from the Coeur d'Alene district, shipped and prepared in the rock mechanics laboratory of the University of Wisconsin-Madison. Phase II consisted of an extensive laboratory study, and in Phase III an analysis of the data obtained and recommendations for in-situ stress measurements were made.

Under Phase I, the original intent was to obtain rock cores from different underground sites in the Coeur d'Alene area. However, all attempts to extract intact cores from the Crescent mine were unsuccessful. Problems related to the high strength and hardness of the local quartzite, the excessive compressive stresses, the large core sizes (4 in. and 6 in. diameter), and the insufficient sturdiness and flexibility of the available drill apparently contributed to the extremely slow coring rate and the inability to extract sufficiently long cylinders ($\triangleright$ 8 in.). It was then decided to abandon the idea of coring and, instead, blocks of typical rock were obtained from blasting piles. Such blocks would, of course, be less representative of the virgin rock because they had been subjected to dynamic stresses due to blasting. It was felt, however, that careful selection would exclude badly damaged pieces and minimize blasting effects.

The rock used in the laboratory tests came in four different shipments from the Star mine. The first shipment contained two large blocks approximately 1x2x3 ft. from the 6100 level. The second and third shipments came in different size blocks from the two separate sites on the 7500 level. The fourth shipment consisted of nine large blocks taken from the 7700 level.

Phase II was divided into three stages:

1 - Determination of mechanical properties of rocks from the four shipments.

2 - Hydrofracturing simulation, using a triaxial cell (equal in-situ horizontal stresses).

3 - Hydrofracturing simulation, using a polyaxial cell (unequal in-situ principal stresses).

The purpose of Stage 1 was to determine the mechanical properties of the rock and verify the existence of any correlation between these properties and hydrofracturing results. The tests were also meant to show the amount of anisotropy and inhomogeneity in the quartzite and study the resulting effect on hydrofracturing. Stage 2 was conducted in rock from the first three shipments. Stage 3 was conducted in rock from the last two shipments. Both Stages 2 and 3 were carried out in two types of specimens, intact and naturally prefractured.

ROCK, LABORATORY EQUIPMENT, AND EXPERIMENTAL PROCEDURES

The Coeur d'Alene Mining District

The Coeur d'Alene mining district, one of the leading silver, lead and zinc producers, is in the Coeur d'Alene mountains of northern Idaho. The surface elevations range between 2,000 ft. above sea level for the lower valleys to 7,000 ft. for the higher peaks. The major bedrock is the Precambrian

metamorphosed sediments of the Belt supergroup which includes the Revett formation. The bedrock has undergone extensive folding, shearing, and faulting. The structural complex is dominated by the Osburn fault, which strikes west-northwest and is of the strike-slip type. The faults south of the Osburn fault tend to be parallel to it. Faults on the northern side strike in the north-south direction (Chan, 1972).

The Star Mine

The Star mine, Burke, Idaho is located in the Coeur d'Alene mining district and has the distinction of being perhaps the deepest lead-zinc mine in the world. The Star-Morning ore shoot is in a nearly vertical shear zone striking N79°W. The wall rock is exclusively hard brittle Revett quartzite (Ageton, 1967a).

Rock Type

The entire testing program was conducted on the Revett quartzite obtained from the Star mine, Idaho. The quartzite is fine to very fine grained consisting of about 75% quartz and 20% mica, varying in color from white to a light greenish or geyish tint. It is traversed frequently by closed fractures and milky white quartz veins, sometimes interspersed with mineralized particles.

Specimen Preparation

1. Hydrofracturing Specimens

Two types of specimens were prepared for hydrofracturing tests. The first was cylindrical in shape obtained by coring 4 in. diameter, 6 in. long cylinders out of the blocks received from the Star mine . These specimens were to be subjected to equal confining pressure in a triaxial cell. The second type was prismatic in shape having a square cross section (3.5 x 3.5 in.) and a 8.25 in. length. The prisms were to be loaded externally by a set of three unequal stresses.

The cylindrical specimens required coring (using 4 in. I.D. self-sharpening diamond bits), cutting the ends to size, and surface-grinding to yield parallel planes to within .005 in. The prismatic specimens were cored as cylinders using a 5 in. I.D. self-sharpening diamond bit. The two ends were cut using a cut-off diamond blade and surface-ground to yield parallel planes to within .005 in. The cylinders were then cut longitudinally along four perpendicular planes. These planes were surface-ground to obtain two pairs of parallel planes (within .005 in.) that were perpendicular to each other and also to the end planes. A 0.3 in. diameter hole was drilled axially in the center of one end to a depth of 4 in. in the cylindrical specimens, and 6 in. in the prismatic specimens. The prepared rock was oven dried at 150°F for three days.

The lower end of the axial hole served as the bottom seal of the pressurized interval. The upper seal was provided by a packer made of rod steel 1.5 in. long and 0.25 in. in diameter. The packer length was essential to ensure that the open hole section was sufficiently removed from the ends of the specimen. The packers were hollow to fit the piston attached to the upper platen of the triaxial or the polyaxial cells, and allow the fracturing fluid to enter the open hole section. The packers were cemented to the wall with a 3M epoxy adhesive (Scotch Weld). The epoxy was allowed to cure for 24 hours before the specimens were ready for hydraulic fracturing tests (see Fig. 1a).

In some of the specimens revealing preexisting fractures, central holes of 0.5 in. in diameter were first drilled. A mixture of plaster of paris and water was poured into the hole and allowed to cure. Then a 0.3 in. diameter hole was drilled concentrically inside the plaster and was packed-off in the same way as described earlier. This arrangement was an attempt to conceal the existing fractures from the pressurizing fluid, at least until breakdown (see Fig. 1b).

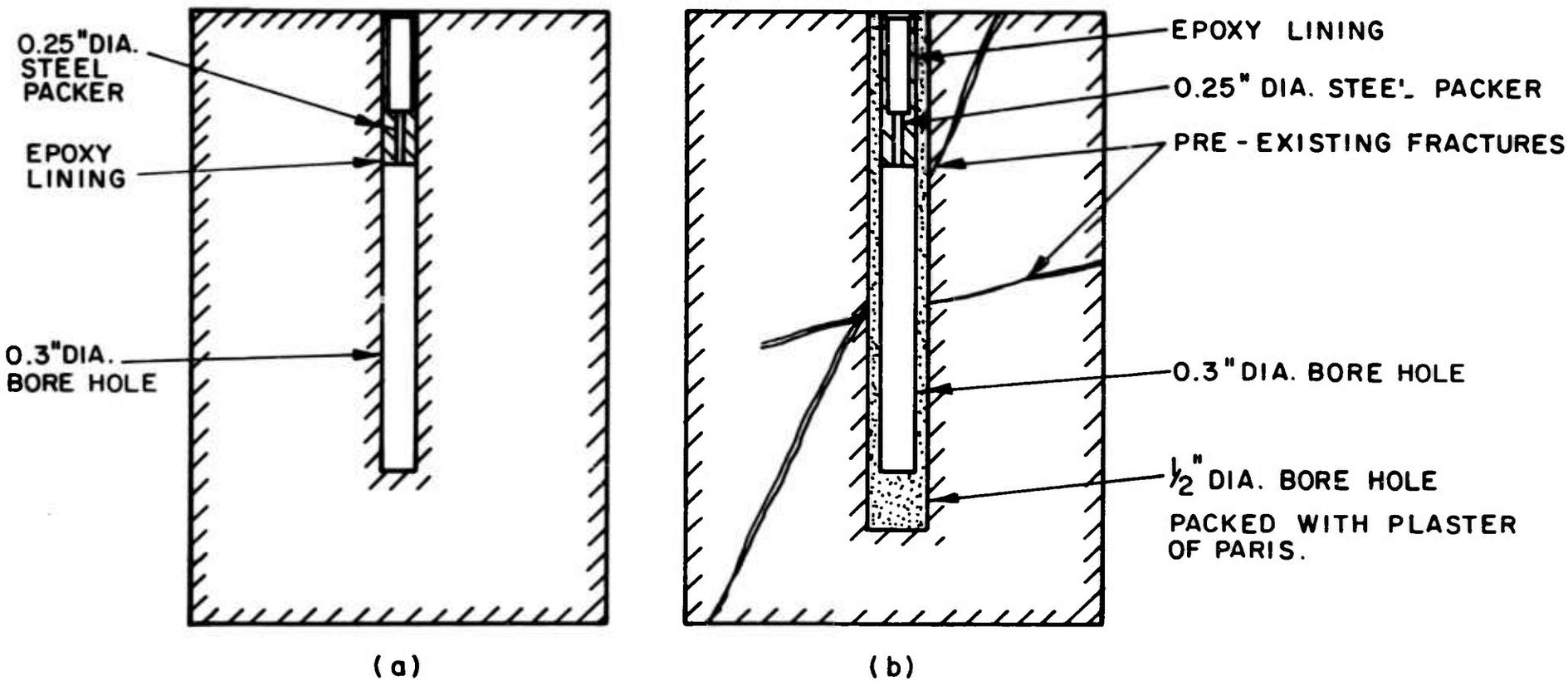

Fig. 1 (a) Vertical cross-section of a hydrofracturing specimen.
(b) Vertical cross-section of a prefractured hydrofracturing specimen treated with plaster of paris.

In a number of specimens, conditions were simulated under which the pressurized borehole was inclined with respect to any of the principal stresses. A 0.3 in. diameter hole was drilled such that it formed a 2.0 in. long segment in the center of the specimen at 30° with the vertical. An additional axial hole was drilled and allowed to communicate with the inclined hole. A hollow steel packer similar to the one described above, but longer, was cemented in the axial hole. A solid metal packer was cemented in the lower end of the inclined hole. The arrangement (Fig. 2) allowed for the pressurization of a centrally located inclined hole without making any equipment changes.

2. Mechanical Property Specimens

The specimens prepared for mechanical property determination were 1.0 in. in diameter and approximately 2.5 in. long. The ends of the specimens were ground flat and parallel to within 0.001 in. The prepared specimens were oven dried at 120°F for a week and thereafter exposed to room conditions for another week prior to testing.

Apparatus

1. Hydraulic Fracturing

a - Triaxial Cell - It can accommodate 4 in. diameter 6.0 ($\pm$ 0.5) in. long rock specimens and can be safely used up to 30,000 psi confining pressure. The cell also enables the pressurization of the simulated hydraulic fracturing borehole in the center of the specimen. Fig. 3 shows a vertical cross section of the triaxial cell.

Insertion and removal of specimens from the cell were easily accomplished. A specimen was first put between the upper and lower platens and a polyolefin tubing was shrunk over using a heat gun. A 3/8 in. band steel and earlocks were utilized to clamp the shrunk jacket over the steel end caps. The whole assembly was lowered into the cylinder and locked with a nut shown on top at the cell in Fig. 3.

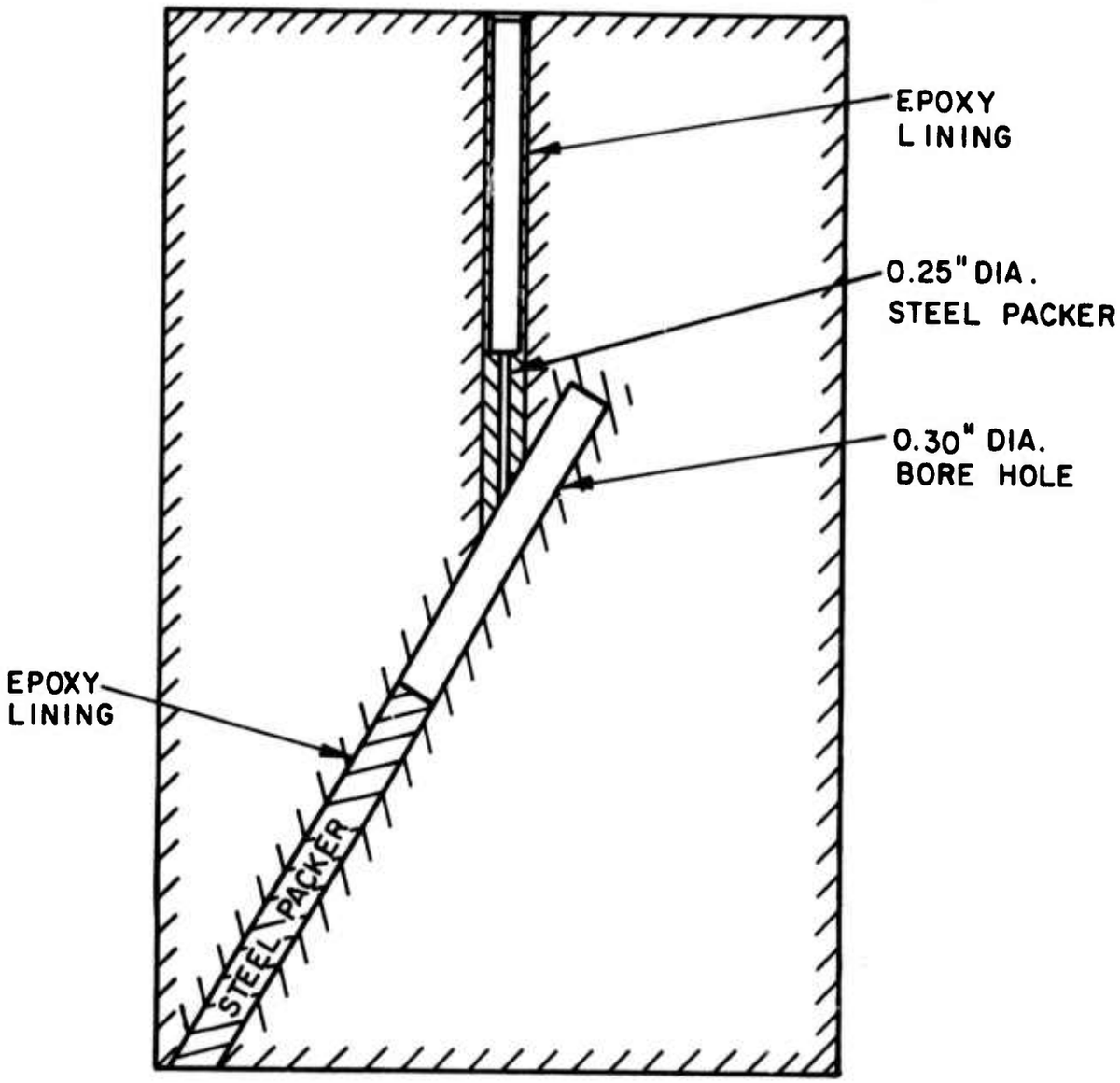

Fig. 2 Vertical cross-section of a hydrofracturing specimen with inclined hole.

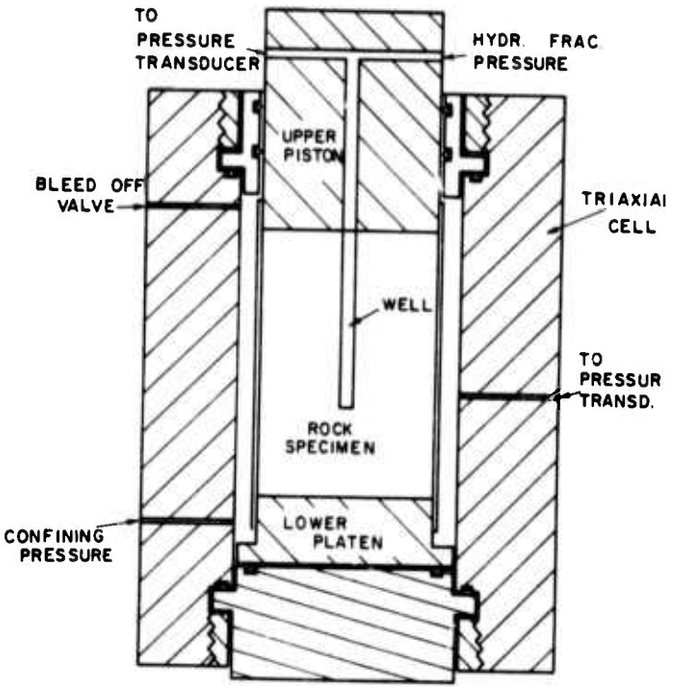

Fig. 3 Vertical cross-section of the triaxial cell.

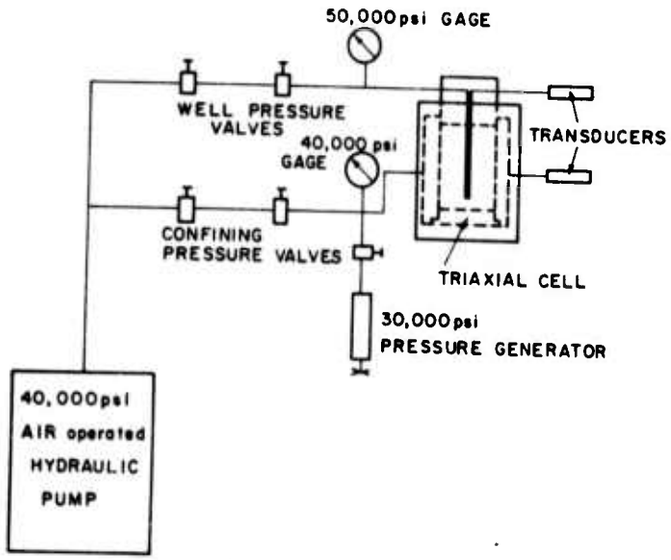

Fig. 4 Hydraulic circuit for hydrofracturing testing in the triaxial cell.

Vertical loading was supplied by a 400,000 lb. Tinius Olsen compression tester. The confining and hydrofracturing pressures were provided by a 40,000 psi air-operated hydraulic pump (Fig. 4). The vertical stress, confining and fracturing pressures were all monitored by pressure transducers and recorded on time-base plotters. The pressures could also be read on pressure gages mounted on the front panel of the air pump. A general view of the complete set-up is shown in Fig. 5. A photograph of the triaxial cell and a specimen mounted between the two platens is shown in Fig. 6. The vertical, confining and fracturing pressures were raised simultaneously so as to prevent the build-up of excessive stresses in the specimens. The vertical pressure was held constant during the fracturing test by controlling the valve of the loading machine pump. When the lateral pressure reached its designated value, its control valve was closed and the air pump was used solely to increase the borehole pressure (Fig. 4). This pressure was raised at an average of 50-100 psi/sec until breakdown occurred. For unloading, the pressures were again reduced simultaneously to prevent additional failure of the rock. The specimen was then removed, sectioned, and photographed.

b - Polyaxial Cell - It can accomodate specimens up to 4.25 x 4.25 in. in cross section and 8.25 in. long. It has four independently actuated pistons for the application of two unequal lateral loads to a prismatic specimen. The pistons are round inside of the cell to facilitate proper fitting and O-ring sealing, but are rectangular outside (4 in. x 8 in.). Pressures up to 30,000 psi can be applied in each of the four pressure chambers inside of the cell. These pressures produce loads of up to 20,000 psi on the specimens. Plan and vertical cross sections of the polyaxial cell are shown in Fig. 7.

Specimens were placed into the cell in a position equidistant from the four pistons in their retracted position. Between the pistons and the specimen sides flatjacks filled with a layer of lead were inserted in order to reduce friction and uneven loading. The cell sat permanently on the lower platen of a 500,000 lbs. loading machine. The locally built loading frame, actuated

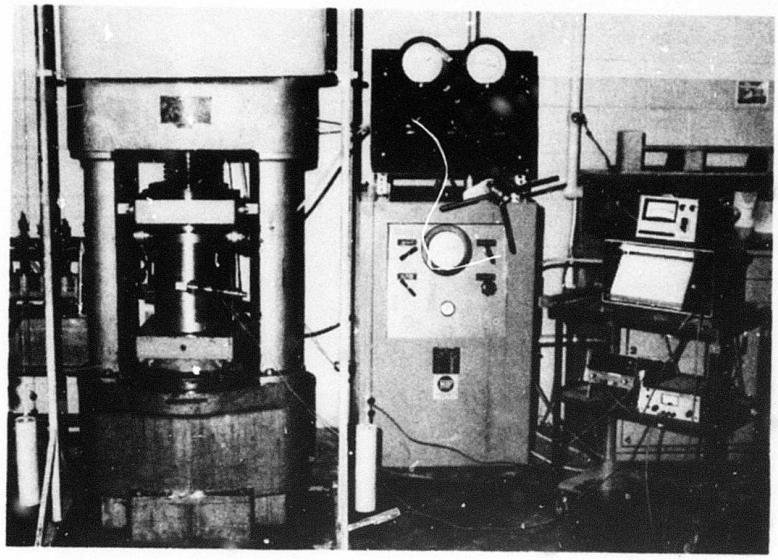

Fig. 5 General view of the hydrofracturing testing system using the triaxial cell.

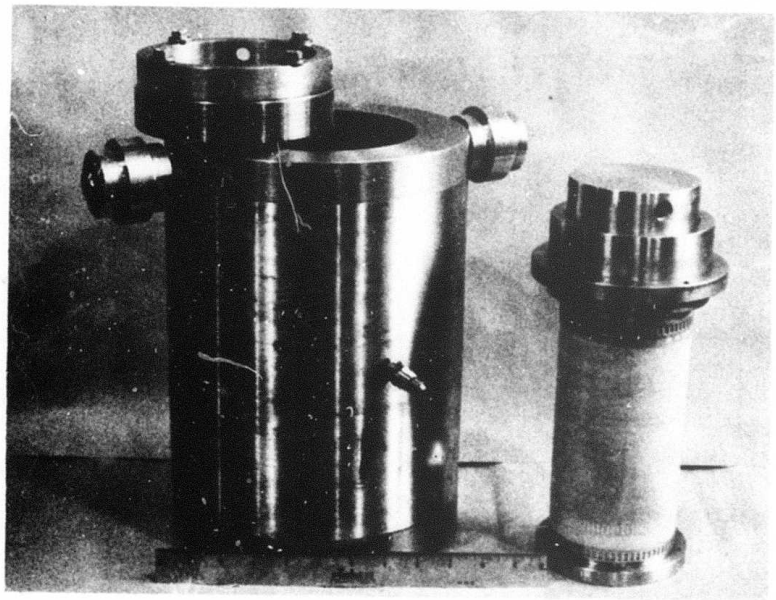

Fig. 6 Triaxial cell, top nut and specimen attached to top and bottom platens.

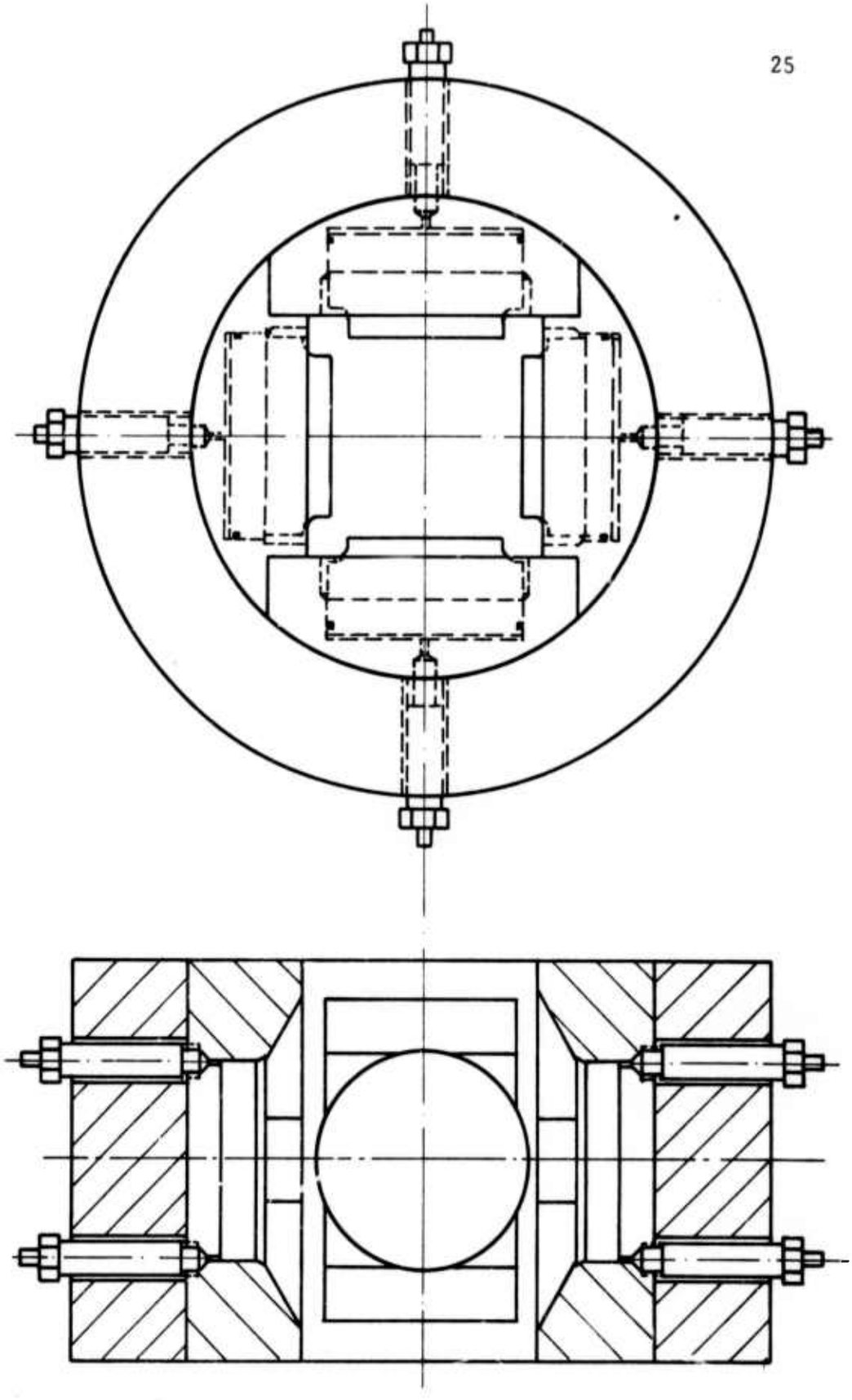

Fig. 7 Horizontal and vertical cross-section (without pistons) of the polyaxial cell.

electro-hydraulically by a servo-controlled unit, applied the external vertical load to the specimen. The external horizontal loads were applied through the polyaxial cell by simultaneously pressurizing opposite pairs of pistons. This was achieved through a 40,000 psi hand pump, in parallel with a precision 30,000 psi pressure generator, and a series of two- and three-way valves as shown in Fig. 8. Borehole pressure for hydrofracturing tests was supplied by a 20,000 psi servo-controlled pressure intensifier, which was programmable and thus ensured that conditions were kept consistent from one test to the next. A block diagram shown in Fig. 9 schematically describes the different loadings applied in each test. The pressures were also permanently recorded on time-base recorders. A general view of the testing system for prismatic specimens and a close-up of the polyaxial cell are shown in Figs. 10 and 11.

Testing procedure was as follows: The three outside loads were first applied simultaneously until the predetermined value of σ_x (designated in these tests as the smallest principal horizontal stress) was reached. At that point the appropriate valve was shut and pressures were raised only in the y and v (vertical) directions until they reached their predetermined magnitudes. The three outside loads (σ_x, σ_y, σ_v) simulating the three principal stresses in the rock were kept constant for the rest of the test. The borehole pressure was then raised at the desired rate by selecting the appropriate ramp function in the function generator. When the critical borehole pressure was reached fracture occurred and the borehole pressure declined suddenly (Fig. 12). The test was then stopped and all the outside loadings removed. The specimen was subsequently removed and observations regarding the type of fracture were made and recorded. Sections of the specimens were photographed for further analysis.

2. Property Determination

Dynamic Properties - An acoustic bench (Fig. 13) was used for the measurement of the dynamic elastic properties. A similar instrument has been described in detail by Thill et al (1968). It consists of a lathe bed with two matching traveling stocks. Each stock supports a transducer holder and enables it to come

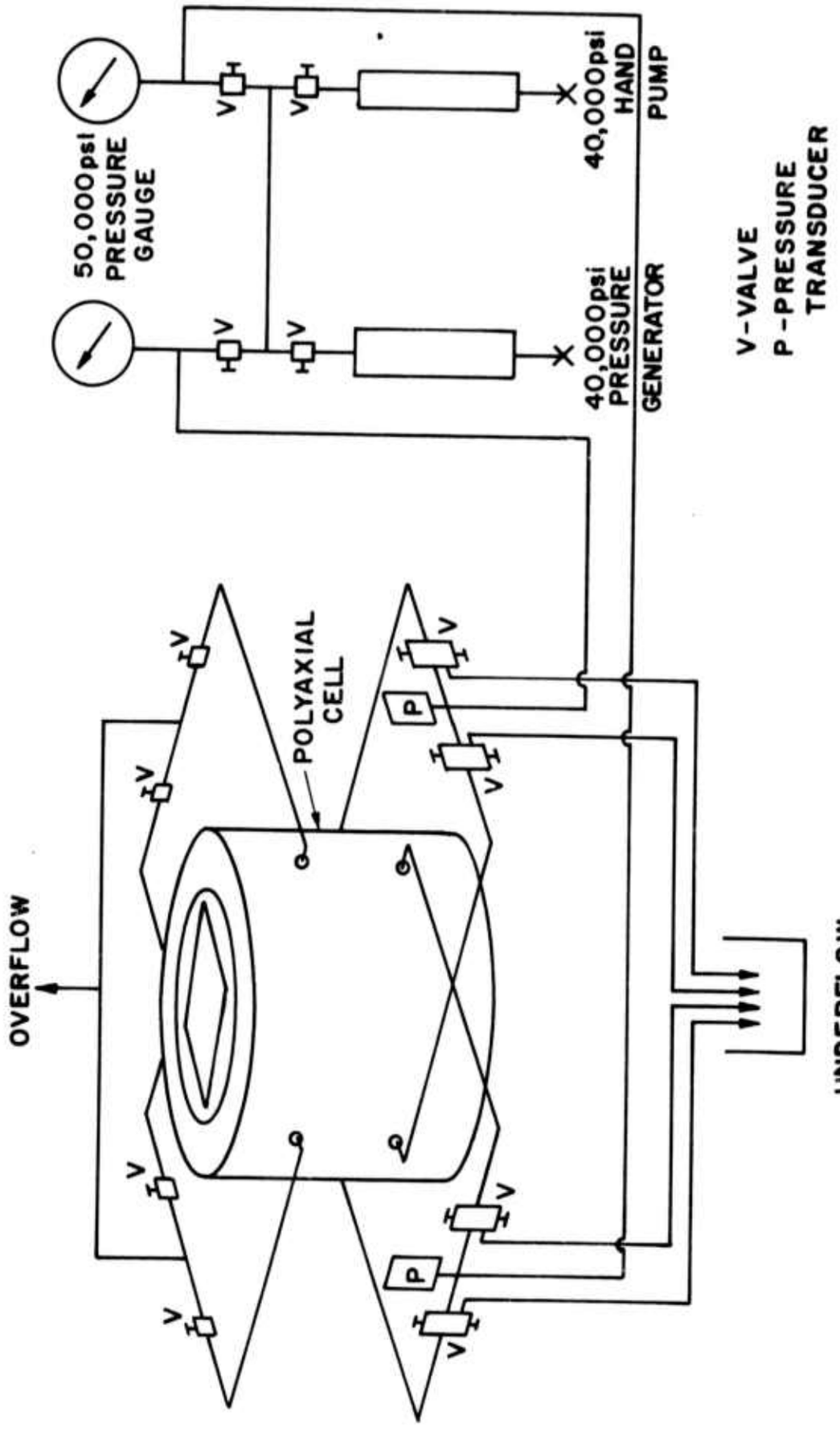

Fig. 8 Hydraulic circuit for hydrofracturing testing in the polyaxial cell.

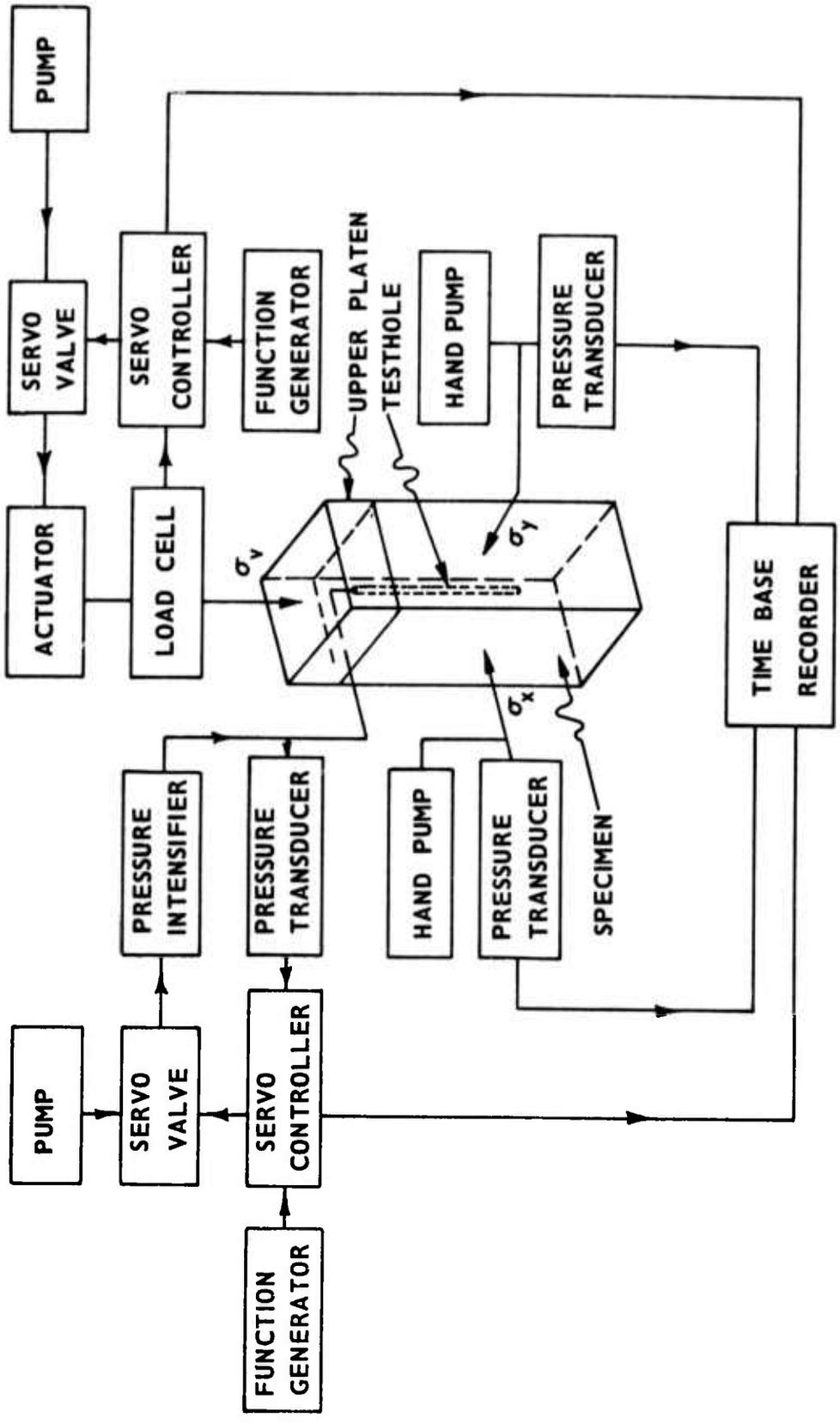

Fig. 9 Block diagram of loading systems and recordings in polyaxial cell testing.

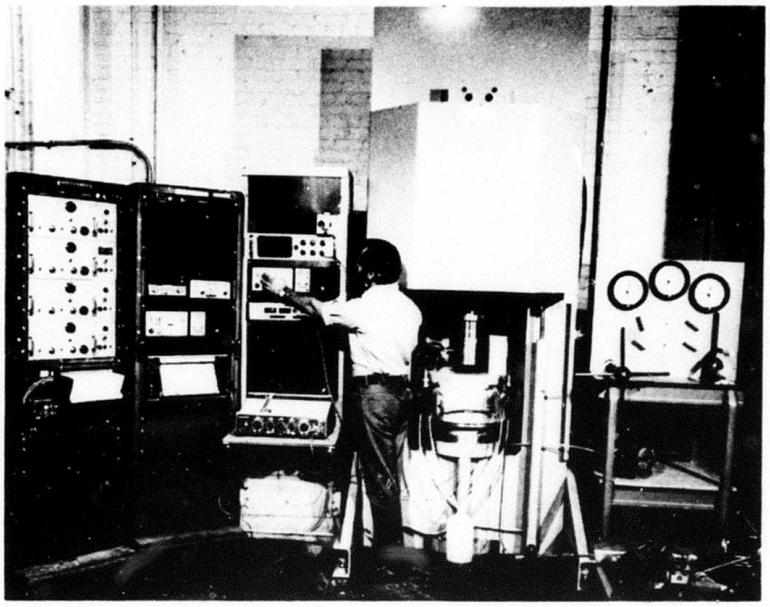

Fig. 10 General view of the hydrofracturing test system using the polyaxial cell.

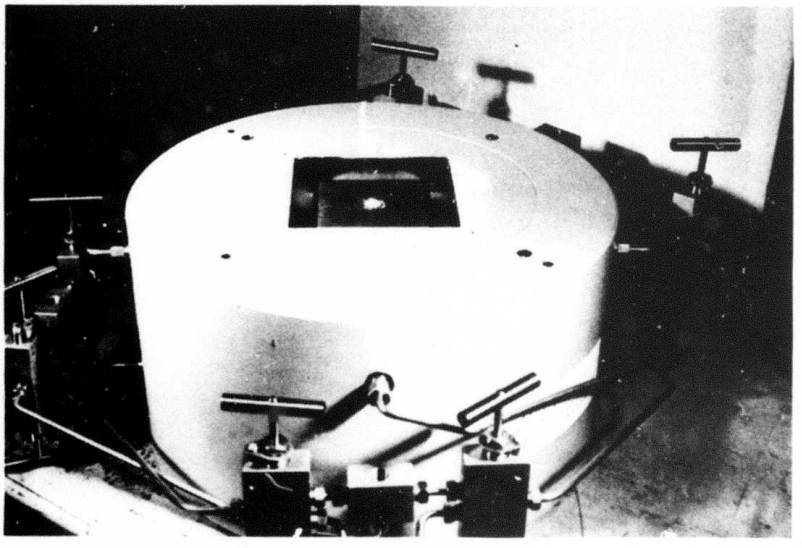

Fig. 11 Polyaxial cell with specimen in place.

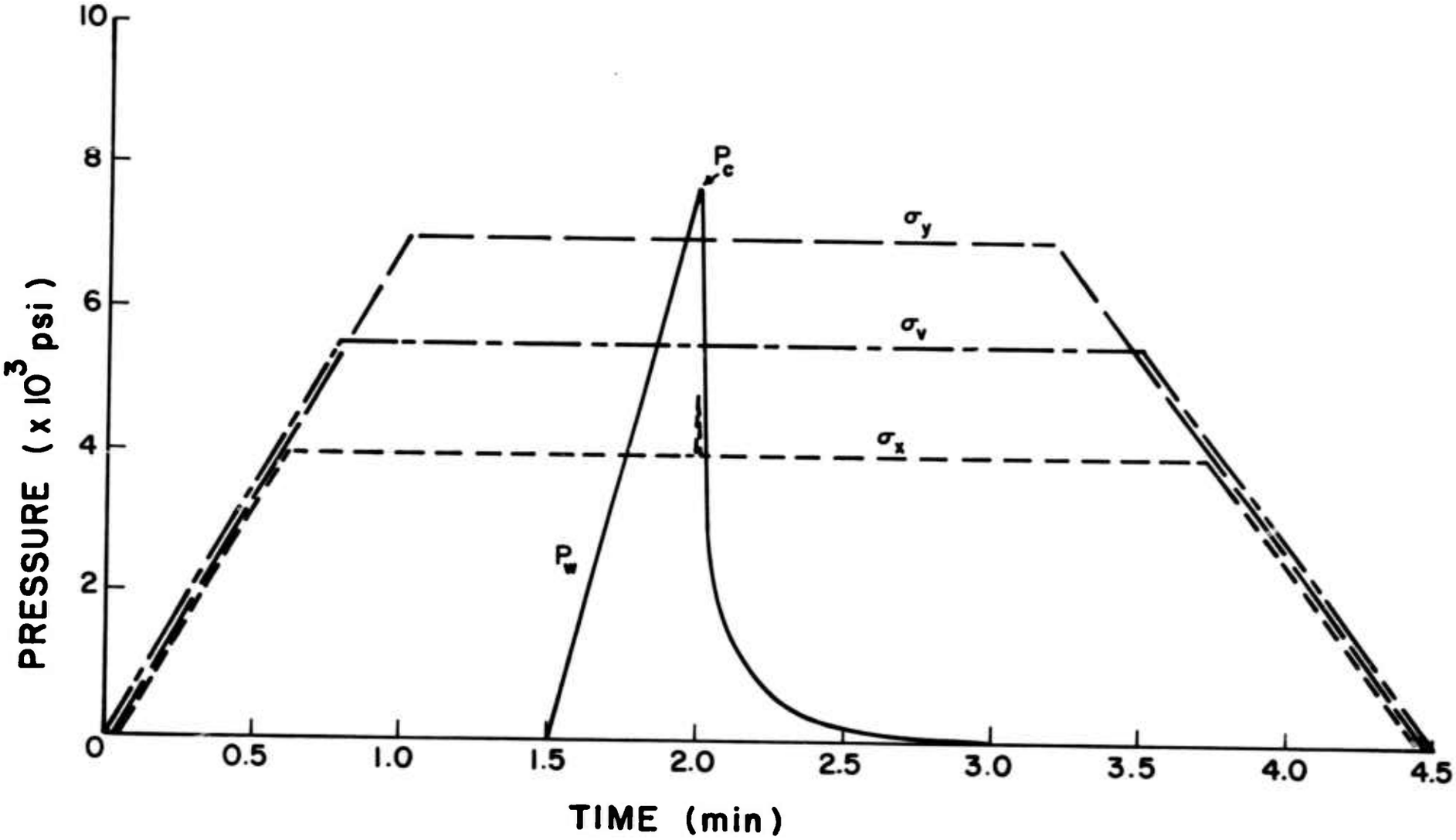

Fig. 12 Typical pressure-time plot during a hydrofracturing test in the polyaxial cell.

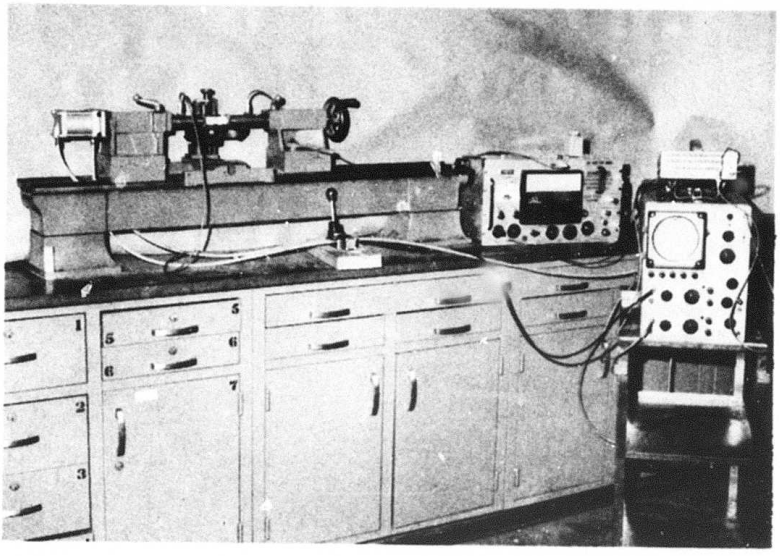

Fig. 13 Acoustic bench used for the determination of dynamic properties.

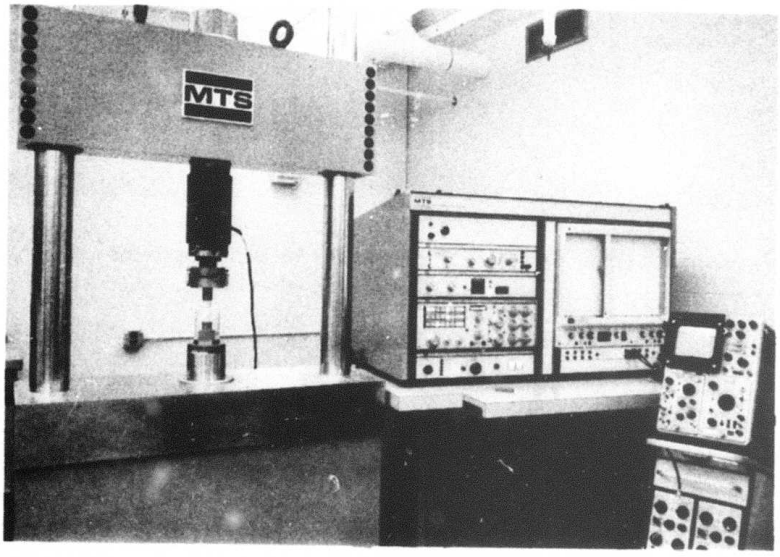

Fig. 14 Loading machine used for the determination of static properties.

in contact with the specimen resting in the stationary holder. The two transducers serving as transmitter and receiver are electrically connected to a pulse generator and an oscilloscope. The electronic circuit generates a pulse, transmits it through the specimen, triggers the oscilloscope, and records its arrival at the receiver's end. The time of pulse travel through the rock is a function of the mechanical properties of the rock.

Static Properties - The static uniaxial compressive and tensile strengths, Young's Modulus and Poisson's Ratio of the tested quartzite, were measured using a servo-controlled hydraulic loading machine (100,000 lbs. capacity). The programmable loading feature of this machine ensures that consistent conditions are applied to all specimens so that differences in results can be wholly attributed to rock property variation (Fig. 14).

For uniaxial compression tests, specimens were mounted in a jig consisting of a lower fixed platen rigidly attached to the hydraulic ram and an upper platen which was part of the swivel head mechanism. The uniaxial load was sensed by a 100,000 lb. load cell. The axial strain was determined either by strain gages or by end to end specimen displacement measurement using a set of double cantilevers mounted at opposite sides of the specimen diameter. Each cantilever was instrumented with four 350 ohms SR-4 foil strain gages connected into a four-arm Wheatstone Bridge circuit. Lateral strain was measured directly by means of two 120 ohms SR-4 strain gages bonded horizontally to the specimen at opposite sides.

The uniaxial tension tests required a more elaborate apparatus and carefully prepared specimens. Steel end-caps were epoxied to all specimens. To guarantee concentricity between rock and end-caps, all three were held firmly against a vertical glass angle bar during the curing period. The top end cap threaded into the loading machine load cell, the bottom cap screwed into a larger bolt which fit loosely into a pot filled with a commercially available "Wood's Metal." The latter has the property of melting at 160°F.

A copper pipe coiled around the pot allowed steam or cold water to melt or solidify the wood's metal as needed. In the molten state, the pot enabled the specimen to hang freely from the top. As the metal solidified, the specimen position remained intact and alignment was assured. Specimens were mounted with two 120 or 350 ohms SR-4 strain gages bonded horizontally to the specimen at opposite sides for lateral strain measurement. Vertical strain was measured by two DCDT displacement transducers mounted axially on opposite sides of the specimen.

MECHANICAL PROPERTIES OF REVETT QUARTZITE

The Revett quartzite, the major host rock in the Coeur d'Alene underground mines, and the rock tested in the reported investigation for its response to hydrofracturing, is not the ideally elastic linear isotropic, homogeneous material as required by the theoretical model upon which the pressure vs. in-situ-stress equations are based. Rather, it is an inhomogeneou s rock, not consistently linear and of questionable isotropy. Chan (1971) divided the Galena mine Revett quartzite into four major groups each exhibiting substantially different mechanical properties: group 1--fine-grained, competent; group 2--argillaceous, fine-grained, thin-bedded; group 3--mineralized, medium to a coarse-grained; and group 4--homogeneous, medium-grained. It was thus found necessary to determine the basic mechanical properties of the rock received from the Star mine for the present study. The two goals of the study were first to verify the extent to which variation in mechanical behavior from the idealized theoretical model affect hydrofracturing results, and second, to obtain the necessary parameter values required in the solution for the in-situ stresses.

The parameters measured were the ultrasonic longitudinal velocities, the static elastic constants, the compressive and tensile strengths, and the jacketed and unjacketed compressibilities. The latter yield the value of the Biot constant α (see Eq. 1). The compressibilities were to be measured by the University of California, Berkeley, which has the appropriate facilities for such tests. Tests were generally conducted on each of the four shipments separately and the results will be presented accordingly.

Dynamic Properties

Originally it was planned to use the acoustic bench for measuring the dynamic elastic properties of the rock. However, due to interactions between the quartz shear crystals and the quartz in the Revett quartzite, shear velocities could not be unambiguously determined. Therefore, only the longitudinal velocities were obtained and an effort was made to use these values for comparison purposes.

Table 1 gives a detailed summary of all longitudinal velocity measurements. Test specimens from a large block, belonging to the first shipment from the 6100 level of Star mine, were obtained in two different manners. First, specimens were cored in three mutually perpendicular directions indicated by x, y, and z (parallel to the three faces of the block). Velocity values show a definite discrepancy between the z and the other two directions. These results are consistent with those obtained by the Bureau of Mines (Thill, 1972). As bedding was clearly visible, specimens were also cored at different bedding inclinations, and velocity values were obtained accordingly and shown in Table 1. There was no clear indication of relationship between bedding inclination and longitudinal velocity except that inclinations 60° - 90° yielded somewhat lower values.

All the remaining rock shipments consisted of several blocks each and specimens were cored only in the direction of the larger cylinders extracted for hydrofracturing tests. Coring in different directions in each block was far beyond the scope of this investigation. It was hoped, however, that since both the rock chunks and the coring directions were picked at random, the total rock mechanical behavior would be determined.

From the second shipment, which consisted of a large number of blocks of varying sizes, an equal number of specimens were obtained from each block and tested. As these specimens were numbered randomly, the results could not be characterized according to blocks. The longitudinal velocity results were widely scattered but appeared to be concentrated

TABLE 1
LONGITUDINAL VELOCITY RESULTS

Shipment	Description	Group	No. of Specimens Tested	Average Longitudinal Velocity (V_p) x 10^4in/sec	Standard Deviation
1	Direction-x		2	23.9	-
	" -y		1	24.9	-
	" -z		2	15.1	-
	Inclination - 0^o		2	20.2	2.0
	" 15^o		4	20.1	0.9
	" 30^o		3	20.2	3.2
	" 45^o		3	21.0	1.4
	" 60^o		1	17.0	-
	" 75^o		2	17.8	1.3
	" 90^o		3	16.7	1.6
2	$V_p<18x10^4$in/sec	I	12	14.4	2.1
	$V_p>18x10^4$in/sec	II	28	19.6	0.8
3	Block - 2	I	12	12.0	0.5
	" 4	"	13	16.6	0.4
	" 6	"	12	15.5	0.5
	" 7	"	9	12.7	0.5
	" 8	"	9	11.9	0.7
	" 1	II	10	18.0	1.0
	" 3	"	10	22.3	1.2
	" 5	"	13	20.3	0.6
4	" 12		11	18.7	1.1
	" 14		8	18.0	0.8

around two means (14.4×10^4 in/sec and 19.6×10^4 in/sec). Hence, the results are presented in two groups, namely group I ($Vp < 18 \times 10^4$ in/sec) and group II ($Vp > 18 \times 10^4$ in/sec).

In the third and fourth shipments, specimens were grouped according to blocks and the velocity results are also presented in this way. The average velocities per block were regrouped according to the above-mentioned arbitrary ranges into groups I and II. The velocities varied from block to block, but within each block, there was considerable consistency. The large variation in velocities between blocks removed from basically the same location indicate strong inhomogeneity and possible anisotropy.

Uniaxial Compression

Uniaxial compression tests were carried out separately on specimens obtained from each shipment. The purpose of these tests was to determine the Revett quartzite mechanical properties such as compressive strength, Young's modulus, and Poisson's ratio, and to observe the extent of inhomogeneity and anisotropy and the variations from level to level in the Star mine. The results obtained are presented in Tables 2, 3, 4, 5, and 6.

The calculated parameters presented in the tables are the failure stress, or more commonly termed the uniaxial compressive strength (Co), the total longitudinal (axial) strain recorded at failure stress, the Young's modulus (E), and Poisson's ratio (ν). Since the quartzite is not consistently linear, neither E nor ν are constants. To provide an indication of the magnitudes, both secant and tangent values of E and ν were calculated at 50% of the failure stress (Co). In addition, the initial tangent Young's modulus was also determined. The measured properties in the first block (Tables 2 and 3) indicate that the Revett quartzite is a very strong rock in compression with Co values ranging from 20,000 psi to 40,000 psi. The considerable variation in strength could not be attributed to the different coring directions. Rather it appeared to be the result of the rock's inherent inhomogeneity. Likewise, no clear anisotropic trends were detected in

TABLE 2
UNIAXIAL COMPRESSION RESULTS
FIRST SHIPMENT - x, y, z DIRECTIONS

Specimen No.	Direction	Longitudinal Velocity (V_p) x 10^4 in/sec	Uniaxial Compressive Strength (Co) psi	Initial Young's Modulus x 10^6 psi	Young's Modulus at 50% of Co		Poisson's Ratio at 50% of Co		Total Long. Strain at Failure μ in/in
					Tangent x10^6 psi	Secant x10^6 psi	Tangent	Secant	
1	x	24.0	36,750	11.3	11.3	11.3	0.25	0.17	3375
2	x	23.7	27,900	11.3	11.3	8.3	0.25	0.12	3100
3	y	24.9	37,250	10.6	10.6	9.4	0.30	0.15	3900
4	z	15.0	31,800	2.0 *	10.3	6.8	0.30	0.13	3650
5	z	15.2	39,200	4.0 *	10.0	7.5	0.30	0.16	5100
Average			34,600		10.7	8.6	0.28	0.14	3825
Standard Deviation			4,600		0.6	0.6	0.03	0.02	775

* between 0-5000 psi.

TABLE 3
UNIAXIAL COMPRESSION RESULTS
FIRST SHIPMENT - DIFFERENT BEDDING INCLINATIONS

Specimen No.	Bedding Inclination	Longitudinal Velocity (V_p) x 10^4 in/sec	Uniaxial Compressive Strength (Co) psi	Initial Young's Modulus x 10^6 psi	Young's Modulus at 50% of Co		Poisson's Ratio at 50% of Co		Total Long. Strain at Failure μ in/in
					Tangent x10^6 psi	Secant x10^6 psi	Tangent	Secant	
1	0^o	-	28,700	11.9	11.9	10.8	0.25	0.10	2850
2	0^o	-	19,600	9.9	9.9	7.6	-	-	2350
3	15^o	19.5	23,500	10.2	10.2	8.0	0.28	0.06	3325
4	15^o	20.6	29,700	11.1	11.1	8.0	-	-	3400
5	30^o	21.8	33,200	10.9	10.9	9.8	0.30	0.04	3350
6	30^o	16.6	31,700	11.3	11.3	9.1	-	-	3250
7	45^o	20.3	37,900	12.0	12.0	10.6	0.31	0.09	3550
8	45^o	22.7	32,000	12.9	12.9	10.2	-	-	3000
9	75^o	16.9	24,800	3.7 *	10.7	7.5	0.10	-0.014[x]	2900
10	90^o	15.6	23,600	3.2 *	11.4	8.3	0.10	0.001[x]	1550
Average		19.25	28,450		11.2	9.0	0.22		2950
Standard Deviation		2.6	5,550		0.9	1.3	0.09		600

* Between 0-5000 psi.
x Lateral strain showed contraction in the range of 0-15000 psi.

the E and ν values at 50% of Co, or in the amount of total strain at failure. All these values indicated a stiff (Young's modulus of about 11×10^6 psi) brittle rock. However, the stress-strain curves were not all alike. Two types were clearly observed, namely a nearly linear curve (Fig. 15) and a nonlinear curve which could be best approximately by a bilinear curve (Fig. 16). In the linear case, the initial and the 50% moduli were approximately the same. In the bilinear case, the initial modulus represented the slope of the lower portion of the curve and the 50% modulus represented the slope of the upper portion. A consistent correlation was found between the longitudinal velocities and the initial modulus. Most of the specimens for which the velocity was low (under 18×10^4 in/sec) yielded a bilinear stress strain curve with a range of initial slope of 2 to 4×10^6 psi prevailing in the first 3,000-5,000 psi of the loading. In two of the bilinear specimens an extremely peculiar behavior was observed. The lateral strain for the first 15,000 psi of the loading range was positive (showing contraction). A typical such stress-strain behavior is shown in Fig. 17. At the time this behavior was observed, no particular attention was paid to it since it was believed to be an isolated case. It was not until specimens of the third shipment were tested that it became clear that some of the Revett quantzite commonly yields a negative or nearly zero Poisson's ratio in the first 5,000-15,000 psi of loading.

Specimens of the second rock shipment from the Star mine were tested without regard to the blocks they represented. No lateral strain measurements were taken. Two groups of behavior were again recognized. Group I (longitudinal velocity under 18×10^4 in/sec) yielded bilinear stress-strain curves, and group II (longitudinal velocity over 18×10^4 in/sec) had basically a linear stress-strain behavior (Table 4). The inhomogeneity within this collection of quartzite blocks was rather spectacular, with compressive strength values ranging between 14,000-50,000 psi, and tangent Young's modulus values at 50% of Co between $8.5 - 15 \times 10^6$ psi.

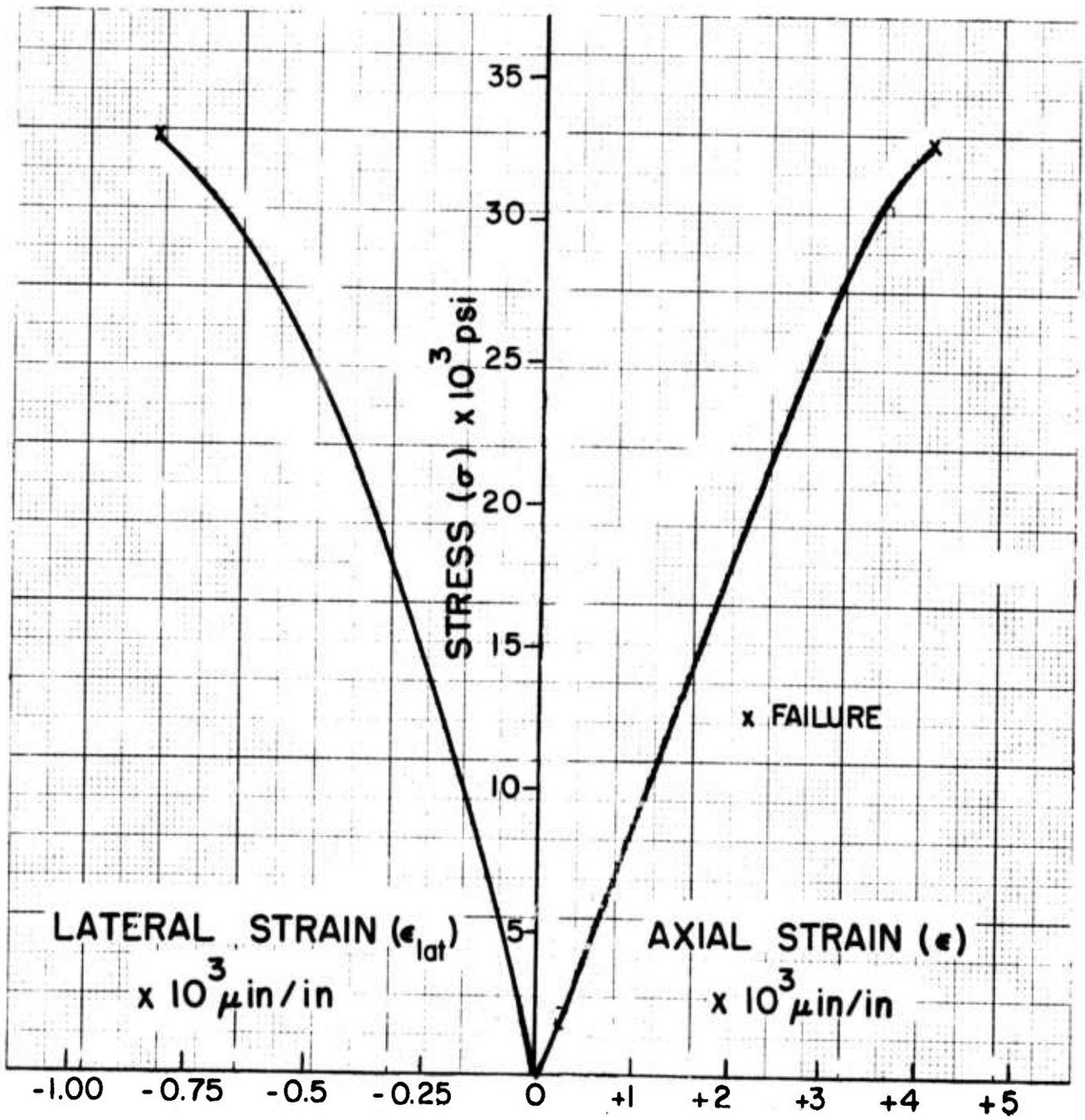

Fig. 15 Typical recording of linear stress-axial strain curve and the corresponding stress-lateral strain.

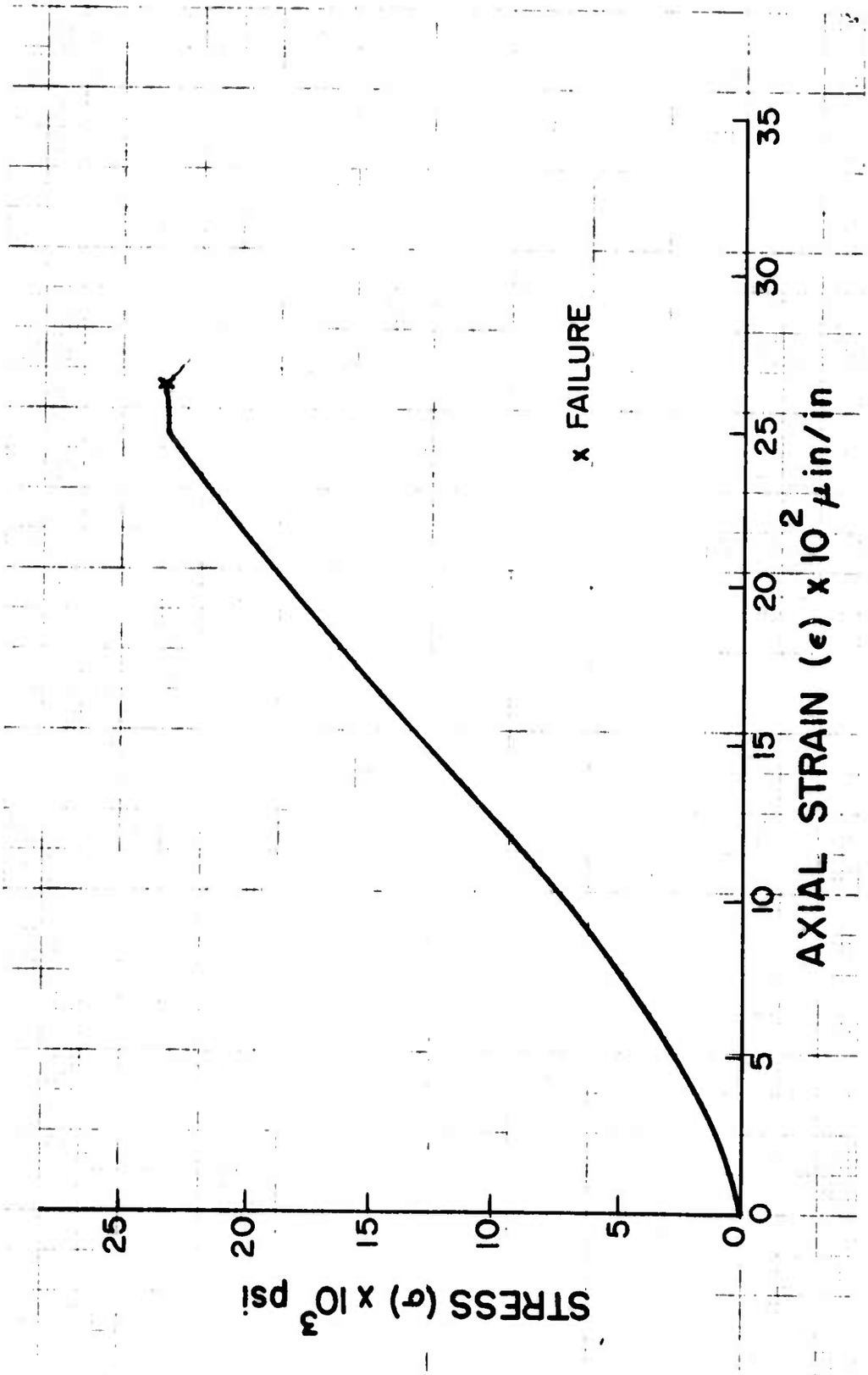

Fig. 16 Typical recording of nonlinear stress-axial strain curve. Such curves can often be approximated by two straight lines (bilinear).

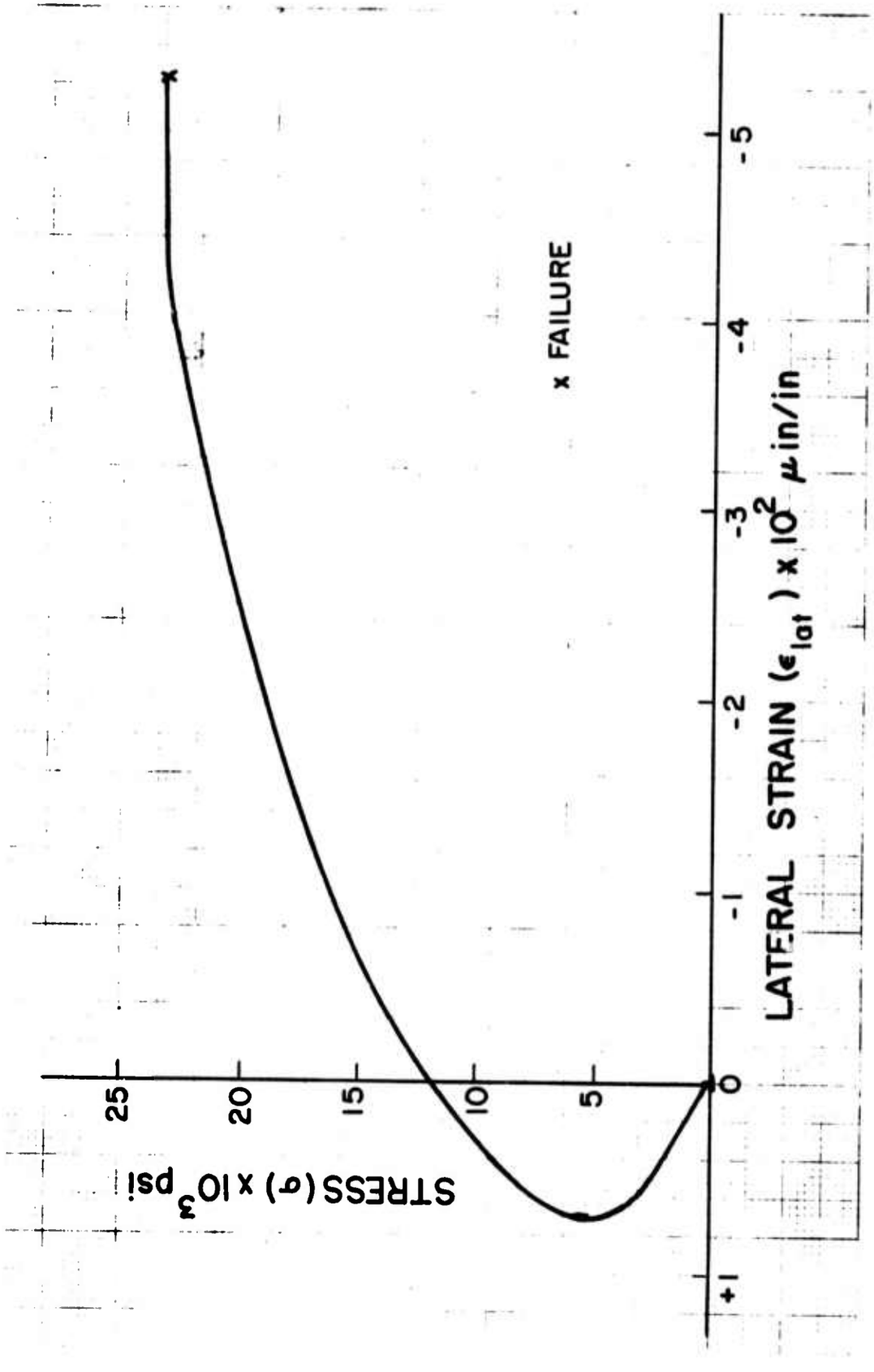

Fig. 17 Recorded stress-lateral strain curve corresponding to the plot in Fig. 16. Note the positive strain (contraction) in the first 12,000 psi of loading.

TABLE 4
UNIAXIAL COMPRESSION RESULTS
SECOND SHIPMENT

Specimen No.	Group	Longitudinal Velocity (V_p) x 10^4 in/sec	Uniaxial Compressive Strength (Co) psi	Initial Young's Modulus x 10^6psi	Young's Modulus at 50% of Co		Total Long. Strain at Failure μ in/in
					Tangent x10^6psi	Secant x10^6psi	
1	I	14.9	34,300	3.8 *	11.7	6.5	4,450
2	"	14.4	48,300	4.6 *	13.0	7.0	5,475
3	"	11.6	41,800	3.0 *	11.0	5.9	5,375
Average		13.6	41,466	3.8	11.9	6.4	5,100
Standard Deviation		1.8	7,006	0.8	1.0	0.5	565
4	II	20.8	40,600	15.2	15.2	14.8	2,750
5	"	19.2	49,400	11.5	11.5	11.3	4,300
6	"	20.5	42,800	11.8	11.8	11.3	3,400
7	"	20.6	44,700	13.6	13.6	12.5	3,600
8	"	20.3	41,300	11.6	11.6	9.3	3,800
9	"	18.9	52,600	12.0	12.0	10.4	4,700
10	"	19.2	36,600	11.9	11.9	9.3	3,400
11	"	19.7	34,000	11.6	11.6	10.1	3,400
12	"	19.9	17,400	9.1	9.1	8.6	2,500
13	"	18.7	27,500	10.5	10.5	10.1	2,200
14	"	18.0	13,600	8.5	8.5	6.9	1,925
15	"	19.5	51,000	13.1	13.1	12.1	4,150
16	"	19.4	46,900	13.2	13.2	11.1	4,025
17	"	19.5	40,600	12.3	12.3	9.6	3,900
18	"	18.9	36,600	11.6	11.6	9.8	3,525
Average		19.5	38,370	11.8	11.8	10.5	3,438
Standard Deviation		0.8	11,438	1.6	1.6	1.8	790

* Between 0-10000 psi.

Specimens of the third shipment were tested according to blocks they represented (Blocks 1 to 8) and the results given in Table 5 show again two distinctly different behaviors. Blocks 2, 4, 6, 7, and 8 belonged to group I as far as their longitudinal velocities and stress-strain behavior (bilinear). Many of the specimens belonging to this group contracted in the lateral direction during the first portion of the uniaxial loading (0 - 15, 000 psi). The result is seen in Table 5 in the form of nearly zero secant Poisson's ratio at 50% of Co. The amount of average strain at failure stress was almost double the one recorded for group II. The average compressive strength and the tangent Young's modulus at 50% of Co, on the other hand, were very close in both groups. A typical stress-strain plot for each of the groups is shown in Fig. 18. The corresponding stress-volumetric strain curves and the resulting dilatancies are given in Fig. 19. The variation of Poisson's ratio with stress in each of the groups, including the negative values obtained in group I are presented in Fig. 20. Note that Poisson's ratio is never really constant, but rather varies linearly with stress.

The fourth shipment specimens were cored out of two large blocks (nos. 12 and 14). The longitudinal velocities of all specimens were within close proximity of 18×10^4 in/sec, i. e. somewhere in between groups I and II. As a result the stress-strain behavior was also intermediate. While a slight bilinear behavior was noticed in some specimens, no positive lateral strains were recorded and no differences in the total longitudinal strain to failure were revealed. While the average secant Poisson's ratio was higher than in previous shipments, the tangent ratio was lower (Table 6).

Table 7 is an attempt to consolidate the average results of the compression tests according to shipments. Variation of 20% in compressive strength, and tangent Young's modulus, and of 100% in Poisson's ratio make the rock appear, in general, highly inhomogeneous.

TABLE 5
UNIAXIAL COMPRESSION RESULTS
THIRD SHIPMENT

Specimen No.	Group	Longitudinal Velocity (V_p) x 10^4 in/sec	Uniaxial Compressive Strength (Co) psi	Initial Young's Modulus x 10^6 psi	Young's Modulus at 50% of Co		Poisson's Ratio at 50% of Co		Total Long. Strain at Failure μin/in
					Tangent x10^6 psi	Secant x10^6 psi	Tangent	Secant	
204	I	11.6	28,900	1.7 *	7.7	3.9	0.14	0.08 x	7075
206	"	10.9	40,650	1.8 *	7.6	2.7	0.22	0.07 x	7900
402	"	15.7	25,600	4.2 *	6.0	5.4	0.17	0.06 x	4100
403	"	16.7	26,350	4.8 *	6.8	4.0	0.12	0.01 x	4400
602	"	15.8	26,400	-	-	-	-	-	-
604	"	16.3	26,350	4.5 *	11.3	5.1	0.16	0.01 x	4875
701	"	12.9	41,300	2.5 *	6.7	4.6	0.19	0.07 x	7370
704	"	12.5	43,400	2.7 *	7.4	4.5	0.29	0.06 x	7950
807	"	11.9	47,700	2.5 *	9.0	4.7	0.15	0.07 x	8000
Average		13.8	34,050	2.8	7.8	4.4	0.18	0.05	6450
Standard Deviation		2.3	9,000	1.1	1.6	0.8	0.05	0.02	1700
101	II	18.7	34,300	6.4	6.4	6.4	0.31	0.31	4450
104	"	16.8	23,600	6.7	6.7	6.1	0.37	0.14	5150
301	"	23.3	40,650	11.4	11.4	11.4	0.19	0.12	4100
304	"	19.7	43,400	11.7	11.7	11.7	0.17	0.12	4350
501	"	21.2	31,400	9.1	9.1	9.1	0.17	0.03 x	3375
505	"	20.9	25,700	8.9	8.9	8.9	0.14	0.02	2775
508	"	20.4	35,750	7.3	7.3	7.3	0.16	0.06 x	3600
Average		20.1	33,550	8.8	8.8	8.7	0.21	0.11	3975
Standard Deviation		2.1	7,300	2.1	2.1	2.2	0.08	0.09	775

* Between 0-15000 psi.
x Lateral strain showed contraction in the range of 0-12000 psi.

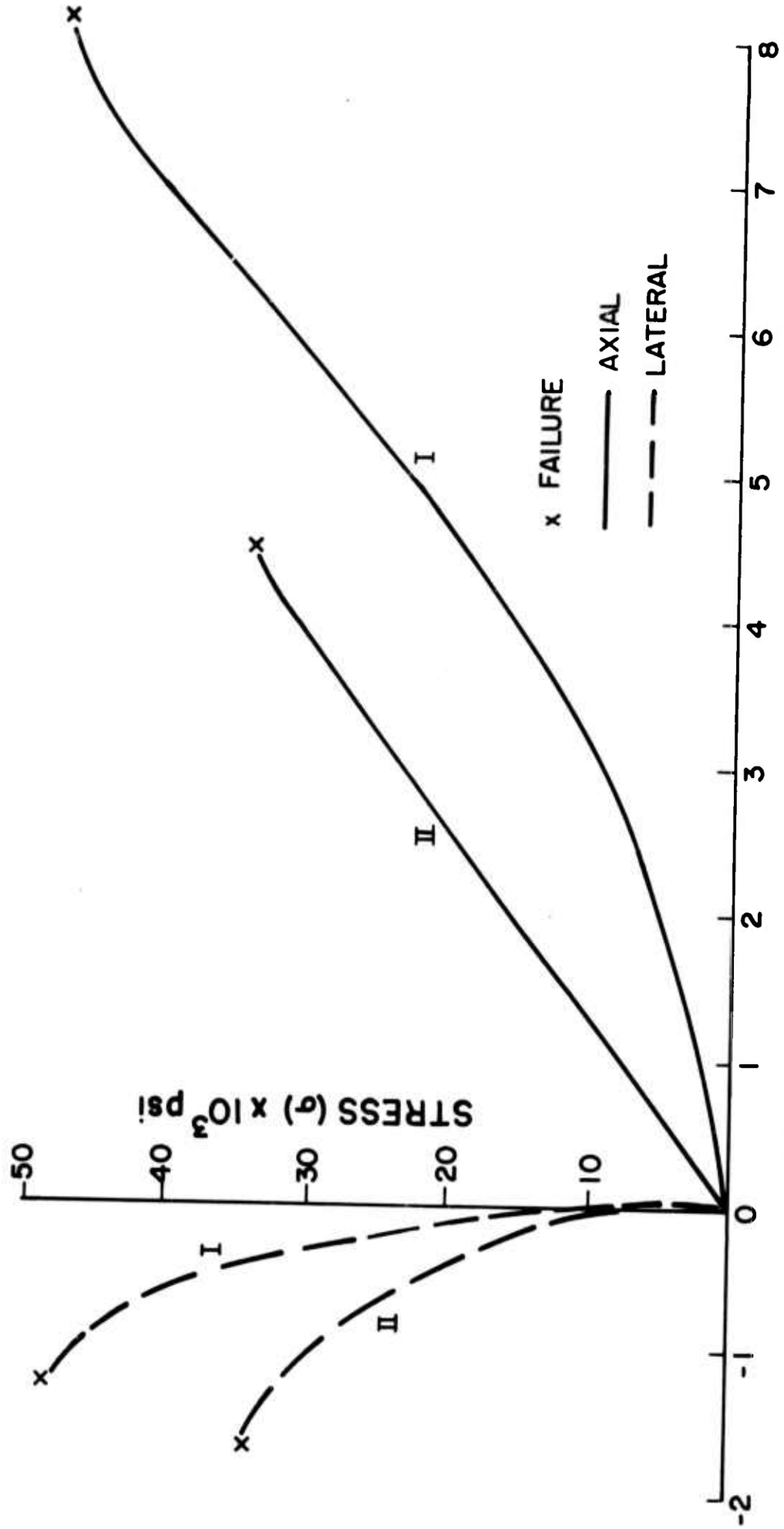

Fig. 18 Typical stress-strain curves representing groups I and II.

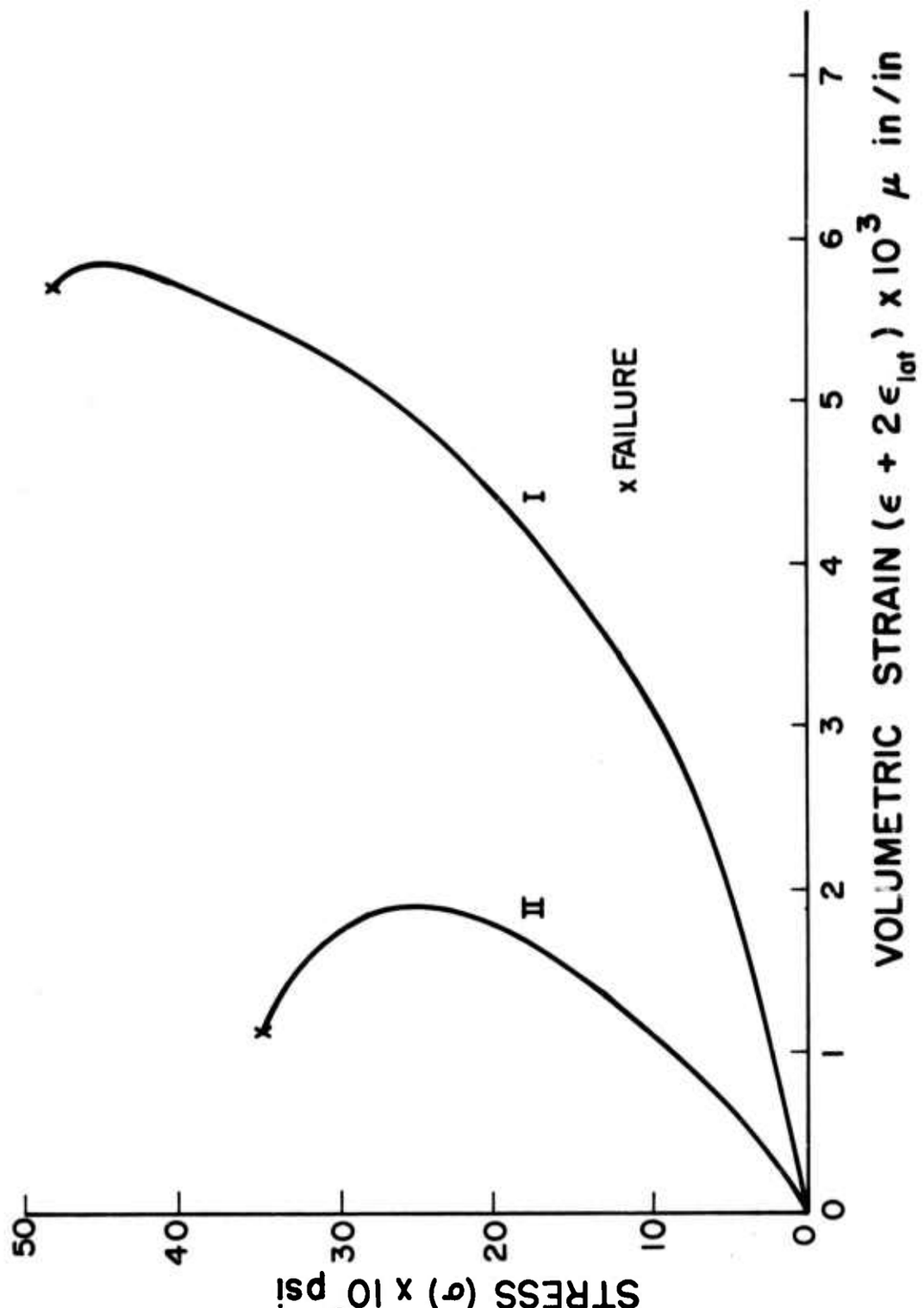

Fig. 19 Calculated stress-volumetric strain curves corresponding to plots in Fig. 18.

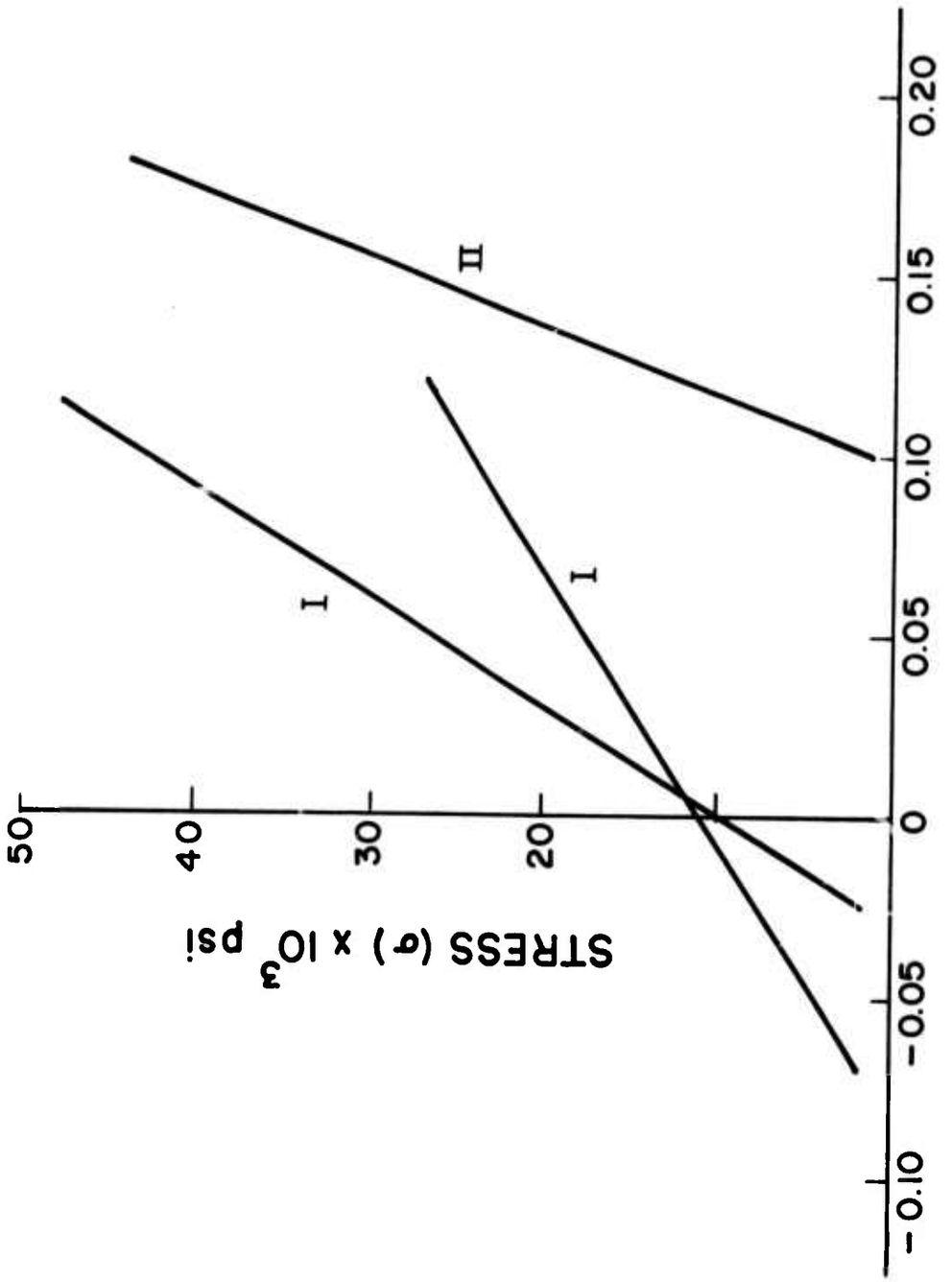

Fig. 20 Variation of Poisson's Ratio with stress in selected typical specimens of groups I and II.

TABLE 6
UNIAXIAL COMPRESSION RESULTS
FOURTH SHIPMENT

Specimen No.	Longitudinal Velocity (Vp) $x10^4$ in/sec	Uniaxial Compressive Strength (C_o) psi	Initial Young's Modulus $x10^6$ psi	Young's Modulus at 50% of C_o		Poisson's Ratio at 50% of C_o		Total Long. Strain at Failure μ in/in
				Tangent $x\ 10^6$ psi	Secant $x\ 10^6$ psi	Tangent	Secant	
1202	18.2	56,900	6.98*	9.4	8.7	0.10	0.18	6050
1203	19.0	44,300	10.40	10.4	10.4	0.15	0.09	4025
1204	18.5	27,200	7.42*	10.2	9.1	0.13	0.24	3225
1401	16.3	25,150	6.20*	8.7	7.1	0.09	0.26	3025
1402	17.7	23,800	5.88*	8.3	6.4	-	-	3575
1403	18.5	28,150	7.2	7.2	7.2	0.13	0.09	4025
Average	18.0	34,250	7.34	9.0	8.1	0.12	0.19	4150
Standard Deviation	0.9	13,350	1.61	1.2	1.5	0.02	0.06	1150

*Between 0-5000 psi

TABLE 7
COMPRESSION TEST RESULTS
COMPARISON

Shipment	Uniaxial Compressive Strength psi	Young's Modulus at 50% of Co		Poisson's Ratio at 50% of Co	
		Tangent x 10^6 psi	Secant x 10^6 psi	Tangent	Secant
1	30,500	11.4	8.8	0.25	0.09
2	38,900	11.9	10.4	-	-
3	33,850	8.5	6.4	0.19	0.08
4	34,250	9.0	8.1	0.12	0.19

In an attempt to improve our understanding of the rock peculiar deformational behavior a microscopic study of typical Revett quartzite thin sections was undertaken. A visual observation indicated that the rock consisted of fine grained quartz (about 75%), mica (close to 20%), some very fine chlorite and about 1% calcite. In bilinear specimens micas appear to be evenly distributed in preferred orientations around the quartz grains. A tempting speculation is that the soft inclusions of mica undergo a contraction which is larger than the overall elastic lateral expansion during the first phase of compressive loading, causing the low initial modulus and the negative Poisson's ratio.

The compression tests have shown in general that the Revett quartzite mechanical properties vary from site to site and even within the same neighborhood, and that a peculiar bilinear stress-strain behavior can be observed in a substantial number of cases. As far as stress measurements, this implies that careful mechanical property determination is required for each hydrofracturing test or group of tests that are to be run in a particular location.

Uniaxial Tension

Uniaxial tension tests were carried out separately on specimens from each shipment. The purpose of these tests was to obtain the Revett quartzite mechanical properties in tension such as the uniaxial tensile strength, Young's modulus, Poisson's ratio, and total strain at failure. The results obtained are presented in Tables 8, 9, 10, and 11.

Specimens from the first shipped block were tested in uniaxial tension at different bedding inclinations, and as shown in Table 8, their overall tensile strength and Young's modulus were rather high, indicating a strong brittle rock. No direct correlation between scatter in results and bedding inclination could be found. Typical stress-axial strain and stress-lateral strain curves in tension are shown in Figs. 21 and 22. The stress-axial

TABLE 8
UNIAXIAL TENSION RESULTS
FIRST SHIPMENT

Specimen No.	Bedding Inclination	Longitudinal Velocity (Vp) x10^4 in/sec	Uniaxial Tensile Strength (T_o) psi	Young's Modulus at 50% of T_o		Poisson's Ratio at 50% of T_o		Total Long. Strain at Failure μ in/in	Rupture Plane Inclination
				Tangent x 10^6 psi	Secant x 10^6 psi	Tangent	Secant		
1	0°	19.0	1,900	13.2	-	0.09	0.09	200	0°
2	0°	18.7	2,700	-	-	-	-	-	35°
3	15°	20.6	850	-	-	-	-	-	15°
4	30°	19.5	1,750	-	-	-	-	-	35°
5	45°	20.3	3,000	12.9	14.5	0	0	250	0°
6	45°	20.3	3,650	-	-	-	-	-	35°
7	60°	17.0	3,750	8.2	10.5	0	0	215	25°
8	75°	18.7	3,000	8.6	10.2	0.03	0.02	465	45°
9	90°	17.9	2,200	9.3	9.3	-	-	290	25°
10	90°	17.9	1,700	10.6	13.2	0.10	0.07	205	45°
Average		19.0	2,450	10.5	11.5	0.07	0.06	270	
Standard Deviation		1.2	925	2.2	2.2	0.04	0.03	100	

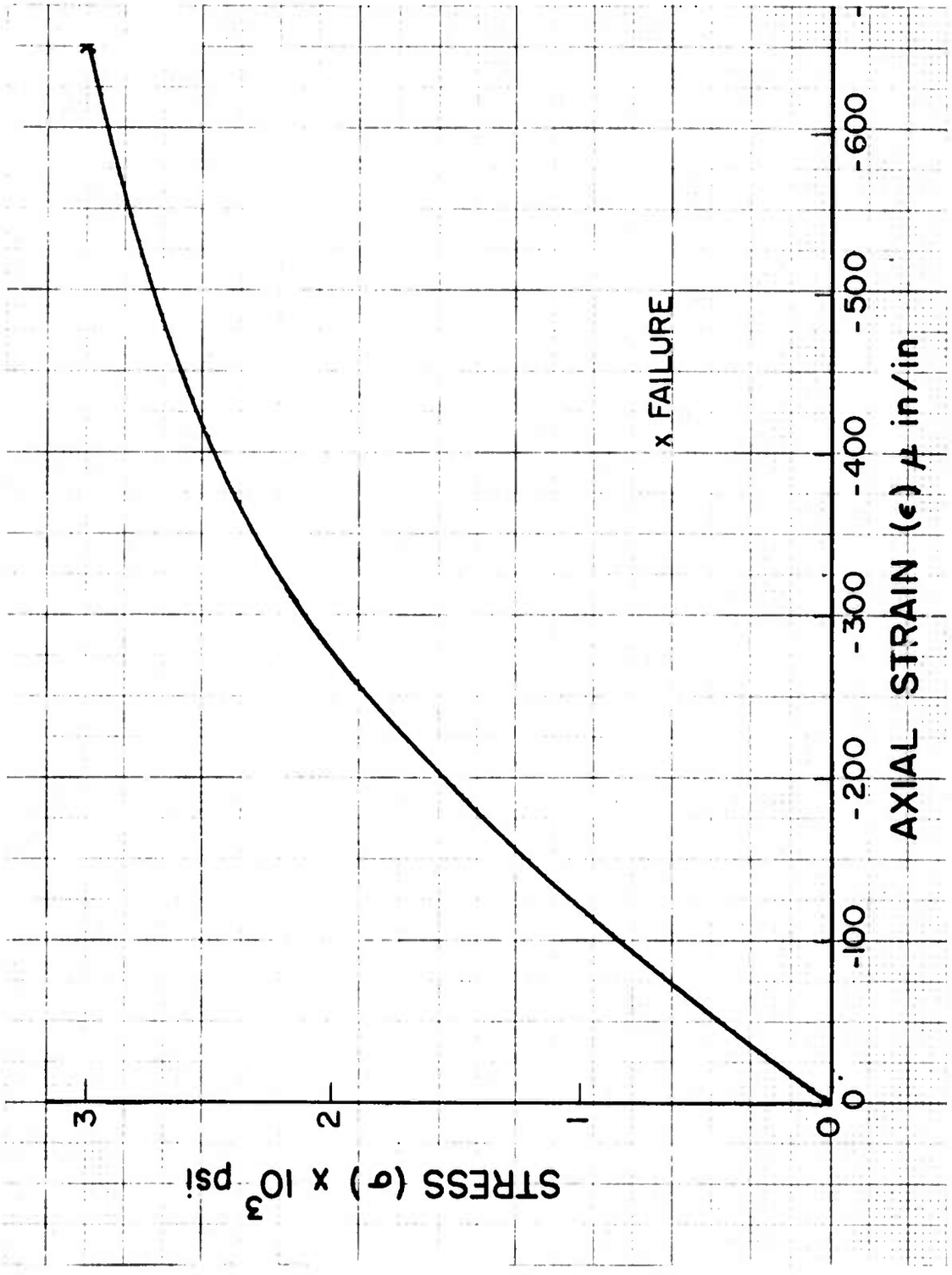

Fig. 21 Typical recording of stress-axial strain curve in uniaxial tension.

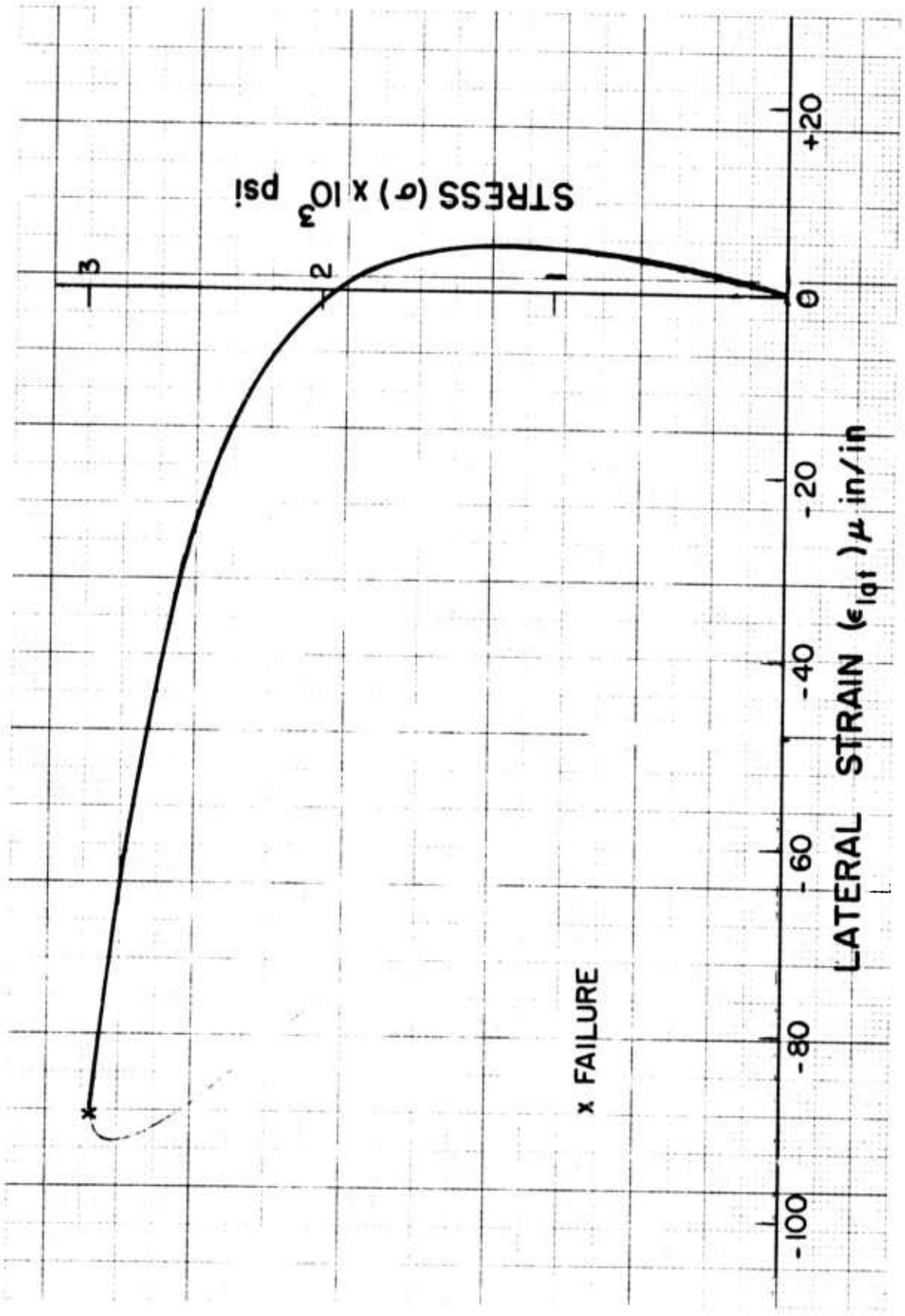

Fig. 22 Typical recording of stress-lateral strain curve in uniaxial tension (corresponding to Fig. 21).

strain (Fig. 21) curve started as a straight line, gradually turning into a concave downward curve. This softening effect was probably due to opening of existing cracks or soft inclusions. The lateral strain (Fig. 22) was first positive indicating, as expected, contraction. As the load was increased, the slope of the stress-lateral strain curve gradually increased until at some point the lateral strain became zero. Beyond that, the lateral strain, and with it the Poisson's ratio, became negative, indicating expansion. Such a behavior has been observed in other rocks and is attributed to the opening of cracks or expansion of soft inclusions. Of major interest is the tensile rupture plane inclination with respect to the lateral direction. Under normal conditions an inclination of 0° to 10° is expected. However, in the reported tests inclinations of up to 45° were observed. This peculiar behavior could be the result of failure along the weak microscopic mica inclusions, which were observed to traverse most of the specimens (see section on "Uniaxial Compression").

Specimens from the second shipment were again grouped into two according to the longitudinal velocities (Table 9). A direct correlation is found between these velocity ranges, and the modulus as well as the total strain at failure. Group I is characterized by low modulus and large total strain, indicating a softer material. The negative Poisson's ratios were a direct result of the lateral expansion, as above. The rupture plane inclination again varied between 0° and 45°.

The results of the third shipment tests, Table 10, are very similar to the previous one given in Table 9, namely, group I showed considerably lower modulus and also increased total strain. No direct correlation to the tensile strength or the Poisson's ratio was detected. The failure planes were again mostly inclined to the lateral direction.

The fourth shipment specimens, as in uniaxial compression, yielded intermediate modulus and total strain values (Table 11). The Poisson's ratio at 50% of the tensile strength was very small or negative and the rupture planes were inclined between 0° and 30°. The tensile strength was lower than in the other shipments.

TABLE 9
UNIAXIAL TENSION RESULTS
SECOND SHIPMENT

Specimen No.	Group	Longitudinal Velocity (Vp) $\times 10^4$ in/sec	Uniaxial Tensile Strength (T_o) psi	Young's Modulus at 50% T_o		Poisson's Ratio at 50% of T_o		Total Long. Strain at Failure μ in/in	Rupture Plane Inclination
				Tangent x 10^6psi	Secant x 10^6psi	Tangent	Secant		
1	I	12.20	1,000	2.00	3.10	-	-	600	12°
2	I	14.60	2,150	3.42	4.80	-	-	780	10°
3	I	13.04	1,550	2.50	3.60	-	-	765	6°
Average		13.28	1,567	2.64	3.83	-	-	715	
Standard Deviation		1.22	575	0.72	0.87	-	-	100	
4	II	18.05	2,175	8.15	9.40	-0.02	-0.03	290	0°
5	II	19.60	2,150	9.32	10.45	-	-	260	23°
6	II	18.50	2,400	4.80	6.10	-	-	470	45°
7	II	19.00	2,200	9.29	10.86	-0.06	-0.09	325	26°
8	II	18.90	3,125	8.70	8.70	0	-0.05	400	8°
9	II	19.70	2,600	12.80	13.90	-	-	285	0°
10	II	18.00	1,300	8.50	9.10	-	-	175	0°
Average		18.82	2,278	8.79	9.78	-0.03	-0.06	315	
Standard Deviation		0.68	551	2.35	2.37	0.03	0.03	96	

TABLE 10
UNIAXIAL TENSION RESULTS
THIRD SHIPMENT

Specimen No.	Group	Longitudinal Velocity (Vp) x10^4 in/sec	Uniaxial Tensile Strength (T_o) psi	Young's Modulus at 50% T_o		Poisson's Ratio at 50% of T_o		Total Long. Strain at Failure μ in/in	Rupture Plane Inclination
				Tangent x 10^6psi	Secant x 10^6psi	Tangent	Secant		
211	I	12.3	1,000	1.5	2.0	-0.01	-0.01	680	0°
412	I	16.6	1,700	4.4	5.2	-0.01	-0.01	225	0°
607	I	15.5	1,800	3.7	4.8	-0.09	-0.07	420	15°
610	I	15.6	1,650	3.0	4.2	-0.10	-0.09	710	30°
706	I	12.7	700	3.7	5.5	-0.07	-0.06	410	0°
710	I	13.3	750	5.1	5.8	-0.10	-0.07	260	30°
801	I	11.9	1,600	-	-	-	-	-	0°
811	I	12.6	550	6.4	6.4	-0.03	-0.03	230	30°
Average		13.8	1,218	3.9	4.8	-0.03	-0.04	419	
Standard Deviation		1.8	518	1.5	1.4	0.03	0.03	204	
110	II	18.0	1,450	5.8	8.1	-0.05	-0.03	310	0°
306	II	22.6	3,500	14.4	15.2	0.02	0.02	260	45°
509	II	20.6	2,150	10.7	11.5	-0.05	-0.04	210	0°
511	II	19.8	2,000	-	-	-	-	-	35°
513	II	20.7	3,500	8.3	10.8	-0.04	-0.06	650	0°
Average		20.3	2,520	9.8	11.4	-0.03	-0.03	357	
Standard Deviation		1.6	931	3.6	2.9	0.03	0.03	200	

TABLE 11
UNIAXIAL TENSION RESULTS
FOURTH SHIPMENT

Specimen No.	Longitudinal Velocity (Vp) x 10^4 in/sec	Uniaxial Tensile Strength (To) psi	Young's Modulus at 50% of To		Poisson's Ratio at 50% of To		Total Long. Strain at Failure μ in/in	Rupture Plane Inclination
			Tangent x10^6psi	Secant x10^6psi	Tangent	Secant		
1201	18.7	2300	5.2	8.5	-0.06	-0.04	530	0^o
1209	17.8	1550	5.8	8.2	-	-	310	25^o
1405	18.8	850	8.8	10.7	-0.06	-0.03	105	15^o
1408	18.0	1450	9.0	9.0	0	-0.01	310	30^o
Average	18.3	1540	7.2	9.1	-0.04	-0.03	310	
Standard Deviation	0.5	600	2.0	1.1	0.03	0.01	170	

TABLE 12
UNIAXIAL TENSION RESULTS
COMPARISON

Shipment	Uniaxial Tensile Strength (T_o) psi	Young's Modulus at 50% of T_o		Poisson's Ratio at 50% of T_o	
		Tangent x 10^6 psi	Secant x 10^6 psi	Tangent	Secant
1	2457	10.48	11.60	0.07	0.06
2	2065	6.83	7.50	-0.03	-0.06
3	1719	6.10	7.22	-0.03	-0.04
4	1542	7.18	9.08	-0.04	-0.03

Table 12 summarizes the uniaxial tension results. There are wide variations indicating the inhomogeneity of the rock. Most of the peculiar behavior resulting in negative Poisson's ratios and inclined rupture surfaces could possibly be traced back to soft mica inclusions and preexisting microcracks.

Triaxial Compression

In order to establish the dependence of the peculiar lateral strain behavior of the quartzite on confining pressure, a series of triaxial compression tests were carried out in specimens from the third shipment (Group I). The confining pressures used were 1, 000 psi, 2, 500 psi, and 5, 000 psi. The specimens were first loaded hydrostatically to the value of the preset confining pressure. Thereafter the confining pressure was kept constant and the axial load was increased until failure. The lateral strain indicated expansion throughout the loading range. No contraction was observed in any of the six specimens tested. The recorded stress-axial strain curves were all linear, unlike the bilinear behavior observed in specimens from the same blocks under uniaxial compression. It is apparent that the confining pressure contributes to the closure of existing microcracks or soft inclusions prior to the initial loading over the preset lateral stress. This preloading closure eliminates the peculiarity observed under uniaxial compression.

Jacketed and Unjacketed Compressibilities

Samples of the second shipment rock were sent to the Petroleum Engineering Laboratory of the University of California-Berkeley for jacketed and unjacketed compressibility measurements. These values were required to evaluate the Biot constant (α) which was to be used in the hydrofracturing pressure vs stress relationships. Only two specimens were tested, yielding very close results. The calculated values of α as a function of the hydrostatic pressure are plotted in Fig. 23. Due to the large expenses involved,

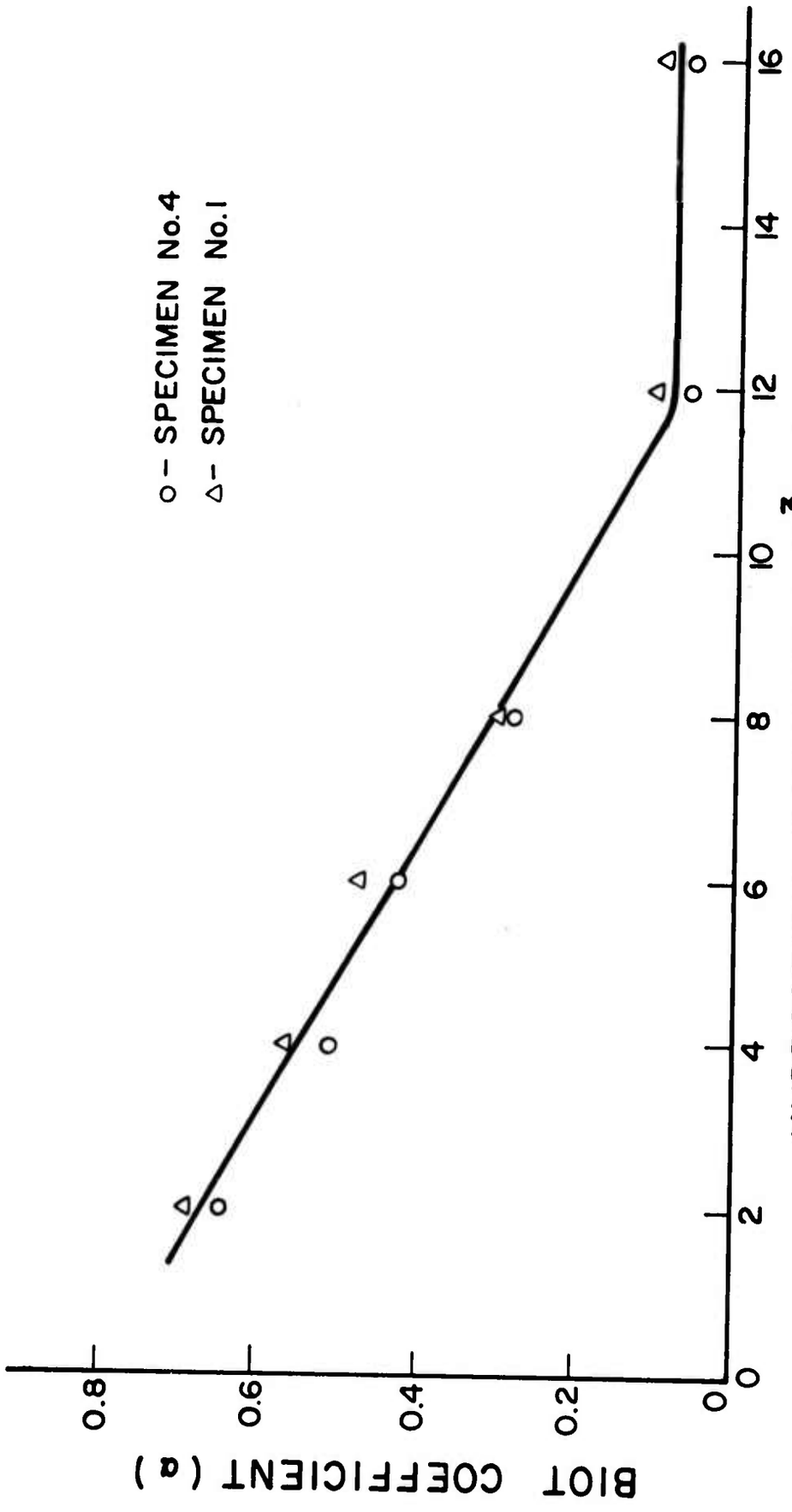

Fig. 23 Variation of Biot cooefficient with pressure in Revett Quartzite.

these were the only tests performed for the evaluation of α, whose value was subsequently considered to be representative of all the rock shipments.

HYDRAULIC FRACTURING

Equal Horizontal Stresses

1. Axial Holes

The first stage of the hydrofracturing laboratory testing was conducted on cylindrical specimens subjected to equal horizontal stresses. This is not the most general simulation of in-situ conditions, where all three principal stresses are considered unequal, but it was preferred for the initial testing because it produced important basic results without necessitating the considerably more substantial effort involved in preparing and testing prismatic specimens.

The first round of tests was run on specimens extracted from a large block which arrived with the first shipment from the Star mine. Coring was done in three mutually perpendicular directions. The objective was to explore the sensitivity of the rock to hydrofracturing and to observe any possible anisotropy with respect to fracturing pressures and directions.

The hydrofracturing test results are given in Table 13 and the breakdown pressure (P_c) vs. the horizontal in-situ stress (σ_H) are plotted in Fig. 24. The breakdown pressure results are definitely independent of the direction of core extraction. They are, however, closely related to the horizontal stress and fall within a narrow band below the theoretical curve for impermeable rock (P_c^i) as given by eq. (7b). Since the tested Revett quartzite is practically impermeable, one would expect that eq. (7b) should represent the experimental results. However, as it has previously been noted (Haimson, 1968, Haimson and Edl, 1972) at high borehole pressures ($>$ 2000 psi or so) there is an apparent pore and crack opening around the hole, the initially impermeable rock becomes locally permeable and the fracturing fluid penetrates a short distance into it.

TABLE 13
HYDRAULIC FRACTURING RESULTS*
FIRST SHIPMENT

Borehole Direction	Vertical Load σ_V(psi)	Horizontal Stress σ_H (psi)	Experimental Breakdown Pressure P_c^e (psi)
x	2,000	0	6,000
z	2,000	0	6,200
x	11,600	5,000	11,500
y	11,600	5,000	11,250**
y	11,600	5,000	10,800
z	11,600	5,000	10,000
z	11,600	5,000	9,300***
z	11,600	5,000	10,800
x	19,400	10,000	16,400
z	19,400	10,000	16,000
z	11,600	10,000	14,300
z	27,000	20,000	26,300
x	27,000	20,000	24,300
y	27,000	22,000	24,500

* All hydrofractures were axial (vertical) fractures emanating from the borehole.

** Preexisting horizontal fracture below borehole did not affect vertical hydrofracture but stopped its extension downward.

*** Preexisting vertical fracture at short distance from borehole did not affect vertical hydrofracture.

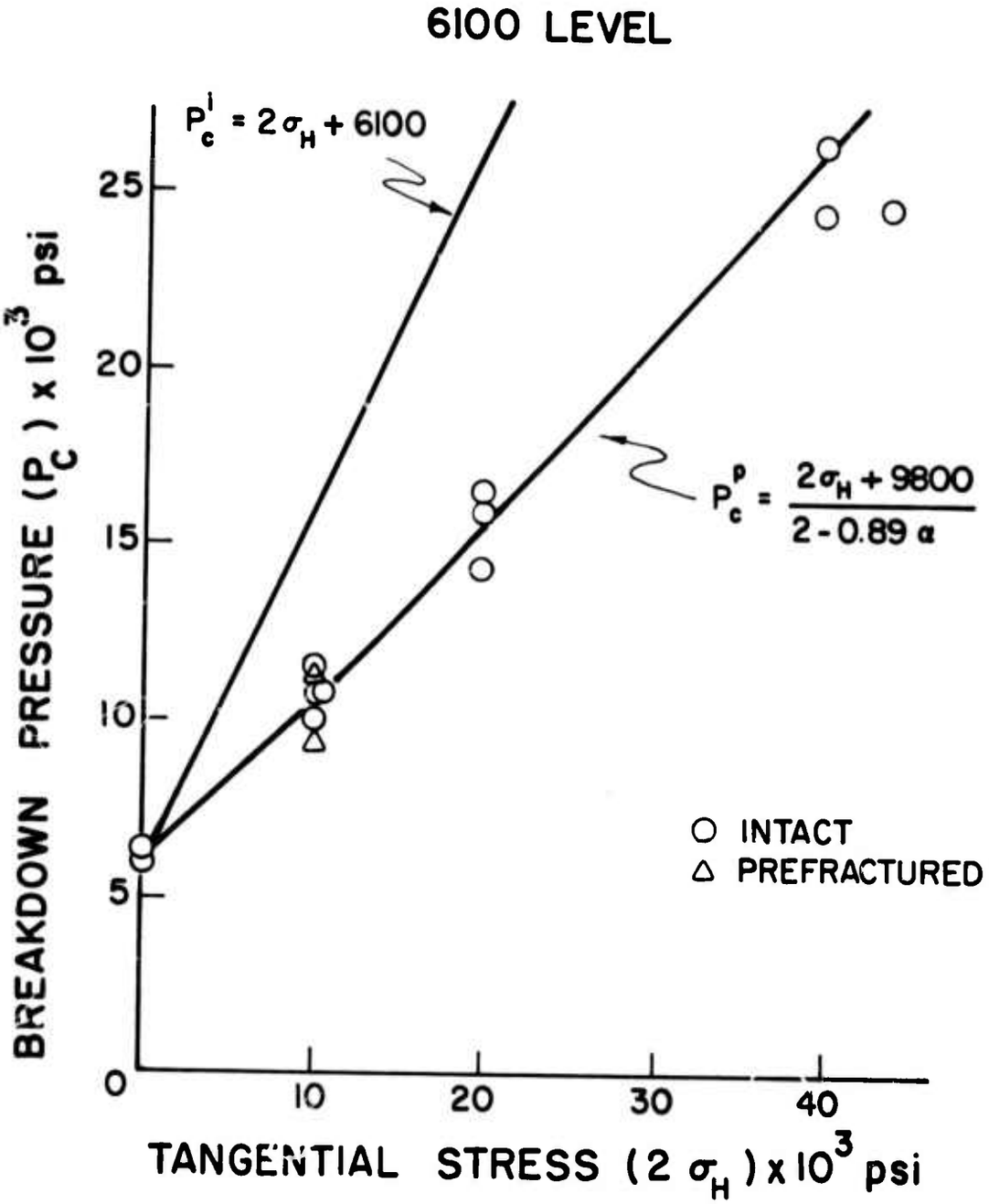

Fig. 24 Breakdown pressure results as a function of tangential stress (cylindrical specimens, first shipment).

This justifies the use of eq. (6) in calculating the expected breakdown pressure. Indeed, in this series of tests the theoretical curve represented by eq. (6) accurately correlated with the experimental points (Fig. 24). It should be noted that the value of T for eq. (7a) was calculated in all cases by taking the average experimental value of P_c for $\sigma_H = 0$ and setting $P_c = T$. The value of T for eq. (6) was calculated similarly by taking the average experimental value of P_c for $\sigma_H = 0$ and setting $P_c = T/[2-\alpha(1-2\nu)/(1-\nu)]$. Poisson's ratio was taken as the average value obtained in the laboratory (0.1). The Biot constant (α) was taken from Fig. 23 for the appropriate value of P_c.

As noted in Table 13 all hydrofractures were vertical, unaffected by core orientation. Not only were the experimental breakdown pressure values unaffected by any anisotropy of the rock, but the vertical fractures appeared insensitive to existing cracks.

Unlike the first set of tests, which were conducted on mostly intact specimens taken from one block, the second round of tests were conducted in largely precracked cylinders extracted from the small blocks (less than 1 cu. ft) that constituted the second shipment. The quartzite itself had variable tint and texture which differed from block to block. The high frequency of fractures could have been the result of excessive exposure to blasting forces. However, most of the existing cracks did not appear to be fresh but rather weakly to strongly cemented, and hence they are believed to have existed in the virgin rock in-situ.

The results of 14 hydrofracturing tests in the second shipment rock are given in Table 14 and Fig. 25. It is noted that most of the specimens had visible preexisting fractures (Table 14) and as a result the hydrofracturing pressures are rather scattered. The majority of the experimental points still lie within the bounds formed by the two theoretical curves for P_c^i and P_c^p. All hydraulic fractures were vertical emanating from the hole and extending all the way to specimen boundary. Figs. 26 and 27 are photographs of two specimens

TABLE 14
HYDRAULIC FRACTURING RESULTS*
SECOND SHIPMENT

Specimen No.	Vertical Load σ_v (psi)	Horizontal Stress σ_H (psi)	Experimental Breakdown Pressure P_c^e (psi)
2	1,000	0	3,000
3	1,000	0	2,500**
24	1,000	0	3,300**
25	1,000	0	2,300
4	2,000	1,000	2,000***
6	2,000	1,000	6,000
9	2,000	1,000	3,400+
13	2,000	1,000	5,000x
7	5,000	2,500	6,100**
10	5,000	2,500	9,600**
5	9,700	5,000	9,600+
8	9,700	5,100	8,800+
11	15,000	6,600	12,800**
12	15,000	7,500	14,700**

*Unless otherwise stated all hydrofractures were axial (vertical) fractures emanating from the borehole.

**Hydraulic fracture joined preexisting fracture(s).

***Hydraulic fracture originated and extended along preexisting fracture which crossed the borehole.

+Hydraulic fracture did not join preexisting fracture although it might have intersected it.

xHydraulic fracture was inclined and parallel to one of many preexisting fractures.

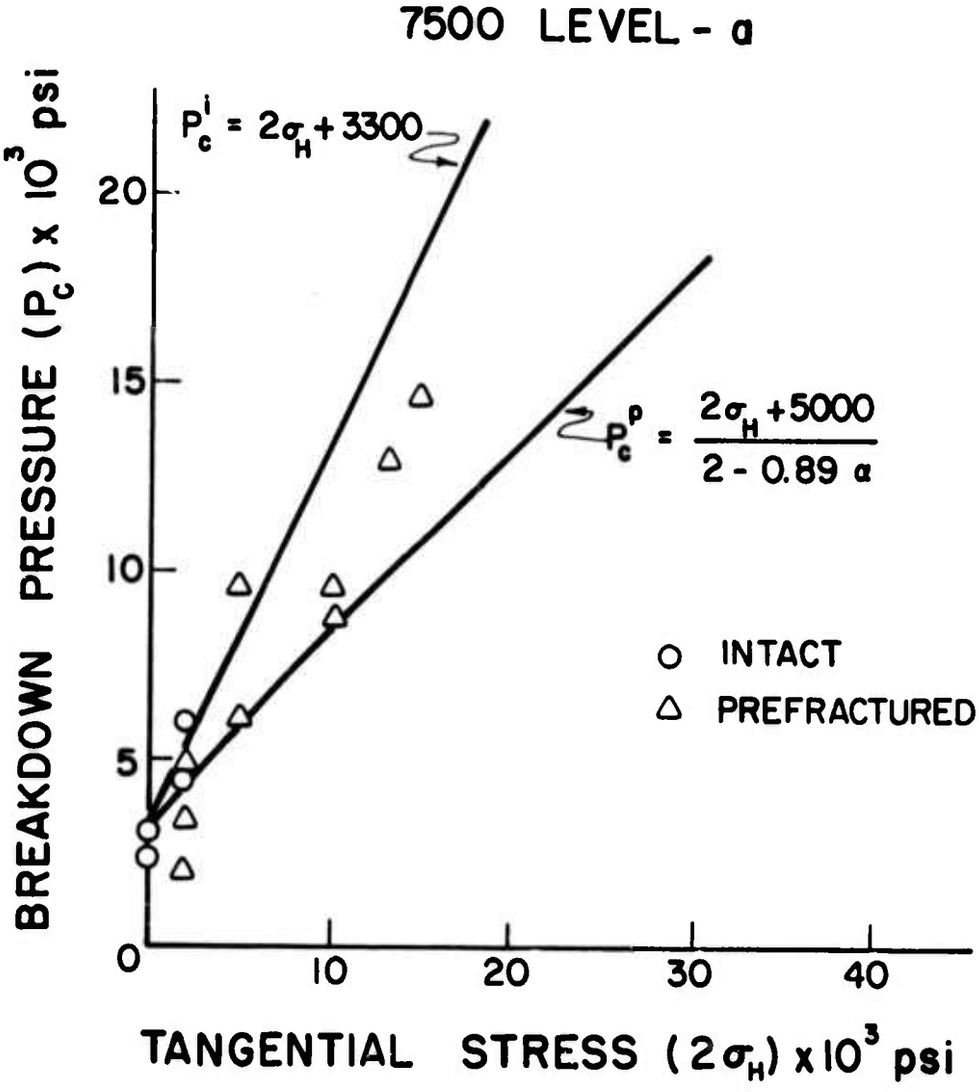

Fig. 25 Breakdown pressure results as a function of tangential stress (cylindrical specimens, second shipment).

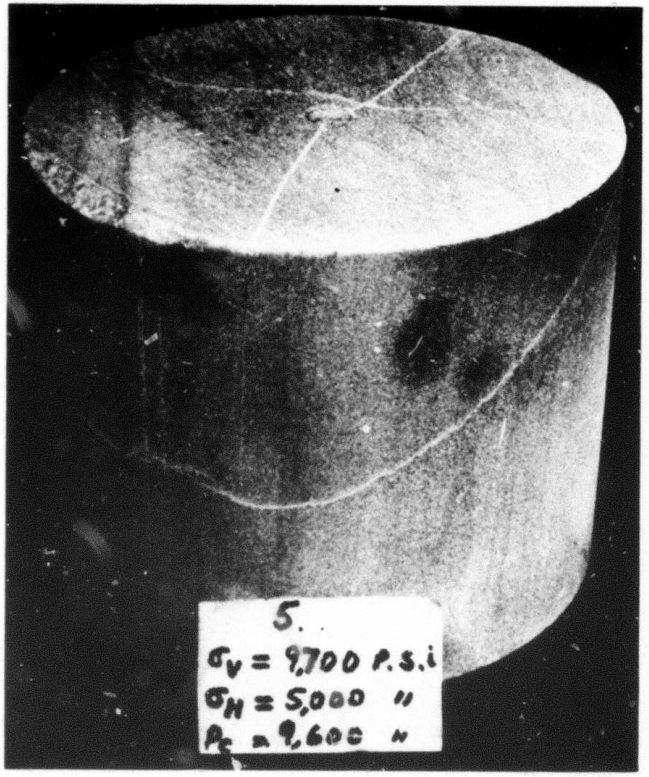

Fig. 26 Vertical hydrofracture crossed preexisting inclined crack.

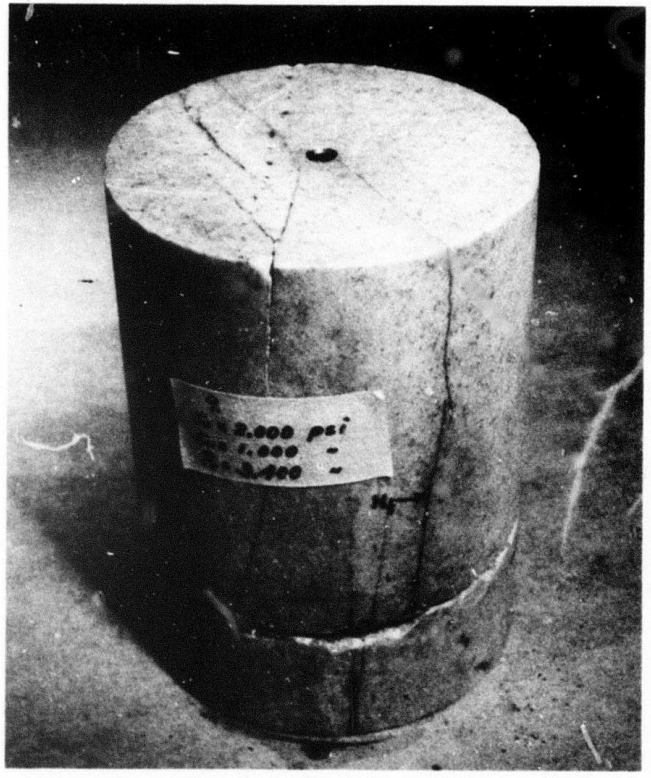

Fig. 27 Vertical hydrofracture (H_f) was unaffected by preexisting vertical crack, but was stopped from extending downward by horizontal crack.

where the hydraulic fracture (H_f in the photos) initiated and extended unaffected by the existence of nearby fractures. Specimen 5 (Fig. 26) was traversed by a preexisting inclined fracture. The induced hydrofracture at the borehole was vertical and crossed the inclined crack. Specimen 9 (Fig. 27) had a number of vertical fractures and a major horizontal one. The hydraulic fracture did not join any of the vertical flaws but was stopped by the horizontal fracture.

The last and largest set of tests under equal horizontal stress conditions was run in specimens obtained from the third shipment. The results are shown in Table 15 and Fig. 28. Generally, the specimens taken from the larger blocks were the less prefractured and yielded more consistent breakdown pressures. Due to the variability of the rock from block to block, however, the experimental P_c^e points are rather scattered, but still contained within the two theoretical curves (Fig. 28). To prevent premature opening of cracks crossing the borehole before hydrofracturing occurred, a lining of plaster of paris was installed in appropriate specimens as described in a previous chapter. The lining kept the fracturing fluid from coming in contact with the existing openings and yielded successful vertical fractures, albeit at somewhat lower breakdown pressures. Fig. 29 shows a specimen that had near vertical cracks cutting through the borehole. The plaster of paris lining helped obtain a normal vertical fracture (H_f). The excellent performance of the lining under difficult conditions surprised the investigators, and promised to be a very useful tool in eventual field tests.

In an attempt to explore the possibility of treating all the three shipments as representing one rock notwithstanding its variability, a combined plot of all the breakdown pressure results was prepared (Fig. 31). It shows that outside of the low horizontal stress range (0-1000 psi), practically all the breakdown

TABLE 15
HYDRAULIC FRACTURING RESULTS
THIRD SHIPMENT*

Specimen No.	Vertical Load σ_v (psi)	Horizontal Stress σ_H (psi)	Experimental Breakdown Pressure P_c^e (psi)
101	1,000	0	4,500
102	1,000	0	4,700
111	1,000	0	4,400
112	1,000	0	3,900
205	1,000	0	5,000
303	1,000	0	3,760
501	1,000	0	2,600
206	1,000	0	4,900
611	1,000	0	4,200
104	2,000	1,000	5,100 **
105	5,840	2,500	8,900
106	5,840	2,500	8,300
201	5,840	2,500	7,500 ***
107	11,600	5,000	10,400
110	11,600	5,000	8,000 ***
202	5,840	5,000	7,000 ***
301	15,550	5,000	11,000
108	15,550	7,700	14,100
503	15,550	7,500	12,500
607	15,550	7,700	17,100
109	21,350	10,000	20,800
401	25,200	12,500	20,200

TABLE 15 (Continued)

Specimen No.	Vertical Load σ_V (psi)	Horizontal Stress σ_H(psi)	Experimental Breakdown Pressure P_c^e (psi)
508	25,200	12,500	16,400
604	25,000	12,500	21,800
203	25,000	12,500	17,300 ***
402	29,150	15,000	23,600
506	29,150	15,000	22,400
610	29,150	15,000	22,200
	30,000	17,500	25,450
	30,000	17,500	25,000 +
609	30,000	17,500	28,600 +
405	30,000	20,000	29,200
602	30,000	20,000	35,000 +

* Unless otherwise stated all hydrofractures were axial (vertical) fractures emanating from the borehole.

** Inclined hydrofracture at 45° originating at bottom of the borehole.

*** Preexisting fracture through borehole treated with plaster of paris, yielding an axial (vertical) hydraulic fracture.

\+ Preexisting fracture did not affect results.

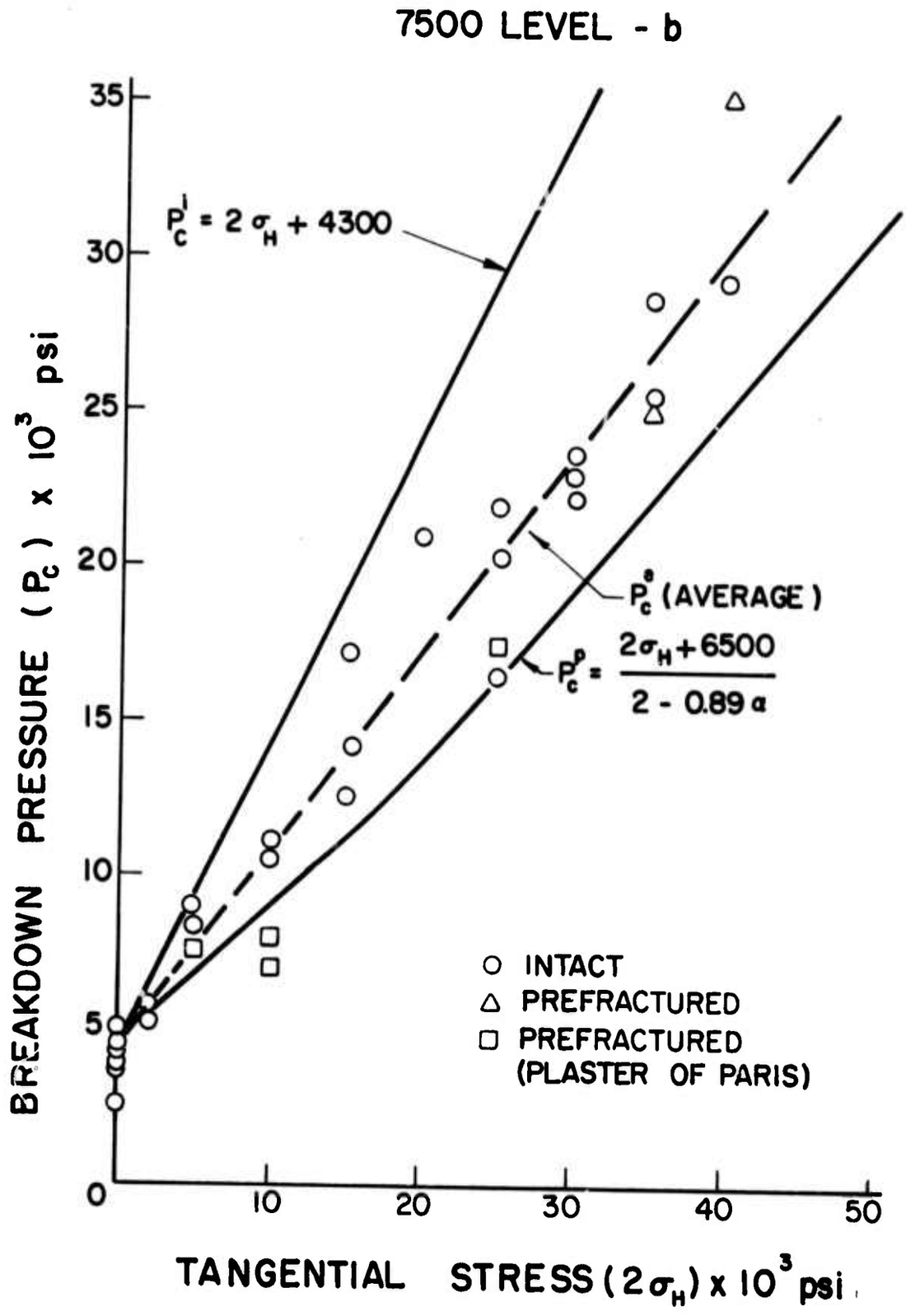

Fig. 28 Breakdown pressure results as a function of tangential stress (cylindrical specimens, third shipment).

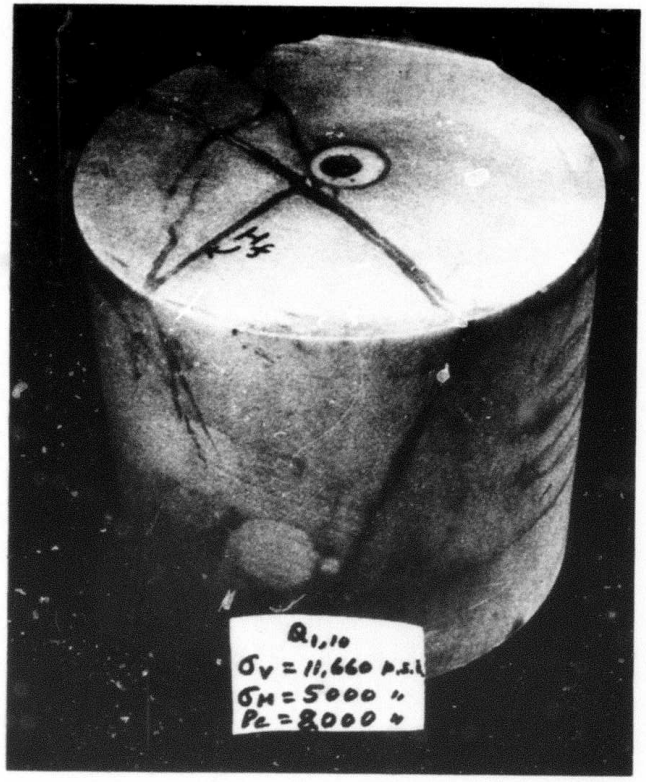

Fig. 29 Plaster of paris lining resulted in a vertical hydrofracture (H_f) unaffected by preexisting inclined crack running through the borehole.

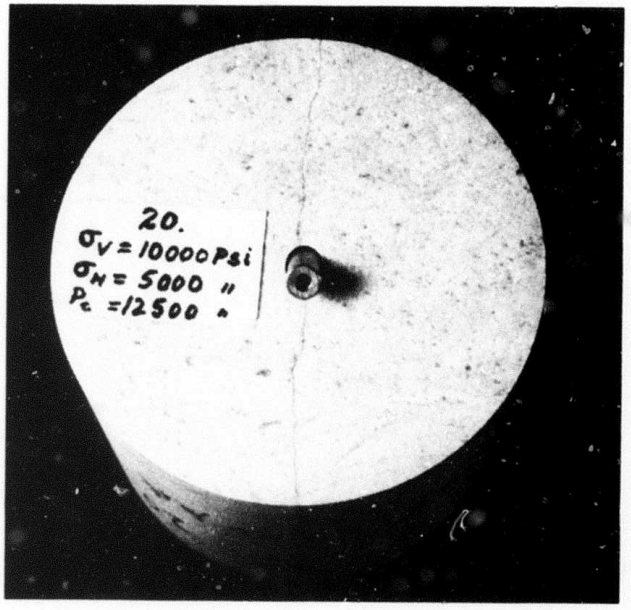

Fig. 30 Typical vertical hydrofracture in an inclined borehole.

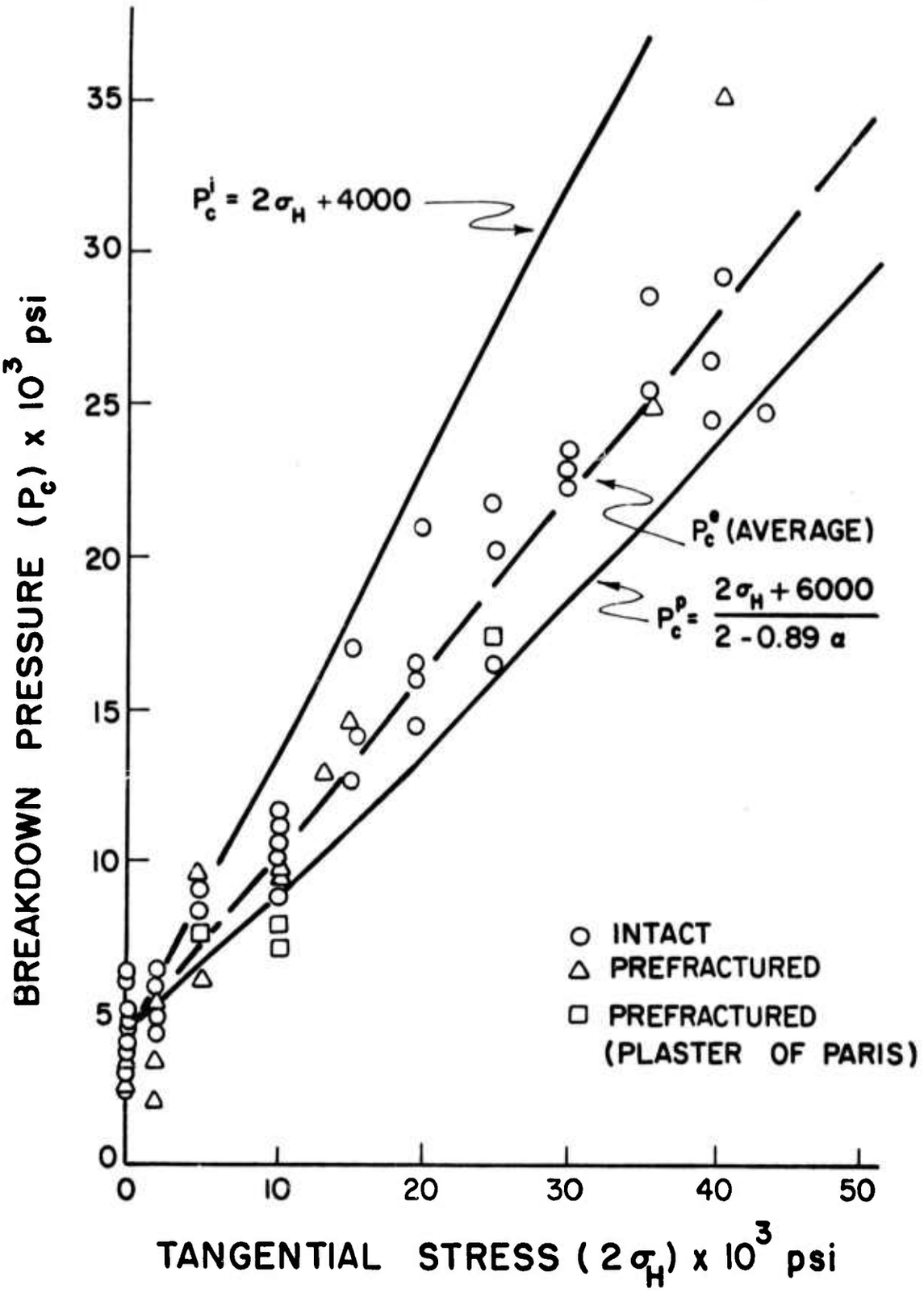

Fig. 31 Breakdown pressure as a function of tangential stress (all cylindrical specimens combined).

pressure results are well within the limits set by the two theoretical values P_c^i and P_c^p . It is interesting to note that the experimental points in this plot refer to rock from three different sites within the mine, and include intact, prefractured, and prefractured rock lined with plaster of paris. The prefractured specimens did show a tendency to yield lower than average breakdown pressure, but this was by no means consistent.

The major conclusion based on the described results is that Revett quartzite is sensitive to hydrofracturing. Because of the variability, the inhomogeneity and the prefractured nature of the rock, one cannot expect very precise maximum principal horizontal stress determination. However, based on Fig. 31 it can be deduced that if a number of tests are run in one location where the in-situ stresses are considered constant, the average calculated σ_H will be approximately within $\pm$ 15% of its real value.

2. Inclined Holes

As described elsewhere in this report, boreholes inclined at 30° to the vertical were drilled in the center of some specimens of the second and third shipment and a series of hydraulic fracturing tests were run in them. The objective of this experiment was to record the breakdown pressures and determine the resulting fracture direction in hydrofractured boreholes that are not parallel to one of the principal stresses. The tests are detailed in Table 16 and Fig. 32. The breakdown pressures obtained were not unlike the values in vertical holes for the same horizontal stress. No particular trend was observed. As to the initiated fractures, they were all tensile ruptures running through the axis of the borehole. In the zero horizontal stress specimens, the fractures were inclined at 30° to the vertical. For all the higher σ_H values the fractures ran vertical. In a horizontal cross section of a specimen, such a

TABLE 16
HYDRAULIC FRACTURING RESULTS
INCLINED HOLES
SECOND & THIRD SHIPMENTS

Specimen No.[a]	Vertical Load σ_V (psi)	Horizontal Stress σ_H(psi)	Experimental Breakdown Pressure P_c^e (psi)
14	1,000	0	4,000 *
15	1,000	0	3,100 *
19	5,000	2,500	5,100 x
204	5,840	2,500	8,200 +
20	10,000	5,000	8,300 +
21	10,000	5,000	12,500 +
608	15,550	7,500	14,000 x
23	15,550	7,500	11,500 +
404	21,350	10,000	14,000 +
590	21,350	10,000	14,000 +
702	25,200	12,500	16,000 +
803	25,200	12,500	16,000 +
606	29,150	15,000	21,700 +
507	29,150	15,000	19,200 +
801	29,150	17,400	21,800 +

a Two digit numbers represent second shipment.
* Inclined hydraulic fracture through borehole axis.
\+ Vertical hydraulic fracture through borehole axis.
x Vertical hydraulic fracture through borehole axis, joined a pre-existing fracture.

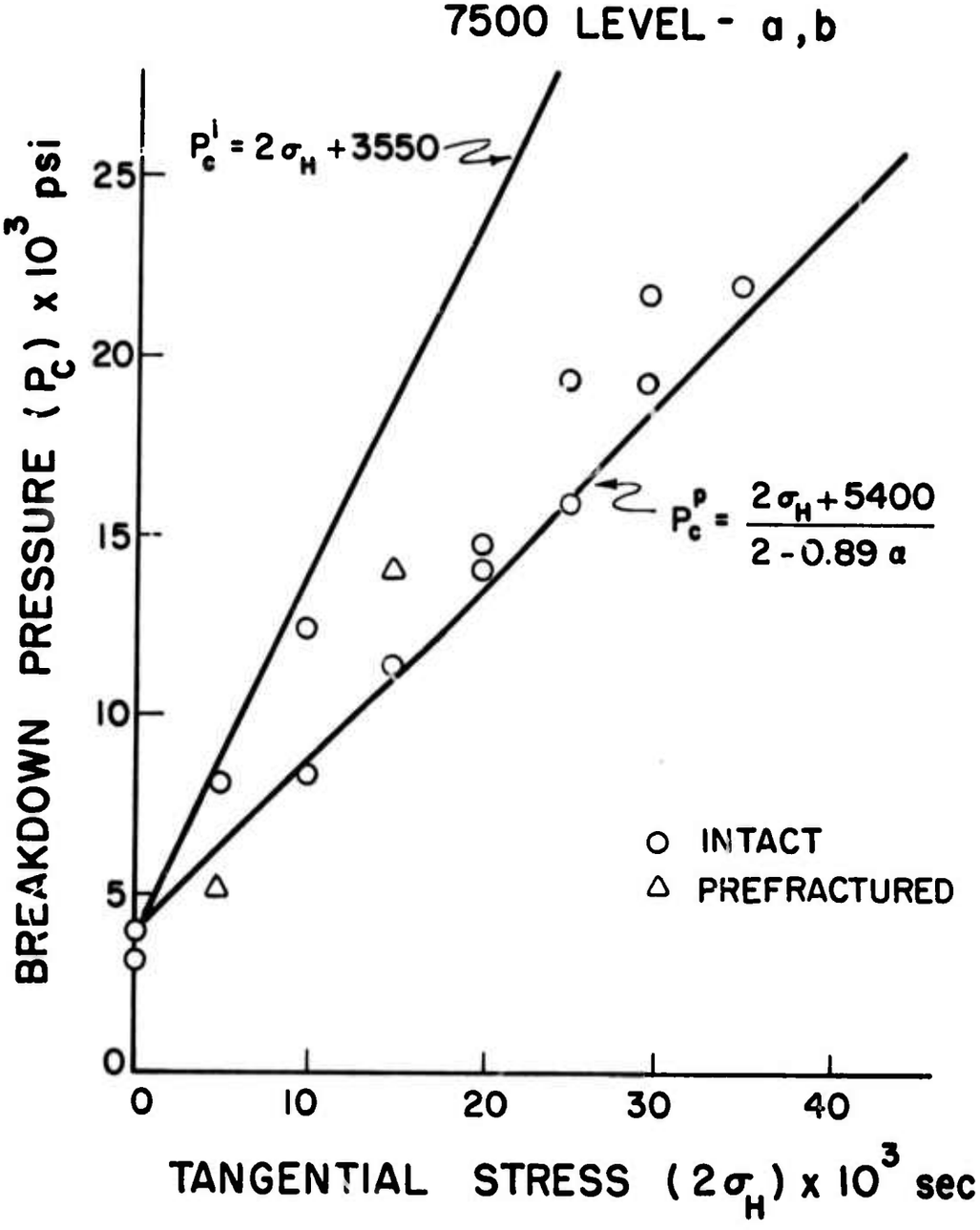

Fig. 32 Breakdown pressures as a function of tangential stress (cylindrical specimens with inclined holes, second and third shipments).

fracture cuts through the long axis of the ellipse formed by the inclined borehole (Fig. 30). This direction appears justified by theory since the tips of an ellipse are its weakest link, the points of the highest stress concentration.

A speculative conclusion to be drawn from this limited series of tests is that hydrofracturing could give a good approximation of principal stresses even if the testhole is not perfectly parallel to one of the principal in-situ stresses.

Unequal Horizontal Stresses - Axial Holes

Although the first phase of hydrofracturing tests run in cylindrical specimens yielded strong evidence that stress magnitudes in the Coeur d'Alene mines could be approximated from hydrofracturing results, it gave no indication regarding the determination of principal stress directions. The tests on prismatic blocks were designed to provide this additional information and to verify the applicability of equations (4) and (7a).

Three series of tests were run, on specimens from the third and fourth shipments. The results were kept separately (Tables 17, 18, and 19, Figs. 33, 34, and 35) due to significant differences in the average tensile strength of the batches of specimens. Plotting $(3\sigma_x - \sigma_y)$ vs P_c (where σ_x, σ_y are the minimum and the maximum applied principal horizontal stresses, respectively), it is again discovered that the great majority of the experimental points fall inbetween the predicted lines for permeable and impermeable rocks. The scatter of results is significant in the specimens of the third shipment and in those of block 12 - fourth shipment (Figs. 33 and 34). It should be noted, however, that most of the specimens in the third shipment were prefractured, many of them requiring plaster of paris lining. These imperfections could account for the somewhat inconsistent results. The origin of the scatter in

TABLE 17
HYDRAULIC FRACTURING RESULTS*
THIRD SHIPMENT-PRISMATIC SPECIMENS

Specimen No.	Horizontal Stresses		Vertical Load	Experimental Breakdown Pressure P_c^e (psi)
	σ_x(psi)	σ_y(psi)	σ_v(psi)	
617	3,150	8,950	8,100	6,300x
406	1,000	3,000	2,550	4,750x
505	3,000	9,150	3,250	5,250+
114	3,000	9,000	3,250	7,400
1102	1,000	3,000	2,150	4,250
618	5,350	10,000	8,100	7,750x
403	7,850	14,350	12,500	11,150x
118	2,500	5,000	3,250	3,400+
511	2,500	5,050	8,100	3,550△
901	5,000	9,800	12,200	7,100△
902	2,900	9,000	6,500	6,850△
119	2,500	4,900	3,250	7,500
1101	3,750	7,400	5,400	6,000△
616	6,000	6,950	6,500	7,400x
615	4,000	5,950	5,400	9,100
408	11,300	15,500	18,400	13,900x
113	4,000	5,950	5,400	10,000
1002	6,000	8,000	10,650	13,450θ
513	10,000	13,050	10,830	12,950
701	8,450	11,700	16,250	13,700△
1001	8,000	10,000	10,850	19,350
619	3,950	5,850	8,100	8,400△

TABLE 17 (Continued)

Specimen No.	Horizontal Stresses		Vertical Load	Experimental Breakdown
	σ_x(psi)	σ_y(psi)	σ_v(psi)	Pressure P_c^e(psi)
903	7,000	8,400	13,000	8,600ø
601	9,600	9,750	20,450	14,400□
1301	550	1,500	1,000	3,250Δ

* Unless otherwise stated, all hydrofractures were vertical and perpendicular to the direction of the smallest horizontal stress (σ_x).

x Preexisting inclined fractures did not effect hydrofracture.

\+ Hydrofracture occurred at an angle to borehole axis, apparently due to preexisting fracture, not previously observed on the outside of the specimen.

Δ Preexisting fractures through borehole treated with plaster of paris, did not effect hydrofractures.

□ Vertical hydrofracture occurred at random (Fig. 36).

ø Hydrofracture followed preexisting fracture due to incorrect plaster of paris treatment.

θ Preexisting fracture parallel to borehole axis and an inclined quartz vein in specimen did not effect hydrofracture.

TABLE 18
HYDRAULIC FRACTURING RESULTS
FOURTH SHIPMENT-PRISMATIC SPECIMENS*
BLOCK 12

Specimen No.	Horizontal Stresses		Vertical Load	Experimental Breakdown Pressure
	σ_x (psi)	σ_y (psi)	σ_v (psi)	P_c^e (psi)
1212	0	0	500	8,350
1213	0	0	500	6,750
1214	0	0	500	7,100
1215	0	0	500	6,850
1206	500	1,500	750	7,500
1203	2,050	5,950	4,350	9,550
1209	2,000	3,950	3,000	9,600
1208	3,950	6,950	5,500	7,300x
1205	5,300	9,000	7,500	15,100
1204	10,000	15,000	12,500	16,850**
1207	5,150	7,000	6,000	9,800+
1210	7,100	9,950	9,000	16,400**
1211	4,850	7,000	6,500	7,500+Δ
1202	6,100	7,950	7,600	12,600x
1201	7,950	10,050	9,750	18,000

* Unless otherwise stated, all hydrofractures were vertical and perpendicular to the direction of the smallest horizontal stress (σ_x).

** Preexisting fracture did not effect hydrofracture.

\+ Preexisting fracture in specimen treated with plaster of paris, did not effect hydrofracture.

Δ Preexisting fracture stopped hydrofracture away from the borehole.

x Inclined fracture at the bottom of the borehole, apparently caused by preexisting fractures.

TABLE 19
HYDRAULIC FRACTURING RESULTS
FOURTH SHIPMENT-PRISMATIC SPECIMENS*
BLOCK 14

Specimen No.	Horizontal Stress		Vertical Load	Experimental Breakdown
	σ_x(psi)	σ_y(psi)	σ_v(psi)	Pressure P_c^e (psi)
1401	0	0	500	2,500
1402	0	0	500	3,600
1403	500	1,500	1,000	3,750
1404	1,000	2,000	1,500	3,200
1405	5,050	9,950	7,500	8,800
1406	6,000	7,900	7,000	12,800
1407	10,070	14,930	12,500	17,600
1409	5,500	8,050	7,000	10,300**
1410	3,050	5,500	4,000	8,100
1411	7,600	10,050	9,000	12,000
1412	2,000	4,000	3,000	6,200
1414	5,050	7,950	7,000	12,000
1415	3,550	6,000	5,000	8,000

* All hydrofractures were vertical and perpendicular to the direction of the smallest horizontal stress (σ_x).

** Preexisting fractures in the specimen treated with plaster of paris, did not effect hydrofracture.

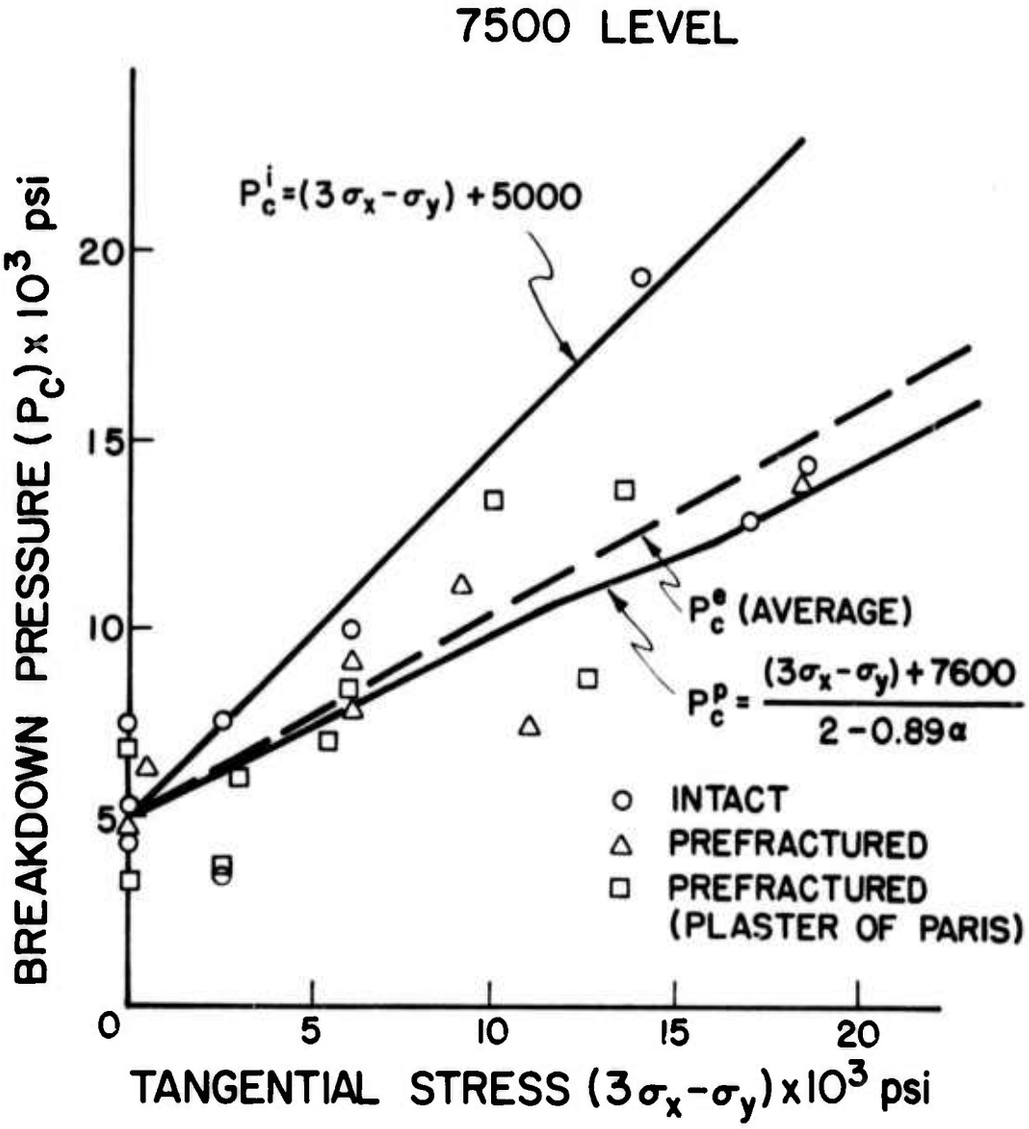

Fig. 33 Breakdown pressure as a function of tangential stress (prismatic specimens, third shipment).

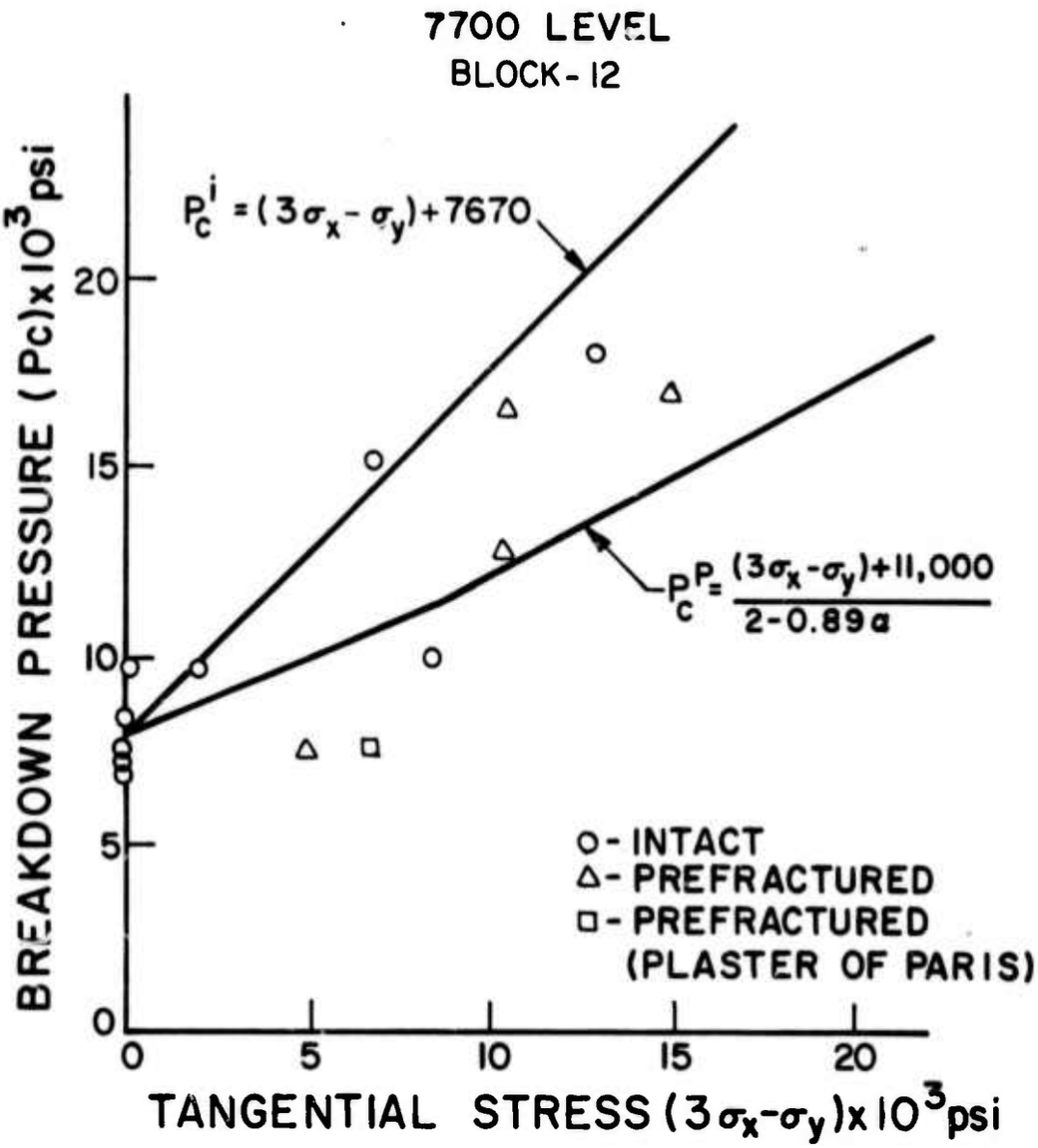

Fig. 34 Breakdown pressure as a function of tangential stress (prismatic specimens, fourth shipment, block 12).

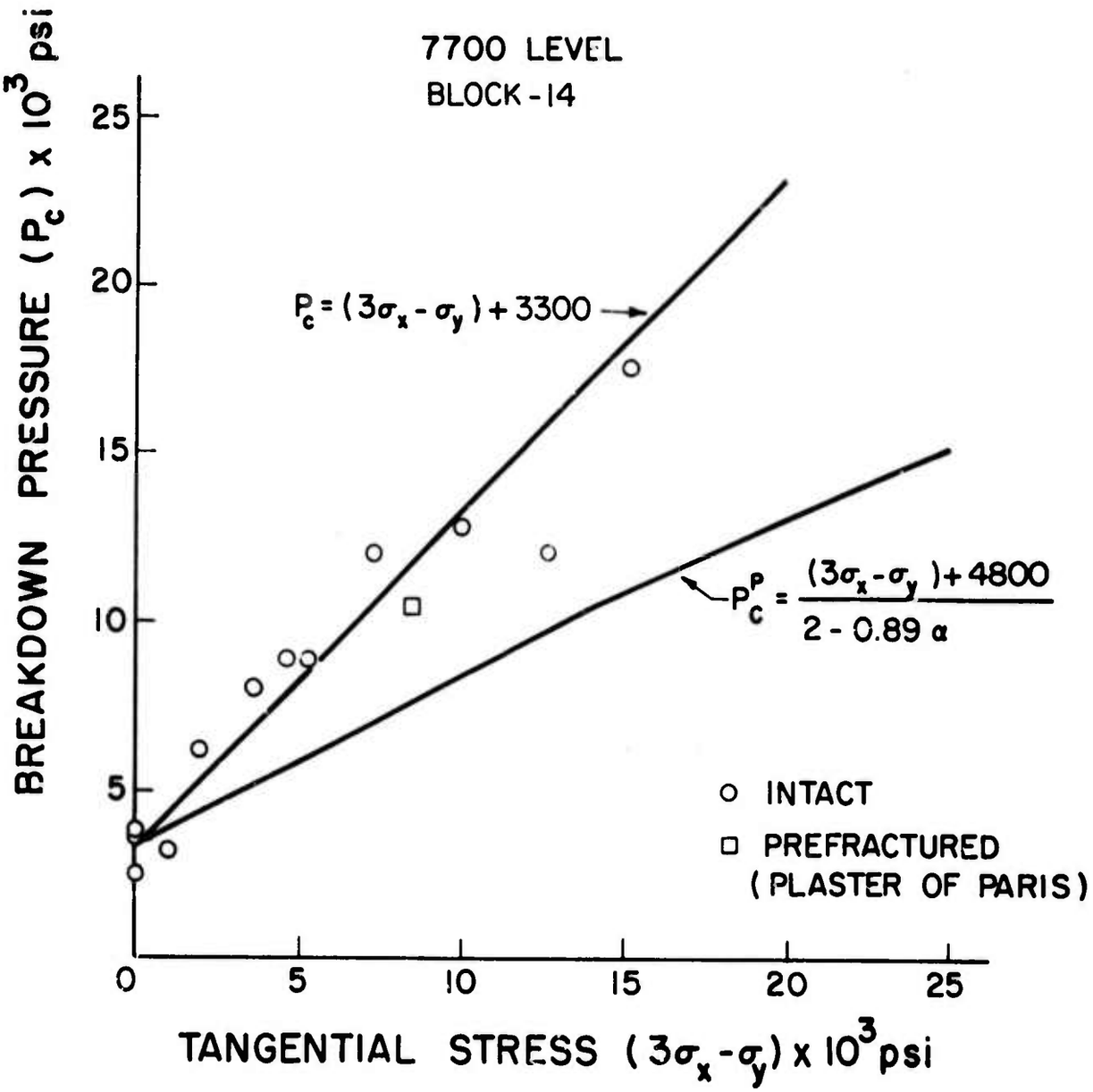

Fig. 35 Breakdown pressure as a function of tangential stress (prismatic specimens, fourth shipment, block 14)

block 12 is unclear, and more tests were necessary, but were not possible because of the block size limitations. Fig. 34 representing the results obtained in block 14 of the fourth shipment not only reveals very consistent results in this nearly intact block, but most of the experimental breakdown pressures lie on the line representing the theoretically expected values for an impermeable rock. It is apparent that the particular version of Revett quartzite represented by block 14 remains impermeable under the borehole pressures used in the reported tests. This is, of course, unlike any of the other blocks previously tested. This result only emphasizes the importance of laboratory testing of rock properties for any location where hydraulic fracturing is to be used in the Coeur d'Alene mines.

As noted in Table 17 most of the third shipment prisms were prefractured and provided a unique opportunity to examine joint effect on the direction and inclination of hydraulic fractures. Intact specimen invariably yielded vertical fractures perpendicular to the smallest horizontal principal stress, as expected. Fig. 37 shows such a typical fracture in a specimen loaded to a ratio of $\sigma_y/\sigma_x = 2$. In instances where $\sigma_x \tilde{=} \sigma_y$ random vertical fractures were obtained (Fig. 36). This again was as expected since no preference existed for a particular direction.

Figs. 38 to 45 show variations of prefractured specimens and the resulting hydraulic fractures (H_f). The common denominator to all hydraulic fractures is that they were not affected by the initial discontinuities. The great majority of hydraulic fractures maintained their direction perpendicular to the smallest principal stress. In most cases they crossed existing fractures as in Figs. 38, 39, 41, and 42. In others the hydrofracture joined the existing fractures (Fig. 40 & 41). The plaster of paris lining appeared to perform excellently and enabled vertical fracture initiation in such unlikely specimens as # 902 and # 1301 (Figs. 44 and 45) where horizontal discontinuities traversed the rock and testhole.

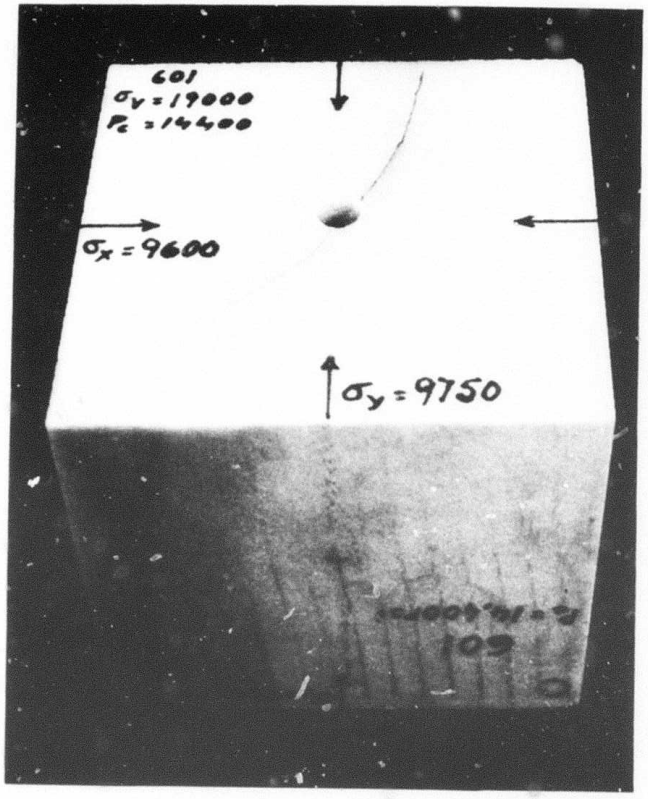

Fig. 36 Vertical hydrofracture at random direction, as expected when $\sigma_x \simeq \sigma_y$.

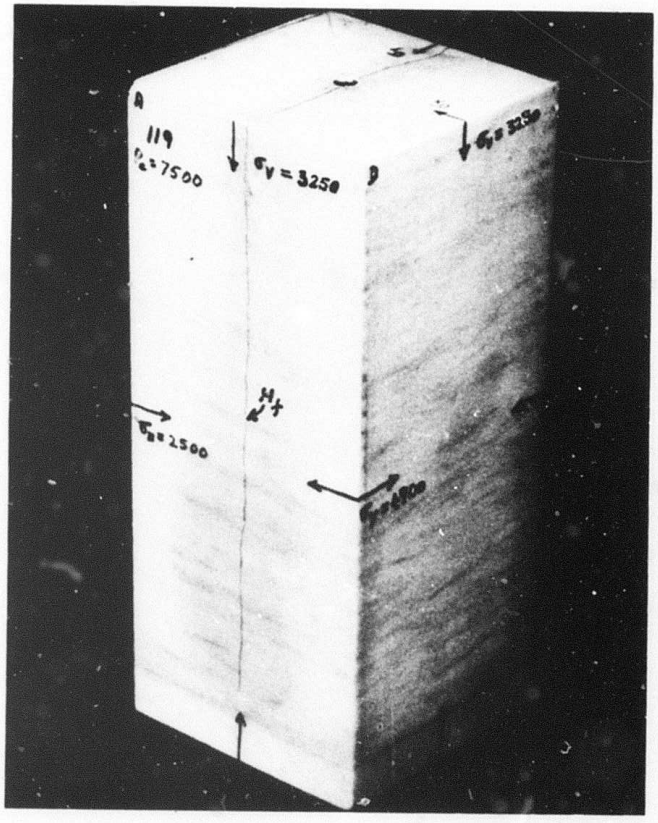

Fig. 37 Typical vertical hydrofracture perpendicular to the smallest horizontal stress (intact specimen with $\sigma_x \neq \sigma_y$).

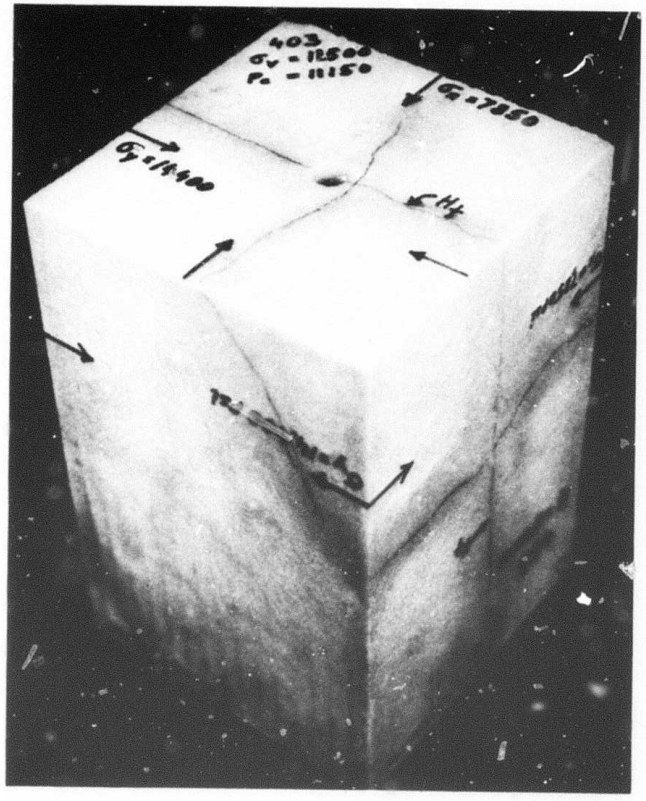

Fig. 38 Vertical hydrofracture (H_f) crossed pre-existing inclined discontinuity and maintained its expected direction.

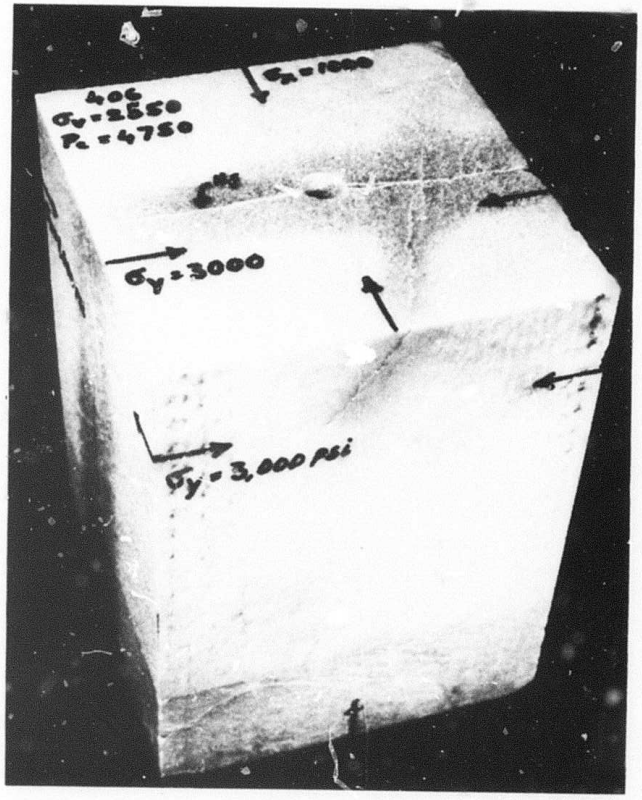

Fig. 39 Vertical hydrofracture (H_f) crossed preexisting inclined fracture and maintained its expected direction.

Fig. 40 Vertical hydrofracture (H_f) developed in its expected direction joined pre-existing fracture. Fracturing hole lined with plaster of paris.

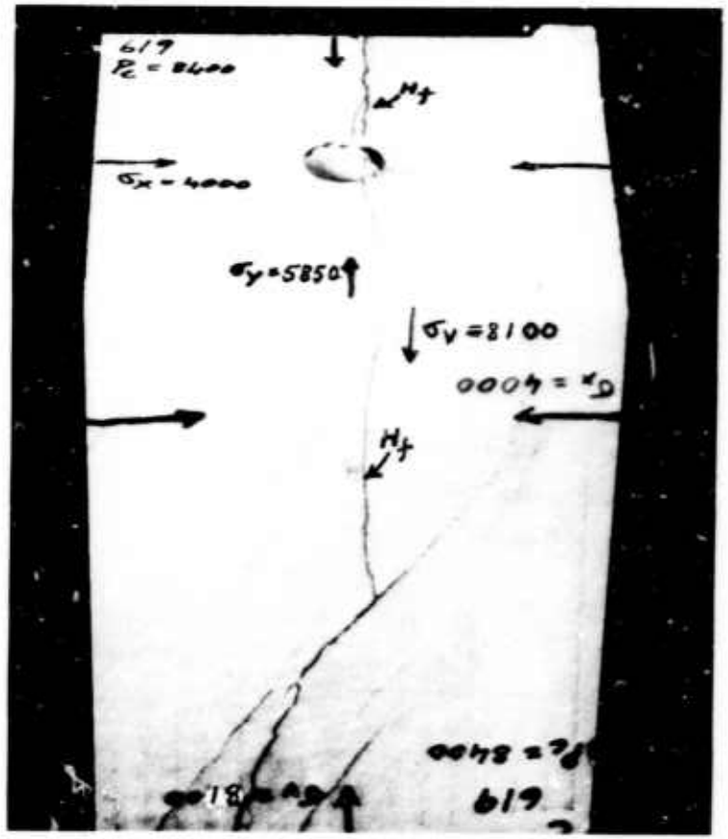

Fig. 41 The presence of a preexisting crack at the hole did not affect the initiation and direction of hydrofracture, probably because of the plaster of paris lining. Away from the hole the hydrofracture joined the inclined crack.

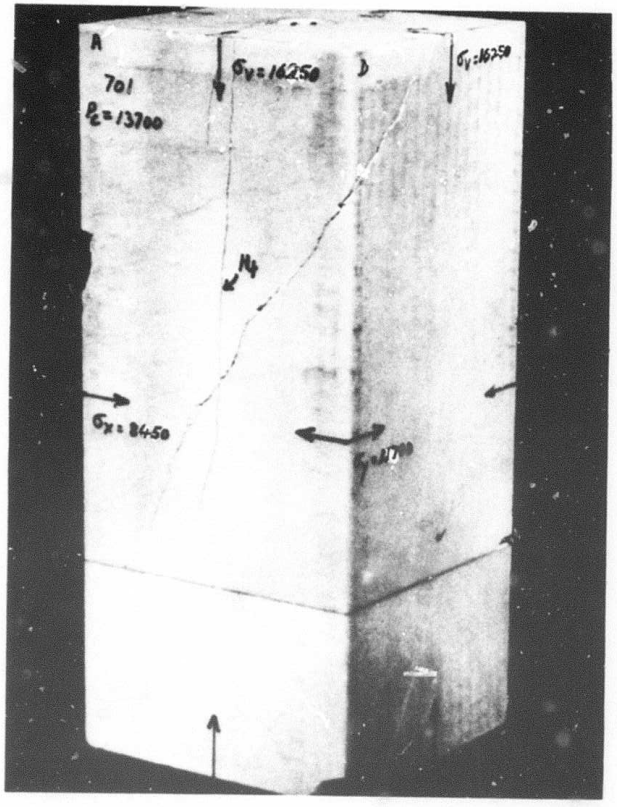

Fig. 42 Vertical hydrofracture in the expected direction, unaffected by preexisting inclined fracture.

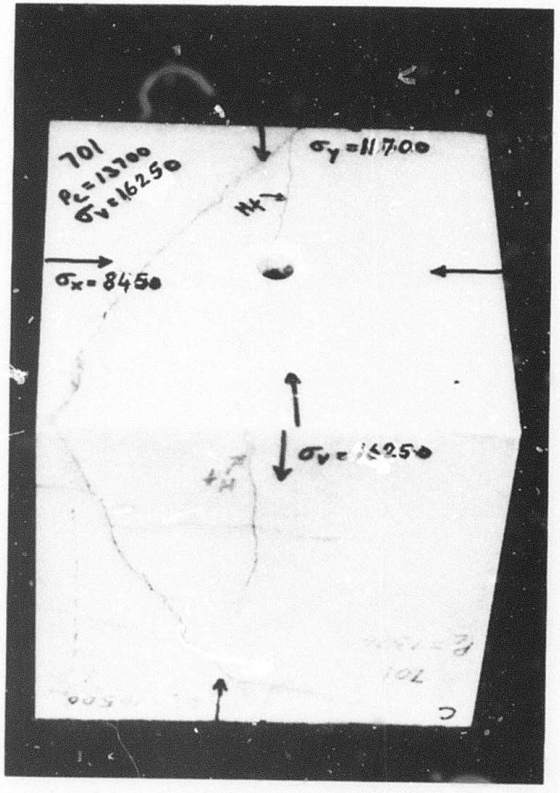

Fig. 43 Horizontal section of the specimen shown in Fig. 42.

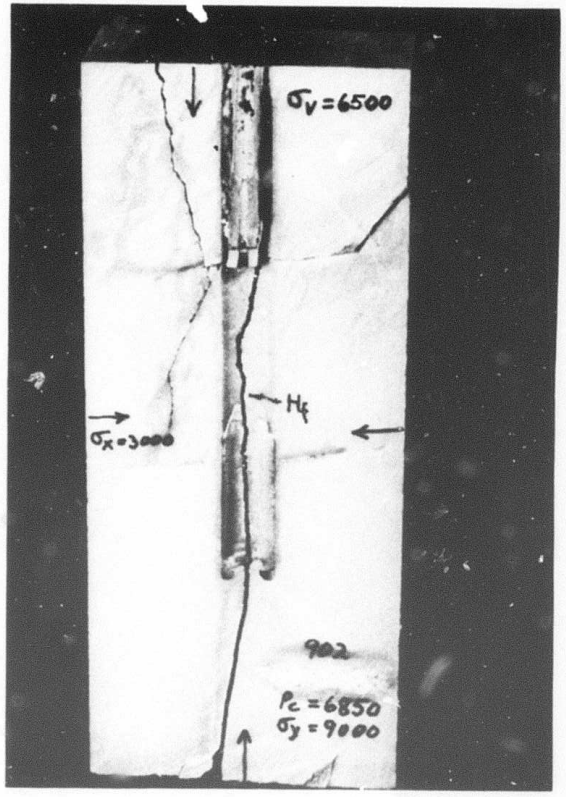

Fig. 44 Vertical section of a specimen traversed by preexisting fractures including two horizontal cracks cutting through the hole. With the help of plaster lining the hydrofracture obtained was unaffected by discontinuities.

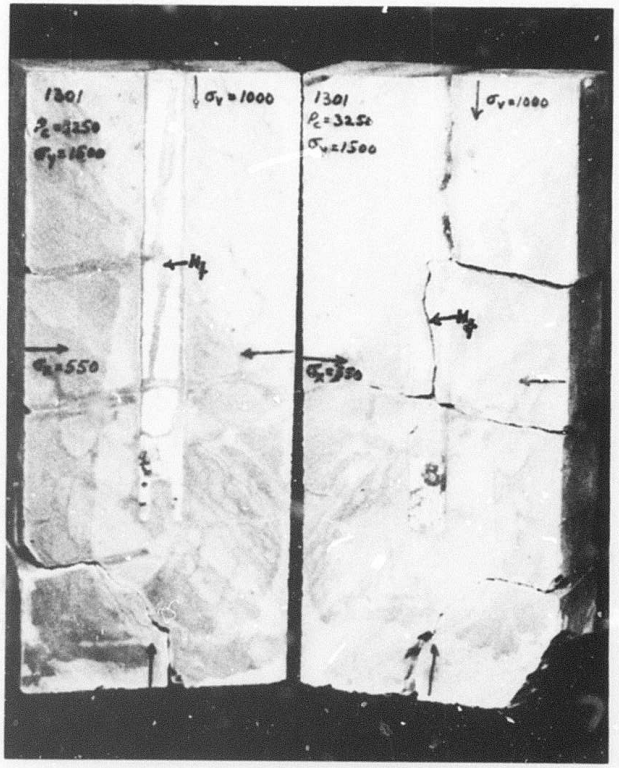

Fig. 45 Vertically sectioned specimen showing preexisting cracks and bands cutting into the hole. The hydrofracture, initiated through a plaster lining, was controlled only by the principal stress directions.

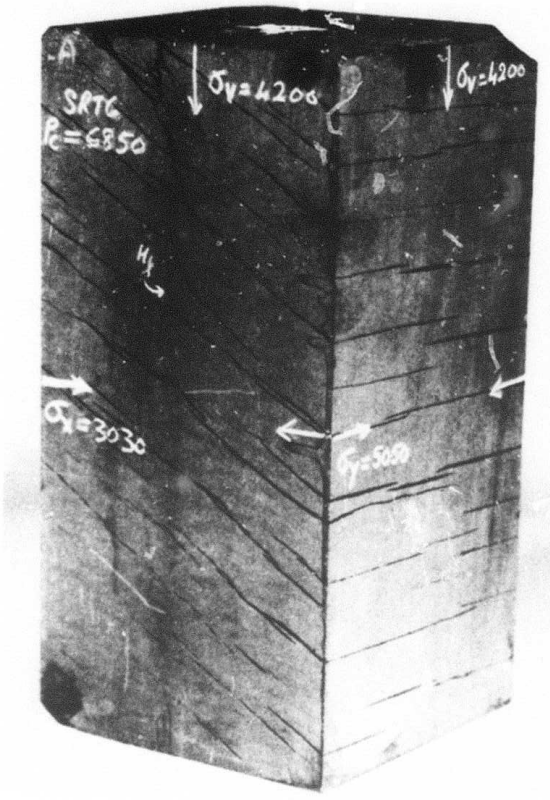

Fig. 46 A pennsylvanian slate specimen with thin beds dipping at 30° yielded a hydrofracture controlled only by the direction of the smallest horizontal stress. Hole was lined with plaster of paris.

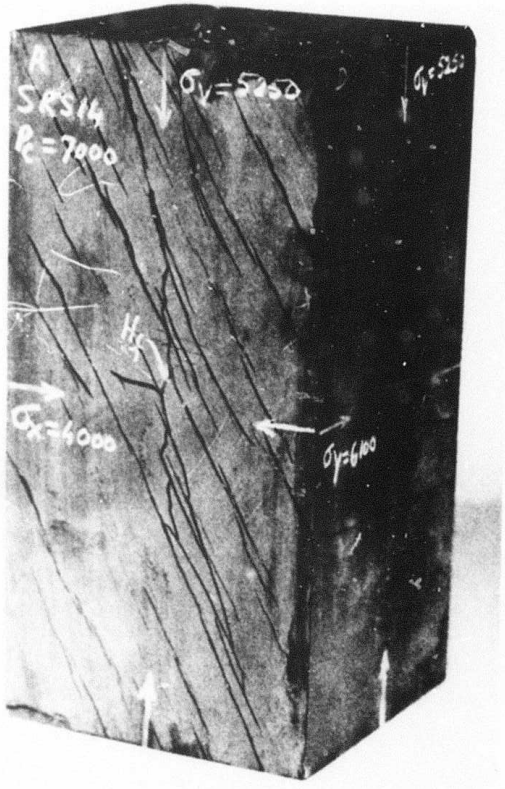

Fig. 47 A pennsylvanian slate specimen with thin beds dipping at 60° yielded a hydrofracture controlled only by the direction of the smallest horizontal stress. Hole was lined with plaster of paris.

To illustrate the extent to which hydrofracture orientation is affected by principal stresses, two additional tested specimens are shown (Figs. 46 and 47). These are thinly bedded pennsylvanian slate prisms. The bedding planes are extremely weak and permeable. Yet with the help of a thin layer of plaster of paris, enough to keep the fracturing fluid from coming in contact with the discontinuities when pressurization initiates, vertical fractures perpendicular to the smallest principal horizontal stress were obtained.

In general, the testing of prismatic specimens was conducted in extremely prefractured, inhomogeneous, variable rock. A look at the mechanical property results in intact specimens will show a nonlinear, inconsistent behavior, including such irrational characterization as lateral contraction during uniaxial tension. Naturally, such rock could hardly facilitate precise measurements of in-situ stresses which are always calculated with the assumption of elastic linear, homogeneous rock behavior. The scatter of experimental results seen in Figs. 33 and 34 is of the type that no theoretical curves would fit any better than the P_c^i and P_c^p shown. The major reason for the scatter appears to be an inconsistent hydrofracture tensile strength (T) which is sensitive to existing discontinuities at the borehole wall. When the specimens are intact, as in block 14 (Fig. 34), T is more consistent and so are the other results. In the worst situation, however, P_c results do not appear to be off by more than 20% from an average between the theoretical P_c^i and P_c^p. To the purist this may seem excessive. To the field practitioner such a result is a considerable improvement over complete ignorance of the stresses, especially that the directions of the principal stresses can be determined quite accurately by hydrofracturing. Indeed, the hydrofracture direction results as proven by photographs in Figs. 37 to 47 are remarkably consistent at 90° to the smallest horizontal stress, notwithstanding the obstacles provided by preexisting fractures.

CONCLUSIONS

A laboratory investigation was conducted to establish the applicability of hydraulic fracturing as a stress measuring method in the Revett quartzite of the Coeur d'Alene mining district. Rock from three different levels (6100 ft, 7500 ft and 7700 ft levels) of the Star mine was tested both for mechanical properties and hydraulic fracturing response.

1. Mechanical properties such as dynamic longitudinal velocity, static compressive and tensile strengths, Young's Modulus and Poisson's ratio show that on the average the Star mine quartzite is a very strong and stiff rock. However, from specimen to specimen the scatter can be substantial. This is believed to be caused by variations in the texture and composition of the rock, both locally and from site to site, and predominantly due to the existence of abundant flaws, fractures, weak bands and mica inclusions.
2. Two basic mechanical behaviors were detected. Specimens for which the longitudinal seismic velocities were above 18×10^4 in/sec yielded linear stress-strain curves in uniaxial compression and tension, and exhibited predictable mechanical behavior of brittle elastic rock. Specimens for which the longitudinal velocities were lower then 18×10^4 in/sec yielded bilinear stress-strain curves in uniaxial compression, with an initial low modulus gradually stiffening in the range of 5,000 psi - 10,000 psi. The lateral strain recorded in the low modulus range was nearly zero, and in many cases positive, indicating contraction. This unusual behavior is suspected to be the result of mica inclusion closure in the first stage of loading. In uniaxial tension the bilinear specimens exhibited lateral expansion throughout most of the loading range. This peculiar characteristic is suspected to be the result of mica inclusion opening.

3. No consistent dependency of mechanical properties on bedding inclination was found. Anisotropy was not positively identified. Rather, the rock can be best described as being inhomogeneous with mechanical property variations depending on the existence and extent of fractures, bands and inclusions.
4. Hydraulic fracturing testing has shown that, in spite of considerable scatter of results mostly at low horizontal stresses, a linear relationship can be approximated to characterize the experimental points of breakdown pressure vs. horizontal stress in most of the blocks tested. This line is almost always bounded by the curves representing the expected relationship for breakdown pressure in impermeable and permeable rock respectively. No modification of the existing theory is required.
5. For the stress conditions simulated in the tests, the great majority of hydraulic fractures were vertical. These fractures emanated from the pressurized borehole in two opposite directions and extended to the specimen face. The direction of the hydraulic fracture was always perpendicular to the smallest horizontal principal stress.
6. The existence of nearby cracks and bands did not appear to affect either the breakdown pressure or the inclination and direction of the fracture at borehole. Away from the borehole, the hydrofractures would at times join the preexisting cracks, but more often cross them and continue to extend in the original direction.
7. In specimens where open preexisting fractures traversed the borehole, a thin lining of plaster of paris provided the necessary barrier between fracturing fluid and open crack, and yielded vertical hydrofractures unaffected by rock condition. The breakdown pressures were often slightly lower than those expected for similar cases in intact rock.

8. Hydraulic fracturing in holes inclined at 30° to the direction of the vertical principal stress resulted in vertical fractures passing through the axis of the hole. Breakdown pressures were not significantly different from those obtained in vertical holes under the same stress conditions.
9. Generally, it can be concluded that the Coeur d'Alene quartzite does react to hydraulic fracturing consistently enough to warrant field testing. It is envisioned that the method could become the only reliable technique of estimating stresses in the Coeur d'Alene mining district because of its simplicity and relative insensitivity to deviations from ideal rock conditions.

REFERENCES

Ageton, R.W. (1967), "Deep Mine Stress Determination Using a Flat Jack and Borehole Deformation Methods", U.S. Bureau of Mines, Report of Investigation 6887.

Ageton, R.W. (1967a), "Stress Ellipsoid Determination in a Rock Burst Prone Area at a 4,000 Foot Depth, Galena Mine, Wallace, Idaho", U.S. Bureau of Mines, Report of Investigation 6997.

Biot, M.A. (1956), "Thermoelasticity and Irreversible Thermodynamics", Journal of Applied Physics, Vol. 27, p. 240.

Biot, M.A. and Willis, D.G. (1957), "The Elastic Coefficients of the Theory of Consolidation", Journal of Applied Mechanics, p. 594.

Blake, W. (1970), "Six Month Progress Report on Rock Burst Research at the Galena Mine; Nov. 1, 1969 through May 1, 1970", U.S. Bureau of Mines, Denver Mining Research Center, Denver, Colorado.

Bredehoft, J.D., Wolff, R.G., Keys, W.S. and Shuter, E. (1973), "Hydraulic Fracturing as a Tool to Determine the State of Tectonic Stress in the Piceance Basin, Northwest Colorado, Abstract, Annual Meeting, the Geological Society of America.

Chan, S.S.M. (1971), "Deformation Behavior of Revett Quartzite Under Uniaxial and Triaxial Loading", 6th Canadian Symposium on Rock Mechanics, May 1970, Montreal, Canada.

Chan, S.S.M. (1972), "A Case Study of In-Situ Rock Deformation Behavior for the Design of Ground Support System", University of Idaho, Final Report to U.S. Bureau of Mines (Grant No. G0110174).

Clark, J.B. (1968), "A Hydraulic Process for Increasing the Productivity of Wells", Trans. AIME, Vol. 186.

Dahl, M.D. and Parsons, R.C. (1971), "A Study of the Causes of Roof Instability in the Pittsburgh Coal Seam", 7th Canadian Symposium on Rock Mechanics.

Fairhurst, C. (1964), "Measurement of In-Situ Rock Stresses with Particular Reference to Hydraulic Fracturing", Rock Mechanics and Engineering Geology, Vol. 2, No. 3-4, p. 129.

Haimson, B.C. (1968), "Hydraulic Fracturing in Porous and Nonporous Rock and its Potential for Determining In-Situ Stresses at Great Depth", Ph.D. Thesis, University of Minnesota, Minneapolis.

Haimson, B.C. (1973), "Earthquake Related Stresses at Rangely, Colorado", New Horizons in Rock Mechanics (Proc. 14th Symposium on Rock Mechanics), Ed. Hardy and Stefanko, ASCE, p. 689.

Haimson, B.C. and Edl, J.N. (1972), "Hydraulic Fracturing of Deep Wells", SPE 4061, 47th Annual Fall Meeting, Society of Petroleum Engineers of AIME, San Antonio, Texas, Oct. 1972.

Haimson, B.C. and Fairhurst, C. (1967), "Initiation and Extension of Hydraulic Fractures in Rocks", Society of Petroleum Engineers Journal, Sept. 1967, p. 310.

Haimson, B.C. and Fairhurst, C. (1970), "In-Situ Stress Determination at Great Depth by Means of Hydraulic Fracturing", Rock Mechanics Theory and Practice (Proc. 12th Symposium on Rock Mechanics), Ed. Somerton, AIME, Ch. 28, p. 559.

Haimson, B.C., LaComb, J., Jones, A.M. and Green, S.J. (1974), "Deep Stress Measurements in Tuff at the Nevada Test Site", Proceedings 3rd Conference, International Society of Rock Mechanics, Denver.

Haimson, B.C. and Stahl, E.J. (1969), "Hydraulic Fracturing and Extraction of Minerals Through Wells", Proc., 3rd Symposium on Salt, Cleveland, Ohio.

Hubbert, M.K., and Rubey, W.W. (1959), "Role of Fluid Pressure in Mechanics of Overthrust Faulting", Bulletin of Geophysical Society of America, Vol. 70, p. 115.

Hubbert, M.K., and Willis, D.G. (1957), "Mechanics of Hydraulic Fracturing", Trans. AIME, Vol. 210, p. 153.

Kehle, R.O. (1964), "Determination of Tectonic Stresses through Analysis of Hydraulic Well Fracturing", Journal of Geophysical Research, Vol. 69, p. 259.

Nowacki, W. (1962), "Thermoelasticity", Pergamon Press.

Raleigh, C.B., Healy, T.H., Bredehoeft, J.D. (1972), "Faulting and Crystal Stress at Rangely, Colorado", in Flow and Fracture of Rocks, Geophysical Monograph 16, Am. Geophysical Union.

Rogiers, J.C., Fairhurst, C., and Rosene, R.B. (1973), "The D.S.P. - A New Instrument for Estimation of the In-Situ Stress State at Depth", SPE 4246, Sixth Conf. on Drilling and Rock Mechanics of the Society of Petroleum Engineers of AIME, Austin, Texas.

Sandia Laboratories (1973), "Coal and Oil Fracturing: A Lab. Proposal", Lab. News, Sandia Laboratories, Vol. 25, No. 23.

Scheidegger, A.E. (1962), "Stresses in Earth's Crust as Determined from Hydraulic Fracturing Data", Geologie und Bauwesen, Vol. 27.

Smith, M., Potter, R., Brown, D. and Aamodt, R.L., (1973), "Introduction and Growth of Fracture in Hot Rock", Geothermal Energy, Ed. Kruger, P. and Otte, C., Stanford University Press.

Terzaghi, K. (1963), "Theoretical Soil Mechanics", J. Wiley, New York.

Thill, R.E., McWilliams, J.R. and Bur, T.R., (1968), "An Acoustical Bench for an Ultrasonic Pulse System", R.I. 7164, U.S.B.M., Dept. of Interior.

Thill, R.E., (1972), Personal communication.

Timoshenko, S. and Goodier, J.N. (1951), "Theory of Elasticity", McGraw & Hill, New York.

von Schonfeldt, H., (1970), "An Experimental Study of Open Hole Hydraulic Fracturing as a Stress Measurement Method with Particular Emphasis on Field Tests", Ph.D. Thesis, Univ. of Minnesota, Minneapolis.